Numerical modeling of thermally induced ground deformations around potential geothermal energy storage wells in northern Quebec

Zhebo Ren

A Thesis

In

The Department

Of

Building, Civil, and Environmental Engineering

Presented in Partial Fulfillment of the Requirements

For the Degree of

Master of Applied Science (Geotechnical Engineering) at

Concordia University

Montréal, Québec, Canada

March 2022

CONCORDIA UNIVERSITY

School of Graduate Studies

This is to certify that the thesis prepared

By: Zhebo Ren

Entitled: Numerical modeling of thermally induced ground deformations around potential geothermal energy storage wells in northern Quebec

and submitted in partial fulfillment of the requirements for the degree of

Master of Applied Science (Geotechnical Engineering)

complies with the regulations of the University and meets the accepted standards with respect to originality and quality.

Signed by the final Examining Committee:

_____ Chair

Dr. Adel M. Hanna

_____ Examiner

Dr. Biao Li

_____ Examiner

Dr. Emre Erkmen

_____ Supervisor

Dr. Biao Li

Approved by: _____

Dr. Ashutosh Bagchi Chair of Department or Graduate Program Director

_____2022 _____

Dean of Faculty: Dr Mourad Debbabi

ABSTRACT

Numerical modeling of thermally induced ground deformations around potential geothermal energy storage wells in northern Quebec

Zhebo Ren

Literature from the past two decades demonstrates the feasibility of utilizing borehole geothermal energy storage (BTES) system for the heating of buildings in the cold climate region like Northern Quebec. However, BTES systems would generate an increase in temperature in surrounding soil formations, which may induce ground deformation and result in unexpected accidents. This study investigates the effect of BTES systems of 50-year service life period on thermal consolidation of surrounding soil formations in northern Quebec, where BTES sites are covered by a large quantity of unconsolidated glacial tills. A fully coupled thermal-hydro-mechanical modeling is conducted using Abaqus, and cases with different configuration and operation temperature are modeled. Thermally induced pore pressure generation and dissipation processes are simulated and analyzed. Thermally induced deformation of soil formations is also addressed. The glacial till in the upper layer is prone to sustain strain softening and the glacial till in the lower layer is prone to sustain strain hardening during the periodical thermal operation. A BTES system with a large geometric scale or with a high operation temperature (60°C in this study) would impose significant influence on the glacial till formation, which is displayed by significant changes in pore water pressure and ground deformations.

ACKNOWLEDGEMENTS

First, I would like to express my heartfelt thanks to Professor Biao Li, my thesis supervisor, for his tireless effort in teaching, assisting, guiding and advising me throughout this research.

I am grateful to the support provided by my family members and friends at difficult times during this whole period. I would like to tell Xiuting: “Our life just begins; a booming future is forward.”

I would also thank the examination committee for reading this thesis and providing critical comments. I would like to offer my deepest gratitude for the guidance of Dr. Hanna and Dr. Erkmen.

Finally, I would like to acknowledge the financial support received from the Department of Building, Civil, and Environmental Engineering at University of Concordia to make this research possible.

TABLE OF CONTENTS

LIST OF FIGURES

LIST OF TABLES

LIST OF SYMBOLS

a_0	Initial yield surface size (Abaqus)
β	Wet yield surface size (Abaqus)
K	Stress flow ratio
M	Stress ratio
λ	Slope of the normally consolidation line
v	Poisson's ratio
κ	Slope of the unloading-reloading line
φ'	Internal friction angle
c'	Effective cohesion
C_c	Compression index
C_s	Swelling index
$\sigma_z^{'}$	Vertical effective stress at depth of z
$\sigma_{zc}^{'}$	Preconsolidation pressure
$\sigma_x^{'}$ and $\sigma_y^{'}$	Horizontal effective stresses at depth of z
u	Pore pressure
$p_z^{'}$	Mean effective stress at depth of z
$p_{z-pre}^{'}$	Maximum mean effective stress at depth of z
q_z	Deviator shear stress at depth of z
q_{z-pre}	Maximum deviator shear stress at depth of z
K_0	Static earth pressure coefficient
$\sigma_{z-pre}^{'}$	Maximum vertical effective stress in the history at depth of z

$p_{cz-pre}^{'}$	Initial yield surface size at depth of z
e	Void ratio
e_0	Initial void ratio
e_N	Void ratio on the normal consolidation line at unit mean effective stress
ρ_{dry}	Dry density
ρ_{sat}	Saturated density
G_s	Specific gravity
k_{sat}	Saturated hydraulic conductivity
C_v	Volumetric heat capacity
C_p	Specific heat capacity
λ_t	Thermal conductivity
$\boldsymbol{\sigma}$	Total stress tensor
$\mathbf{L}$	Differential operator
$\mathbf{k}$	Permeability matrix of the total fluid phase
μ	Viscosity of the total fluid phase
ϕ	Porosity
β_w	Pressure and thermal expansion coefficient of water
β_s	Pressure and thermal expansion coefficient of solid
$\boldsymbol{\varepsilon}$	Strain
Q_e	Volumetric outflow of the fluid per unit volume of the solid
Q_h	Outflow of heat per unit volume of solid
J^{pl}	Plastic part of rate of volumetric change

α_s	Thermal expansion coefficient of glacial till solid
α_w	Thermal expansion coefficient of water

1 Introduction

1.1 Background

A borehole thermal energy storage (BTES) system is promising in cold regions like northern Quebec. Using soil and groundwater for heat storage offers an opportunity to increase the potential for renewable energy sources. Geothermal energy storage systems show a huge market in local communities in cold region suffering from fuel shortage (Giordan and Raymond, 2019; Giordano et al., 2017).

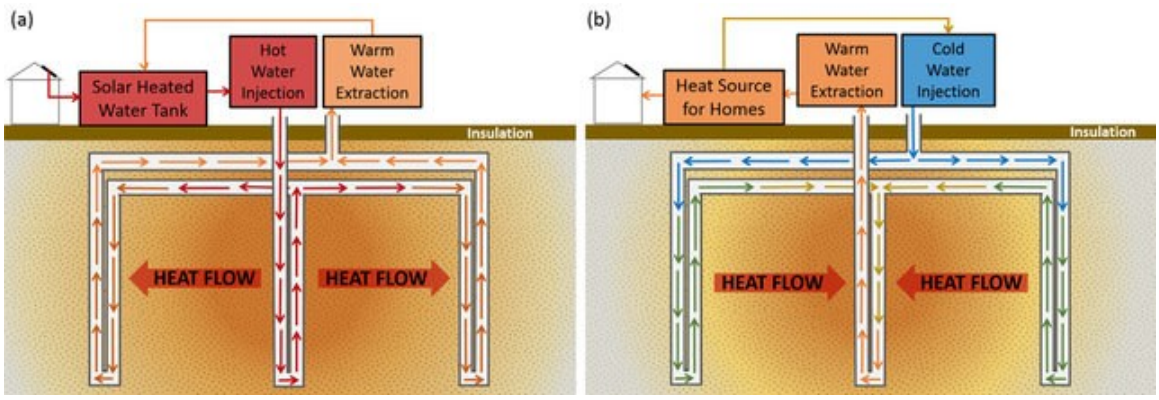

Figure 1.1 Simplified schematic of a borehole thermal energy storage system during (a) summer heat storage of solar energy and (b) winter heat extraction (Catolico et al., 2016).

The literature from the past two decades has demonstrated the feasibility of utilizing geothermal energy storage (GTES) systems for the heating of buildings in the cold climate region like Northern Quebec. The idea to couple a solar collector to the borehole heat exchanger, by means of which solar energy can be stored in the ground, was first proposed by Penrod in 1956. Then he extended this idea to storing solar thermal energy underground

(Penrod & Prasanna, 1962). Solar GTES is reported a viable choice for heating-dominated communities in the aspect of both working efficiency and economic assessment by previous researchers (Chiasson & Yavuzturk, 2003; Gunawan et al., 2020; Han et al., 2008; Yang et al., 2010). Gabrielsson et al. (2000) studied the economic performance and thermal influence on surroundings of a heat storage in clay. Groups of researchers have completed preliminary studies for evaluating the viability of shallow geothermal applications in Kuujjuaq (Miranda et al., 2017). However, the previous research focused on the feasibility of Borehole Thermal Energy Storage (BTES) systems in northern Quebec area only from the economic, working efficiency and environment aspect, lacking assessment on geotechnical influence in local geology, where glacial till is wide distributed.

The operation of a BTES system would lead to temperature evolution beyond natural seasonal variations and thermally induced pore pressure in surrounding soil, which may induce continuous ground deformation and result in unexpected accidents during the service period. This emphasizes the importance of estimating the geotechnical influence of a potential BTES system in cold region on soils surrounding the boreholes.

1.2 Objectives of the Current Study

This study investigates the effect of geothermal energy storage (GTES) systems of 50-year service life period on thermal consolidation of surrounding soil formations in northern Quebec, where GTES sites are covered by a large quantity of unconsolidated glacial tills.

To evaluate the potential influence of Borehole Thermal Energy Storage (BTES) systems on the surrounding soil at a site located in northern Quebec, a potential 50-year life-cycle Borehole Thermal Energy Storage (BTES) in glacial till is simulated in this study. Temperature variation and induced ground deformation are studied using ABAQUS software. The following three major objectives will be achieved through this study:

1) Collecting thermal-hydro-mechanical properties of glacial tills from the studying site at northern Quebec for numerical simulation.
2) Performing numerical analyses of glacial till consolidation behavior around a single borehole. Thermal-hydro-mechanical coupled responses of glacial till formations will be investigated. An elastoplastic model will be applied to quantify the deformation behavior of soil ground.
3) Performing numerical analyses of cases with borehole groups to investigate multiple borehole impacts.

1.3 Structure of thesis

This thesis has been prepared according to the guidelines of the Faculty of Graduate Studies at Concordia University. It is comprised of six chapters. The purpose of this work is to perform numerical modeling of thermally induced ground deformations around potential geothermal energy storage wells in northern Quebec. Chapter 1 introduces the background and brief content about thesis. Chapter 2 summarizes previous studies on geothermal energy storage systems, including borehole optimized configuration and

temperature evolution during service life period. Chapter 3 introduces the elastoplastic model (Modified Cam-Clay model) and governing equations for thermally induced poromechanical processes. Chapter 4 summarizes the mechanical properties of glacial till and gives the details of numerical modelling of soil responses surrounding a single thermal well. In chapter 5, numerical modellings of soil responses surrounding bore hole groups are studied. Conclusions and recommendations for further work are presented in chapter 6.

1.4 Original Contributions

Previous research did not pay enough attention on the feasibility of Borehole Thermal Energy Storage (BTES) systems in geotechnical aspect. The neglecting of assessment of geotechnical influence may results in severe structure failure in BTES systems. In this research, BTES systems of different scale built in glacial till in northern Quebec are simulated to study the potential impact of thermal operation on ground deformation behaviors.

2 Literature Review

The published research on underground Borehole Thermal Storage (BTES) systems, operation temperatures, and related boundary conditions are presented in this chapter. The summarized data will be used for the subsequent numerical modeling work.

2.1 Geothermal energy storage

Geothermal energy storage (GTES) in soils combined with solar energy collectors refers to systems that use buried devices designed to exchange heat with the surrounding ground. It consists of solar thermal collectors, water storage tanks, boreholes, storage space, water circulation loop. The GETS systems are typically categorized in four types: hot-water thermal storage, borehole thermal energy storage, aquifer thermal energy storage and water gravel pit storage. In a borehole thermal energy storage (BTES) system, vertical or horizontal pipes are inserted into the field for injecting or extracting the heat. BTES works in seasonal and periodic modes. In warm months, sufficient sunshine duration and intensity guarantee abundant supply of solar energy. After being heated in storage tanks by the solar energy harvested by solar collectors, water flows into underground along pipes. Water temperature decreases as it flows underground till water flows back to storage tanks. Consequently, heat energy transfers from water into surrounding soils steadily. In cold months, soils around geothermal energy storage systems are much warmer than atmosphere. Cold water is injected into underground to get heated by warm soils. Thermal energy

transfers from soils into running water. As a media, water brings thermal energy to local communities and then returns into underground to absorb heat energy during cold months.

The first community-scale borehole thermal energy storage (BTES) system in North American was installed in 2007 at the Drake Landing Solar Community (DLSC) in Okotoks, Alberta. Solar thermal energy is collected in the summer, stored underground, and then returned to the homes as heat during the winter. More than 90 percent of space heating needs for community's 52 single-detached homes is met by solar energy. There are five main components of the DLSC project: the solar collection, the Energy Centre with short-term energy storage, the seasonal Borehole Thermal Energy Storage (BTES) system, the district heating system, and the energy efficient homes certified to the R-2000 Standard.

For the borehole thermal energy storage (BTES) system, the ground is used as a heat storage medium. In this kind of systems, vertical or horizontal pipes are inserted into the field for injecting or extracting the heat. The depth depends on the heat load, ground temperature, thermal conductivities, and groundwater level. Comprehensively, borehole thermal energy storage (BTES) systems have some geological requirements: drillable ground (preferably groundwater), high heat capacity, high thermal conductivity and low hydraulic conductivity. Higher heat capacity permits more energy stored in a storage volume. High thermal conductivity adjacent to the boreholes guarantees the efficiency of heat transfer between circular fluid and storage medium. Lower hydraulic conductivity

causes less storage heat loss. The vertical boreholes are usually in the range of 30~200 m in depth with approximately 3~4 m separation (Rad et al., 2017; Shah et al., 2018).

Gunawan et al. (2020) pointed out that shallow geothermal energy is financially interesting option to northern communities like Kuujjuaq in Quebec, Canada. Technical viability of underground thermal energy storage in subarctic climates has been validated and such storage could help reduce fossil fuel consumption in remote arctic regions across the world (Giordano & Raymond, 2019). Inspired by this sustainable technology, this thesis is conducted on thermally induced ground deformations around potential geothermal energy storage wells in northern Quebec.

2.2 Borehole thermal energy storage systems and geotechnical engineering

Coupled thermal-hydro-mechanical modeling of a BTES system should focus on the key factors: storage temperature evolution, borehole dimension and array. A BTES system consists of energy collectors, water storage tanks, water circulation loop, boreholes, storage space. A thermal storage system is designed based on the heat demand, heat source availability and cost. The operation and design parameters are thermal storage temperature, heat loss, storage interval, and storage medium. The performances of BTES depends on its configuration such as single or double U-tube heat exchangers as well as the depth of borehole, heat conduction in the ground and heat convection inside the U-tube. In some BTES systems, the heat pumps are utilized to upgrade the low-grade heat to high-grade heat suitable for space heating (Shah et al., 2018). However, for coupled thermal-hydro-

mechanical modeling, excessive parameters are undesired. The whole simulation should be simplified to be boreholes with temperature change buried underground. Heat transfers continuously across the interface of soils and boreholes, inducing stress evolution and deformations in surrounding soils. Solar energy supply, heat loss or heat conducting efficiency are not included in this numerical modeling because previous research has proposed detailed storage temperature profiles based both field tests and simulations.

The storage temperature evolution directly determines to what degree the soils could be influenced. The depth and area of borehole groups directly determine the volume of the influenced zone.

2.2.1 Borehole dimension and storage scale

In a BTES system, the part that directly exchanges heat with the soil is the borehole. In heat injection phase, warm fluid heated by solar energy flows into boreholes through heat exchanger tube, bringing heat energy to surrounding soil because of the temperature gradient between soil and fluid. Accordingly, heat energy is continuously stored, and soil is continuously heated in storage. In heat extraction phase, heat energy transfers from heated soil to cold fluid. As the fact that the outside surface of boreholes contacts soils directly, the temperature of outside surface of boreholes and that of the soil immediately adjacent to the borehole should be nearly identical.

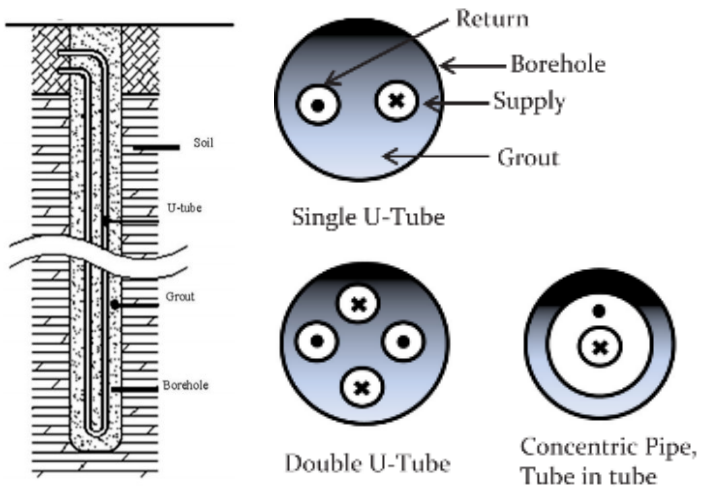

Figure 2.1 Schematic of a vertical borehole (after Shah et al., 2018).

Boreholes come in a variety of sizes, with diameters in a range of serval tens to hundred millimeters. In the vertical borehole thermal energy storage (BTES) systems, the ground heat exchanger (GHE) configurations may include one, tens, or even hundreds of boreholes, each containing one or double U-tubes through which heat exchange fluid is circulated. Typical U-tubes have a diameter in the range of 19–38 mm and each borehole is normally 20–200 m deep with a diameter ranging from 100 mm to 200 mm (Yang et al., 2010). The design of boreholes has been studied lately.

The dimension of boreholes and storage scale of BTES systems from the world or from simulation models are listed in Table 2.1. The summarized information about the number, depth, diameter, and spacing distance of boreholes in BTES system is consistent with Rad et al., (2017) and Yang et al. (2010).

Table 2.1 The characteristic of BTES systems (after Baser & McCartney, 2015; Gabrielsson et al., 2000; Giordano & Raymond, 2019; Lanini et al., 2014; Pahud, 2000; Rad et al., 2017; Reuss et al., 1997; Shah et al., 2018).

	Location		Number of boreholes	Depth, m	Diameter, mm	Spacing, m	Storage shape	Shape factor	Reference
Single U-tube	Quebec, Kuujjuaq, 2019	TRNSYS & FEFLOW model	50/100/150	30	-	1.9-4.1		0.8-1.5	(Giordano & Raymond, 2019)
Single U-tube	Sweden, Linköping, 1992	test field	120	10	-	1.0/2.0	Square		(Gabrielsson et al., 2000)
double U-tube	Switzerland	TRNSYS model	-	-	115	2.0-3.0	Cylinder		(Pahud, 2000)
	Germany	laboratory experiment, test field	140	30	100-150	2	Square		(Reuss et al., 1997)
	Canada		90	59	-	3	Circular		(Reuss et al., 1997)
	Canada, DLSC, 2007		144	35	-	3	Octangular		(DLSC)
Single U-tube	Corolado School of Mines Campus	COMSOL model, test field	5	10	140	1.0/2.0/2.5			(Baser & McCartney, 2015)
	Denmark, Braedstrup		50	47-50					
			3	180	160	5			(Lanini et al., 2014)
double U-tube	France		2	90					(Shah et al., 2018)
	Sweden, Anneberg, 2002		99	65	115				
	Germany, Neckarsulm, 1999			30-100	150				
	Germany, Crailsheim, 2007		80	55					
	Australia, University of Melbourne		2	40	115	3			
	French, Eastern pyrences		3	180					
	China, Tianjin		8	12					
	China, Tianjin, 2007		1	50	220				
	Sweden, Anneberg		100	65					
	Six climate zone		4	50	140				
Single U-tube	China, Harbin		12	50					
	Canada, kotos		144	35	150				
	Germany, Attenkirchen, 2002		140	30					
	China, Shijiazhuang, 2011		5	21					
	Turkey, Erzurum, 2008-09		2	53	200				
	China, Harbin		12	50	76				
	China, Harbin, 2008	Numerical modeling	3	60	40				
	China, Qingdao, 2011			55	110				
	Sweden, Stockholm, 2009		1	60-250					
	China, Tianjin, 2012		25	50					
	Turkey, Izmir, 2003-2005		1	50	105				
	China, Tianjin		580	120					

The depth and diameter of boreholes and distance between boreholes differs from case to case. In this study, the diameter of a single borehole is designed as 160 mm.

Baser and McCartney (2015) and Lanini et al. (2014) studied the effect of depth and spacing room of boreholes on storage system. Depth of boreholes has an affect on the efficiency of heat injection and heat extraction (Lanini et al., 2014). The energy storage is based on the heat transfer fluid (HTF). HTF flows in the loop, taking heat energy from heat temperature section to low temperature section. Heat loss is common in such a loop system, and it increases with the length of loop. If the loop is too short, the heat energy in fluid may not sufficiently be transferred into storage. Too short or too long will reduce the efficiency of storing heat energy. It is recommended by Lanini et al. (2014) that, the depth of boreholes should not exceed 100m. There are serval BTES systems with a diameter of around 50 meters in Table 2.1. In this study, the depth of borehole is designed as 35 m.

The depth and number of boreholes are also dependent on the local geology formation and energy demand. As a preliminary work, the glacial till is assumed to be distributed approximately 40 meters from the ground surface based on other research (Giordano et al., 2017; Rosenberg & Journeaux, 1978; St-Amour et al., 2017; Thomson et al., 1982). The bedrock lies beneath the glacial till. Boreholes in this study are supposed to be less than 40 meters considering highly construction cost for drilling on bedrock. The depth of 35 meters is in good agreement in the work conducted in Kuujjuaq by Giordano

and Raymond (2019). They discussed kinds of borehole configuration with depth of 30 meters in their research.

Heat demand of consumers determines the scale of Borehole Thermal Energy Storage (BTES) system. Three different-scale BTES systems are studied in this paper, they are single borehole system, five-borehole system, and 100-borehole system. Spacing room of five-borehole system and 100-borehole system are referred to the work by Baser and McCartney (2015) and Giordano and Raymond (2019). To study the deformations of surrounding glacial till, the entire thermally influenced zone must be included in the ABAQUS model. For single borehole system, a cylinder volume with a diameter of 40 meters is considered. For 100-borehole system, the simulated diameter is expanded to 400 meters. It is found that severe deformation would happen in multi-borehole systems.

2.2.2 Temperature evolution

Building a Borehole Thermal Energy Storage (BTES) system in cold region like northern Quebec results in periodical ground temperature change. In warm seasons, thermal energy is collected, transferred and stored in ground, leading to underground temperature increase. In actual scenarios, thermal energy injection is discontinuous because solar energy cannot be collected at night or on days without the sun. However, in the long run, the temperature evolution shows a trend of continuous increase in energy injection period. In cold seasons, heat energy is extracted from the ground, leading to the underground temperature decrease.

Given that precious research on BTES systems has provided sufficient knowledge on the storage temperature evolution. Instead of defining heat flux on the interface between boreholes and soil, directly defining temperature evolution on the interface is adopted in this study. As a result, boreholes in storage are regarded as heat source with continuous temperature evolution. Heat transfers continuously between boreholes and surrounding soil due to the temperature gradient. The benefit is focusing on the heat transferring between boreholes and soil and avoiding the heat transferring between boreholes and fluid, between fluid and solar collectors.

It is defined in this study that the temperature on the interface rises from undisturbed value to the highest at a varying rate during heat injection period and decreases to the lowest value at a changing rate due to heat consumption of local community in heat extraction phase. The highest temperature on the interface can be reached in the system depends on the solar energy collected. The lowest temperature after extraction period depends on user consumption. In this study, it is assumed that: 1, the stored energy is the same for every year. 2, the stored energy can be used up exactly in every service circle. That is to say, the temperature evolution on the interface in such BTES system is a perfectly periodic curve.

During thermal operations, thermally induced pore pressure can be developed in the till formation around boreholes and thermal pore pressure may lead to plastic yielding in the till. Storage temperature evolution is closely related to thermally induced pore

pressure. Heat escaping from boreholes gives rise to a gradual increase of the temperature in the surrounding ground. The magnitude of thermally induced excess pore water pressure in the thermally influenced zone significantly depends on the rate of the temperature increase, the maximum temperature level in the soil (Gabrielsson et al., 2000). To study the ground deformations, a reasonable temperature evolution rule (extreme value, evolution rate, and period) is crucial in simulation.

Initial underground temperature: 1°C

Before thermal operations, underground temperature is stable over seasons. Previous research has revealed the underground temperature in northern Quebec.

Raymond and his team conducted detailed geological investigation in Kuujjuaq (Giordano et al., 2017; Kanzari, 2019; Miranda et al., 2017, 2018). The results of ERT surveys include local underground temperature profile, geological section, thermal properties. Temperature-depth profile measured in wells W19, W18 and W16, which locate in Core Zone of Southeastern Churchill Province, Quebec, indicates the subsurface temperature varies within a narrow range from surficial to the depth of around 100 meters: 0.5°C – 1.75°C for W19, 0°C – 1.5°C for W18, 1°C – 1.5°C for W16 (Figure 2.2). Results from two other sites, to southwest of Kuujjuaq, are provided in Miranda et al. (2017). A slightly higher underground temperature is reported: 1.5°C – 2.5°C at depth within 120 meters.

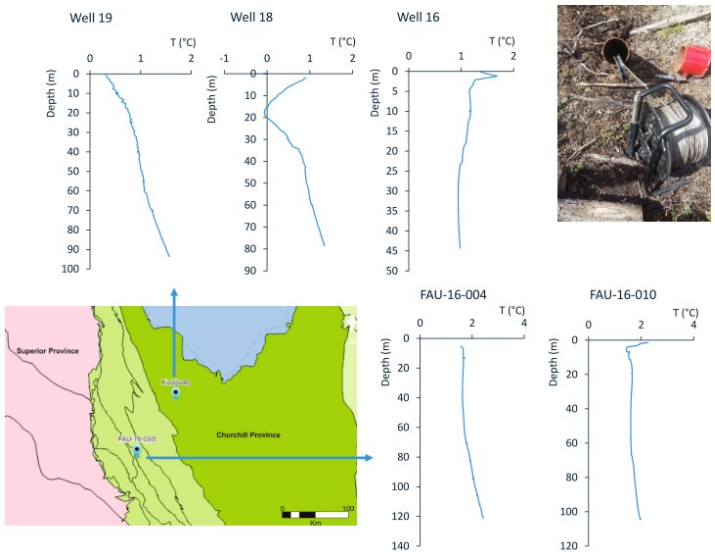

Figure 2.2 Temperature-depth profile at five sites (Miranda et al., 2017).

The data of ground temperature at depths within 0 – 2.4 meters in Kangiqsualujjuaq in 1998 reveals temperature perturbation caused by an annual cycle was significant within 0 – 1 m (Belzile et al., 2017). At the depth of 2.4 meters, despite the temporary decline in 3 months, the ground temperature almost kept unchanged at 0°C (Figure 2.3).

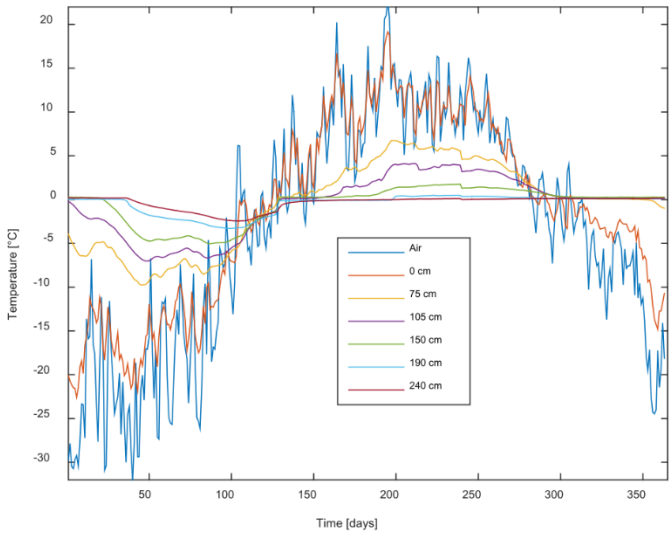

Figure 2.3 Ground temperature at different depths measured in 1998 at KANGTMA in Kangiqsualujjuaq (Belzile et al., 2017).

Considering the narrow underground temperature range from surficial to 100 meters depth and the fact that temperatures below a certain depth show little seasonal variation, a constant undisturbed temperature was set for the simulated formation in this study. Although the underground temperature profile differs from places, a preliminary assumed value is 1°C.

A temperature-depth profile near a road embankment at Umiujaq in Nunavik was reported by Fortier et al. (2011) when studying the permafrost degradation. The results of a piezocone test carried out in the field in July 2008 shows the underground temperature below 4 meters is 2°C. And the undisturbed temperature would be slightly lower. The assumed underground temperature (1°C) in ABAQUS simulation is in good consistent with the field measurement in Kuujjuaq, Kangiqsualujjuaq and Umiujaq.

The rate of temperature change of soil adjacent to the borehole: sinusoidal

With the operation of geothermal storage system, continuous underground temperature change will happen in surrounding glacial till. Such change depends on the amount of injected heat energy and the consumption of local community. Rapid underground temperature evolution would happen in the vicinity of boreholes when the temperature gradient between circular fluid and adjacent till is high. For instance, solar radiation is high in the middle of heat injection stage, thus the circular fluid will reach a high temperature, bringing abundant heat energy into underground. As a result, the underground temperature in the vicinity of boreholes rises more rapidly than lower solar

radiation scenarios. Similarly, the underground temperature falls at a high rate in the middle of the heat extraction phase. Besides, the underground temperature reaches annual peak after heat injection phase, while the circular fluid temperature becomes cold in the heat extraction phase. Accordingly, high temperature gradient at the early stage of heat injection and heat extraction period would also induce rapid underground temperature evolution.

While the problem remained is to quantify the rate of evolution. Evolution rate is crucial to study the thermally induced pore pressure. A steep rate means a dramatic pore pressure evolution.

The general approach is to consider the evolution of underground temperature as periodic (Gabrielsson et al., 1997, 2000; Giordano & Raymond, 2019; Pahud, 2000; Rad et al., 2017; Reuss et al., 1997; Sibbitt et al., 2012; Sweet & McLeskey, 2012).

Giordano and Raymond (2019) calculated the subsurface temperature in the centre of storage, which locates at Kuujjuaq, using TRNSYS and subsurface temperature at different distance to centre at 15 meters depth using FEFLOW in their study. Specifically, the rate of temperature evolution is fast at the early stage and keeps decreasing at the rest of heat injection and extraction phases. A maximum temperature increment of over 30°C is reported.

They set the total injected energy as between 604.2 to 1328.5 GJ for different models. The existence of heat loss was taken into account. It was found that core temperature was different for every model. The smaller the storage volume, the higher the

core temperature. And models in underground without groundwater flow can reach higher temperature than those with groundwater flow. Among these models, a highest temperature of over 30°C was found for SC3. And the evolution is similar to a sinusoidal rule. Besides, the observation points at different distance from center at 15 meters depth in FEFLOW simulation reveal the existence of temperature gradient between central boreholes and boreholes on borders when there is groundwater flow. A maximum of 10°C is found in circular-shaped model, while 2°C in square-shaped storage.

In addition, the measured and calculated mean store temperatures evolution over six temperature cycles at the SGI test field showed an approximate sinusoidal rule (Gabrielsson et al., 2000 and Gabrielsson et al., 1997).

Pahud (2000) reported the temperature evolution of ground duct store (borehole) for a single year in the operation period. A similar is reported by Sweet and McLeskey (2012). Both results are in good agreement with sinusoidal rule.

Sibbitt et al. (2012) used TRNSYS model to simulate DLSC. They found the calculated core temperature cycled over 5 years of operation, with an increasing trend. Same rule is also observed in Rad et al. (2017); Reuss et al. (1997). Regardless of the increasing trend over years, a perfect sinusoidal rule is reasonable for a system where consumption is equal to injection.

Gabrielsson et al. (1997, 2000) investigated the thermal effects on clayey soils and surrounding soft clay at the SGI test field. It is a square-shaped storage, with boreholes of

depth of 10 meters and top insulated. Both measured and calculated underground temperatures at different observation points over several years were reported. It was reported that underground temperature fluctuated with an increasing trend before equilibrium with the operation. They also estimated the settlement in soft clay using empirical calculation model without counting thermal expansion and contraction and then predicted the development of real settlements.

Pahud, (2000) carried out an integrated simulation on a central solar heating plant with seasonal ground storage. It is a vertical cylindrical storage with boreholes of diameter of 0.115 m and top insulated. A sinusoidal evolution rule was reported for the duct store (borehole) temperature for the 12^{th} year of operation. From early June to late September, corresponding to the "Summer" mode, the borehole temperature rises continuously. From early December to late February, corresponding to the "winter" mode, the borehole temperature drops continuously. In two transition periods, the operation strategy of the system would influence the thermal performances. Based on their setting, the borehole temperature evolved at a slow rate during these two transition periods.

In the study by Sweet and McLeskey (2012), a TRNSYS model is used to simulate underground Seasonal Solar Thermal Energy Storage for a single family dwelling in their research. Among the results, the bed temperature profile of one model shows a sinusoidal rule.

Reuss et al. (1997) study an underground storage with 140 heat exchangers, borehole spacing of 2 meters and depth of 30 meters. Calculation based on the boundary conditions that fluid inlet temperature will not exceed 80°C and outlet temperature will not decrease below 35°C revealed mean ground temperature fluctuated with rising trend before it reached equilibrium in the first 10 years. It was highlighted in their research that thermal properties are strongly dependent on the temperature.

Sibbitt et al. (2012) used TRNSYS model to simulate DLSC. They found the calculated core temperature cycled over 5 years of operation, with an increasing trend.

In Rad et al. (2017), based on the DLSC, a new storage with different borehole layout is designed and simulated using TRNSYS. The average ground temperature cycled over 5 years with an increasing trend. After two years, the annual temperature profile was nearly the same.

Based on above information, a sinusoidal rule is adopted to define the temperature evolution on the interface of boreholes and soil in this study. A perfect temperature evolution rule during a service process means energy equilibrium between heat injection and heat extraction. Under the perfect temperature evolution rule, the temperature, also the energy, at the end of discharge period is equal to that at the beginning of charge period. It is assumed there will be no accumulated heat in the boreholes.

Operation period

The thermal operations of BTES systems are divided into two modes: heat injection phase and heat extraction phase. Generally speaking, BTES systems are in heat injection phase only in warm seasons where solar energy is sufficient and in heat extraction phase in cold seasons where heat demand is huge. Various settings are shown in Table 2.2. However, it can be concluded that each phase takes half a year. Such, the heat injection period is 15,768,000 seconds, and the heat extraction period is also 15,768,000 seconds every year.

Table 2.2 Period of heat injection and extraction phase.

Charing period/summer mode/heat injection	**Discharging period/winter mode/ heat extraction**	**Reference**
April to September	October to March	(Giordano & Raymond, 2019)
Mid April to Mid August (4 months)	Mid August to February (6 months)	(Gabrielsson et al., 1997, 2000)
March to October	October to March	(Reuss et al., 1997)
Early June to late September	Early December to late February	(Pahud, 2000)
May to August	September to March	(Sweet & McLeskey, 2012)
March to late September	October to late February	(Sibbitt et al., 2012)
April to Mid October	Mid October to the end of March	(Rad et al., 2017)
6 months	6 months	(Lanini et al., 2014)
March to August	September to February	(Catolico et al., 2016)

Highest temperature evolution

The climate data for a site in Northern Quebec is shown in Table 2.3. Built in a subarctic area, the storage temperature is difficult to reach a high value. The highest storage temperature is set as around 30°C in this study, which is consistent with Giordano and Raymond (2019).

Table 2.3 Climate data in Kuujjuaq.

Month	Jan	Feb	Mar	Apr	May	Jun	Jul	Aug	Sep	Oct	Nov	Dec
Average high °C	-19	-18	-12	-3	5	13	18	16	10	3	-4	-14
Average low °C	-28	-28	-23	-14	-4	2	6	6	2	-3	-11	-22

Actually, the exact highest temperature is designed according to the demand. By optimizing system and reducing heat loss, for example, modifying the borehole spacing, storage shape, borehole connections, insulation, a higher borehole temperature could be reached. Thus, an extreme value of 60°C is considered in this study. In this case, violent pore pressure evolution and severe deformation are likely to happen. A higher temperature is not discussed because a huge change in thermal properties may occur for glacial till beyond 60°C (as cited in Reuss et al., 1997). Although there are storages with highest temperature of over 90°C in other places, such a high underground temperature is difficult to obtain considering the Latitude and geological situation in northern Quebec. Besides, such a high temperature may induce severe ecological impact.

In the situation where extracted energy is less than injected energy, the thermally influenced zone would expand and temperature would stack year by year. In this study, a

conservative assumption is applied: the underground temperature of till adjacent to boreholes would fall back to initial temperature after each cycle.

Fluid temperature is highest before flow into boreholes but decreases gradually as flowing path in boreholes increases. In this study, a relatively small temperature gradient, 5°C, between central boreholes and boreholes at borders are set.

2.3 Summary

In BTES systems, heat energy transfers from circular fluid into surrounding soil through boreholes. The interfaces between boreholes and surrounding soil are well analyzed.

The dimension of boreholes, including depth, diameter and space room, is designed in good agreement with previous work. Three BTES systems in different scales are studied: single borehole system, 5-borehole system, and 100-borehole system. For 100-borehole system, three groups are designed according to different space room.

The temperature evolution on the interfaces between boreholes and surrounding soil is input, instead of heat flux. A practical temperature evolution rule contributes to an accurate result. To describe the evolution rule, three parameters (extreme value, evolution rate, and period) are crucial.

The temperature of ground soil under a certain depth is stable seasonably in northern Quebec. From surficial to the depth of 40 meters, the ground temperature is close

to 1°C. Considering the local solar energy, highest storage temperature is set as around 30°C. In addition, groups of 60°C are studied in consideration of extreme scenarios. In this study, temperature evolution is assumed as sinusoidal. Natural ground temperature is set as 1°C along the whole depth for the whole year. Heat injection and heat extraction phase both take 1,5768,000 seconds in a single year. While, for specific energy supplication and community consumption, a practical temperature evolution rule and period can be designed.

Table 2.4 Group setting in the research.

Group		Boreholes	Space room	Highest temperature
Model 1	a	1	-	30°C
	b	1	-	60°C
Model 2	a	5	2	30°C
	b	5	2	60°C
Model 3	a	100	1.9	35°C
	b	100	1.9	60°C
Model 4		100	3.8	30°C
Model 5		100	2.9	30°C

3 Governing equations and constitutive models

3.1 Governing equations for thermal-hydro-mechanical coupled processes

Thermal-hydro-mechanical (THM) coupled numerical modeling is needed to carry out the geomechanical analysis of BTES operations in a soil ground. We will highlight the poromechanical governing equations herein. We neglect the complicated multiphase flow equations of air and water in porous media herein. In addition, thermal convection is ignored in the current formulation. According to Lewis et al. (1986), the governing equation can be formulated as:

$$\begin{cases} \mathbf{L}^T\boldsymbol{\sigma} + \rho\mathbf{g} = 0 \\ -\nabla^T\left\{\dfrac{\mathbf{k}}{\mu}\nabla\left(p+\rho_w g z\right)\right\} + \mathbf{m}\dfrac{\partial\boldsymbol{\varepsilon}}{\partial t} - \phi\beta_w\dfrac{\partial T}{\partial t} - \left(1-\phi\right)\beta_s\dfrac{\partial T}{\partial t} + \dfrac{\partial Q_e}{\partial t} = 0 \\ \left[\left(1-\phi\right)\rho_s C_s + \phi\rho_w C_w\right]\dfrac{\partial T}{\partial t} - \nabla^T\lambda\nabla^T - \dfrac{\partial Q_h}{\partial t} = 0 \end{cases} \tag{3.1}$$

where $\boldsymbol{\sigma}$ is the total stress tensor; $\mathbf{L}$ is the differential operator; $\mathbf{k}$ and μ are permeability matrix and viscosity of the total fluid phase, respectively. ϕ is the porosity. β_w and β_s are pressure and thermal expansion coefficient of water and solid, respectively. $\boldsymbol{\varepsilon}$ is the rock's strain, and $\mathbf{m} = \left[1,1,1,0,0,0\right]^T$. λ is the thermal conductivity. C_s and C_w are the heat capacities of the solid phase and the fluid phase, respectively. Q_e is the volumetric outflow of the fluid per unit volume of the solid. Q_h is the outflow of heat per unit volume of solid. Eq. (3.1) describes a coupled THM process and convection is not considered in the thermal transport equation. The thermal transport is decoupled from Eq. (3.1) by

considering the assumptions: (1) The thermal convection effects can be ignored during the mechanical failure of geomaterials; (2) The fluid flow and mechanical deformation do not change the thermal properties. Thus, Eq. (3.1) can be simplified to two equation systems: the fully coupled Biot consolidation problem and the thermal conduction problem. ABAQUS can be applied to conduct finite element analysis considering above mentioned THM coupled process.

3.2 Elastoplastic model

The elastoplastic model used in this study is Modified Cam-Clay model. Plasticity theory was originally developed to predict the behavior of metals subjected to loads exceeding their elastic limits. Similar models were developed lately to calculate the irreversible strains in concrete, soils, and polymers. It is customary in plasticity theory to decompose strains into elastic and plastic part. A plasticity model includes (1) a yield criterion that predicts whether the material should respond elastically or plastically due to a loading increment, (2) a strain hardening rule that controls the shape of the stress-strain response during plastic straining, and (3) a plastic flow rule that determines the direction of the plastic strain increment caused by a stress increment.

The Cam-Clay model, one of the representative elastoplastic models, was developed in Cambridge by Roscoe and Schofield. This constitutive model can properly simulate triaxial test on sand and normal consolidated clays, but it cannot cope with the softening behaviour of over-consolidated clay. Therefore, the Cam-Clay model was

extended using critical state theory (Schofield and Worth, 1968), commonly known as the Modified Cam-Clay model (Roscoe & Burland, 1968), in which one elliptical yield surface is defined for both shear and compressive failure (see $p-q$ diagram in Figure 3.1). Both the Cam-Clay and Modified Cam-Clay models can describe the stress-strain behavior of soils; in particular, the models can predict the pressure-dependent soil strength and the compression and dilatancy (volume change) caused by shearing. Because the models are based on critical-state theory, it predicts unlimited soil deformations without changes in stress or volume when the critical state is reached.

Soil is composed of solids, liquids, and gases. The Cam-Clay model assumes that the voids between the solid particles are filled only with water. When the soil is loaded, significant irreversible (plastic) volume changes occur, due to the water that is expelled from the voids. Realistic prediction of these deformations is crucial for many geotechnical engineering problems. Formulations of the Modified Cam-Clay model are based on plasticity theory, through which it is possible to predict realistically volume changes due to various types of loading.

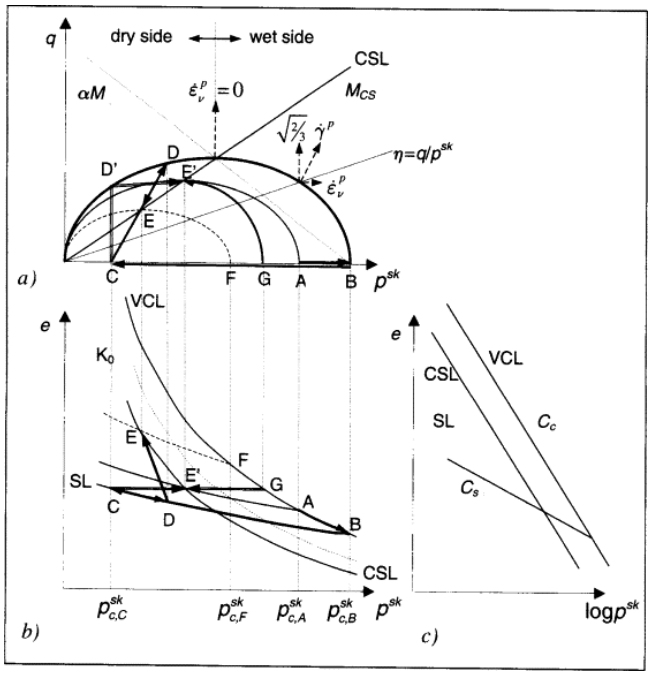

Figure 3.1 Modified Cam-Clay model (Winterwerp & Kesteren, 2004).

Yield surface

In the $p-q$ plane (mean stress-Mises equivalent shear stress), the Modified Cam-Clay yield surface is an ellipse given by

$$\frac{q^2}{p'^2} + M^2\left(1 - \frac{p_c'}{p'}\right) = 0 \tag{3.2}$$

Hardening and softening behavior

OCR: normally consolidated and lightly overconsolidated soil (OCR < 2); overconsolidated soil. Consider a soil specimen that is isotropically consolidated to a mean effective stress p_c' and then is unloaded slightly to p_0', as shown in Figure 3.2. The soil is lightly overconsolidated with OCR < 2. The effective stress path touches the initial yield surface to the right of the point at which the CSL intersects the yield surface, hardening behavior, accompanied by compression, will occur. During shearing, the specimen sustains

only elastic strains within the initial yield surface. When the stress state of the soil specimen touches the yield surface, the specimen will sustain plastic strains as well as elastic strains. The yield surface will expand (hardening), causing further plastic strains, until the stress state of specimen touches the critical state line, where failure occurs; the soil will continue to distort without change in shear stress or volume.

Consider another soil specimen that is isotropically consolidated to a mean effective stress $p_c^{'}$ and then is unloaded slightly to $p_0^{'}$ such that the specimen is heavily oveconsolidated (OCR > 2), as shown in Figure 3.3. The effective stress path traverses the critical state line before touching the initial yield surface and without causing failure in the soil specimen elastic behavior. When the effective stress path touches the yield surface, the yield surface will contract (softening), causing further plastic strains, until the stress state of the specimen touches the critical state line, where failure occurs.

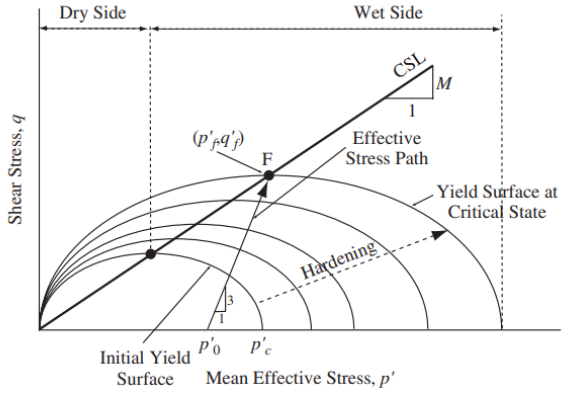

Figure 3.2 Modified Cam-Clay hardening behavior: evolution of a yield surface during hardening (Abaqus, 2016).

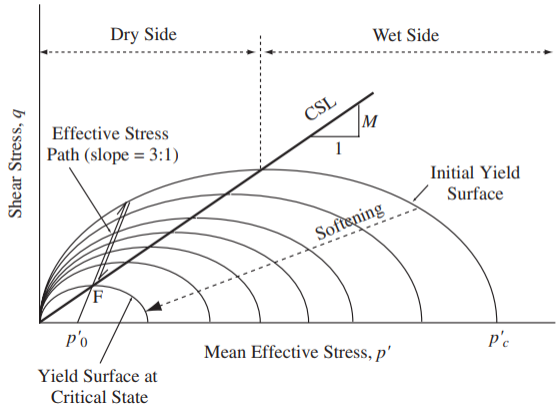

Figure 3.3 Modified Cam-Clay softening behavior: evolution of a yield surface during softening (Abaqus, 2016).

There are two ways to define hardening law in ABAQUS:

1. Exponential form

$$a = a_0 \exp[(1+e_0)\frac{1-J^{pl}}{\lambda-\kappa J^{pl}}] \tag{3.3}$$

where J^{pl} is the plastic part of rate of volumetric change, e_0 is initial void ratio, λ is the slope of normally consolidation line (NCL) in $e-\ln p'$ plane, κ is the slope of unloading-reloading line in the $e-\ln p'$ plane. As plastic volumetric strain $\varepsilon_{vol}^{pl} = \ln J^{pl}$, above function can be write as $a = a_0 \exp[-\frac{1+e_0}{\lambda-\kappa}\varepsilon_{vol}^{pl}]$ for small strain cases.

2. Piecewise linear form: by listing data of p_c and plastic volumetric strain (ε_{vol}^{pl}).

Flow rule

A plastic potential is often defined in principal stress space and then the plastic strain increment vector is normal to this surface. If the plastic potential is the same as the yield surface, the material is said to have an associated flow rule. In CCM, the plastic flow

is defined by a flow potential that is identical to the yield surface (i.e. associated flow). Associated plastic flow rule given by Roscoe and Burland (1968):

$$\frac{d\varepsilon_v^p}{d\varepsilon_s^p} = \frac{M^2 - \eta^2}{2\eta} \tag{3.4}$$

Define initial yield surface size

a_0 shows the initial yield surface size, it can be defined directly or indirectly by giving initial void ratio and analytical expression:

$$a_0 = \frac{1}{2}\exp\left(\frac{e_1 - e_0 - \kappa \ln p'_0}{\lambda - \kappa}\right) \tag{3.5}$$

where, e_1 is the intercept of normally consolidation line (NCL) at $\ln p' = 0$ in $e - \ln p'$ plot, p'_0 is initial mean effective stress.

3.3 Define Modified Cam-Clay model in ABAQUS

Summary of Modified Cam-Clay model parameters

Slope M of the critical state line (CSL) The slope M of the critical state line in the $p' - q$ plane can be calculated from the internal friction angle φ' obtained from triaxial tests results at failure:

$$M = \frac{6\sin\phi'}{3 - \sin\phi'} \tag{3.6}$$

λ and κ slope λ and κ of the normally consolidation and unloading-reloading lines in the $e - \ln p'$ plane are related to the compression index C_c and swelling index C_s obtained from an isotropic consolidation test:

$$\lambda = \frac{C_c}{\ln 10} = \frac{C_c}{2.3} \text{ and } \kappa = \frac{C_c}{\ln 10} = \frac{C_c}{2.3}$$

Define Modified Cam-Clay model

Modified Cam-Clay model can be defined in both ABAQUS/Standard and ABAQUS/Explicit. The parameters needed are listed in Table 3.1.To adapt the Modified Cam-Clay model in Abaqus correctly, it's essential to understand the Extended Cam-Clay model. The Modified Cam-Clay model is a special case of the Extended Cam-Clay model. The Extended Cam-Clay model yield surface, in a three-dimensional yield surface, is given by the function:

$$f(p,q,r) = \frac{1}{\beta^2}\left(\frac{p}{a} - 1\right)^2 + \left(\frac{t}{Ma}\right)^2 - 1 = 0 \tag{3.7}$$

where $p = \frac{J_1}{3} = \frac{\sigma_1 + \sigma_2 + \sigma_3}{3}$

$$q = \sqrt{3J_{2D}} = \sqrt{3(J_2 - \frac{J_1^2}{6})} = \sqrt{\frac{1}{2}[(\sigma_1 - \sigma_2)^2 + (\sigma_1 - \sigma_3)^2 + (\sigma_2 - \sigma_3)^2]}$$

$$r = (\frac{27}{2}J_{3D})^{1/3} = (\frac{27}{2}J_3 - 9J_1J_2 + J_1^3)^{1/3}$$

$$t = \frac{q}{2}[1 + \frac{1}{K} - (1 - \frac{1}{K}(\frac{r}{q})^3)]$$

$$g = \frac{2K}{1 + K + (1 - K)\left(r/q\right)^3}$$

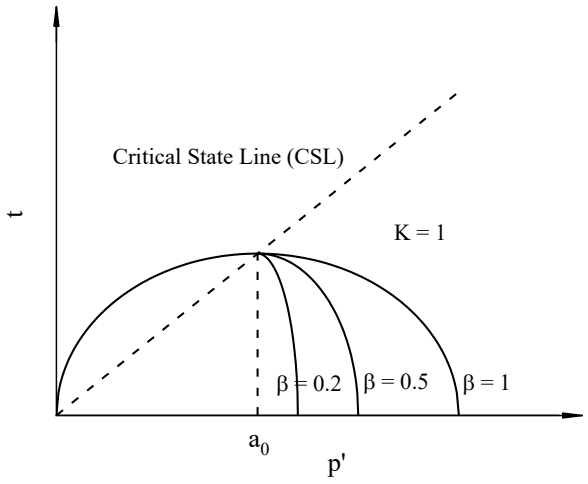

Figure 3.4 Extended Cam-Clay yield surface in the $p-t$ plane (after Abaqus, 2016).

The Modified Cam-Clay yield surface is an ellipse in $p'-q$ space. While the Extended Cam-Clay yield surface consists of two elliptical arcs in $p'-t$, where t is a measure of shear stress related to q as $t = q/g$. g is a function used to control the shape of the yield surface in the Π-plane. K is the ratio of the flow stress in triaxial tension to the flow stress in triaxial compression and determines the shape of the yield surface in the plane of principal deviatoric stresses. In Modified Cam-Clay model, $K = 1$, where the yield surface is independent to the third stress invariant, and the Π-plane section of the yield surface is a circle: this choice gives the original form of the Cam-Clay model. $K = 1 \rightarrow g = 1 \rightarrow t = q$, comprehensively, the Modified Cam-Clay model is a special case of the Extended Cam-Clay model (Abaqus, 2016).

M is the slope of the critical state line (CSL) in $p-q$ space. In the Extended Cam-Clay model, β is a constant used to modify the shape of the yield surface on the "wet" side of the critical state; $\beta = 1$ can be used on the "dry" side of the critical state, and $\beta < 1$

can be used in the most cases on the “wet” side to make the curvature of the elliptic arc on the wet side different from that on the dry side. In the Modified Cam-Clay model, β is always equal to 1. a_0 is a hardening parameter defined as the point on the p -axis at which the evolving elliptic arcs of the yield surface intersect the critical-state line. a_0 is related to β as $a_0 = p_c / (1+\beta)$, when β =1, $a_0 = p_c / 2$.

Table 3.1 List of parameters for define Modified Cam-Clay model in Abaqus.

Parameters	λ	M	a_0	β	K
Value	-	-	$p_c / 2$	1	1

4 Numerical modeling of soil responses surrounding a single thermal well

4.1 Geological and geotechnical characterizations

In this section, the author summarized the extensive existence of glacial till in Canada, especially in Northern Quebec, geological conditions and the fact that glacial till is widely used as construction material. Glacial till has good characteristics and is adorable material for BTES storage medium.

4.1.1 Geology

Glacial till distributes wide through Canada, especially in northern Quebec region. In Kuujjuaq, the unconsolidated deposits above the bedrock are coastal and pre-coastal marine sediments, alluvial deposits from ancient river terraces and glacial tills reworked into continuous cover (Kanzari, 2019). Figure 4.1 shows the map of unconsolidated deposits in Kuujjuaq. Maps of eastern coast of Hudson Bay shows a large-scale of glacial landforms between Kuujjuaraapik and Puvirnituq (Lajeunesse, 2008).

Glacial deposits, both basal till and ablation till, account for 29% of the total land surface in the region of Narsajuaq river valley, Nunavik (Gagnon & Allard, 2020). It is also reported in their research that that Basal till could reach depths of exceeding 10 m before reaching the bedrock. Basal till consists of diamicton dominated by sand (21%–28%

gravel, 43%–50% sand, 26%–31% silt) with scattered boulders. Ablation till consists of very coarse gravel, cobbles, and large boulders scattered over the bedrock in local region.

In the James Bay region, deposits of glacial and glaciofluvial origin cover most of the region (Pare et al., 1978; Paré et al., 1983). Till, consisting generally of nonplastic silty sand and gravel, is widespread in the form of ground moraine, locally including some drumlin deposits in that region.

It is reported by Liang et al. (2019) that, glacial till deposits in the Greater Toronto Area (GTA) usually comprise fine-grained (clay and silt) and coarse-grained (sand, gravel, cobbles, and boulders) fractions, which are substantially heterogeneous in characteristics. The glacial till found at the O'Conner Station site varies, from having some sand to being sandy, and having trace to some gravel. Generally, they considered the glacial till there as a fine-grained soil.

Based on literatures (Gunawan et al., 2020; Klohn, 1965; Rosenberg & Journeaux, 1978; St-Amour et al., 2017; Thomson et al., 1982), glacial till distributes within tens to a hundred meters in Canada.

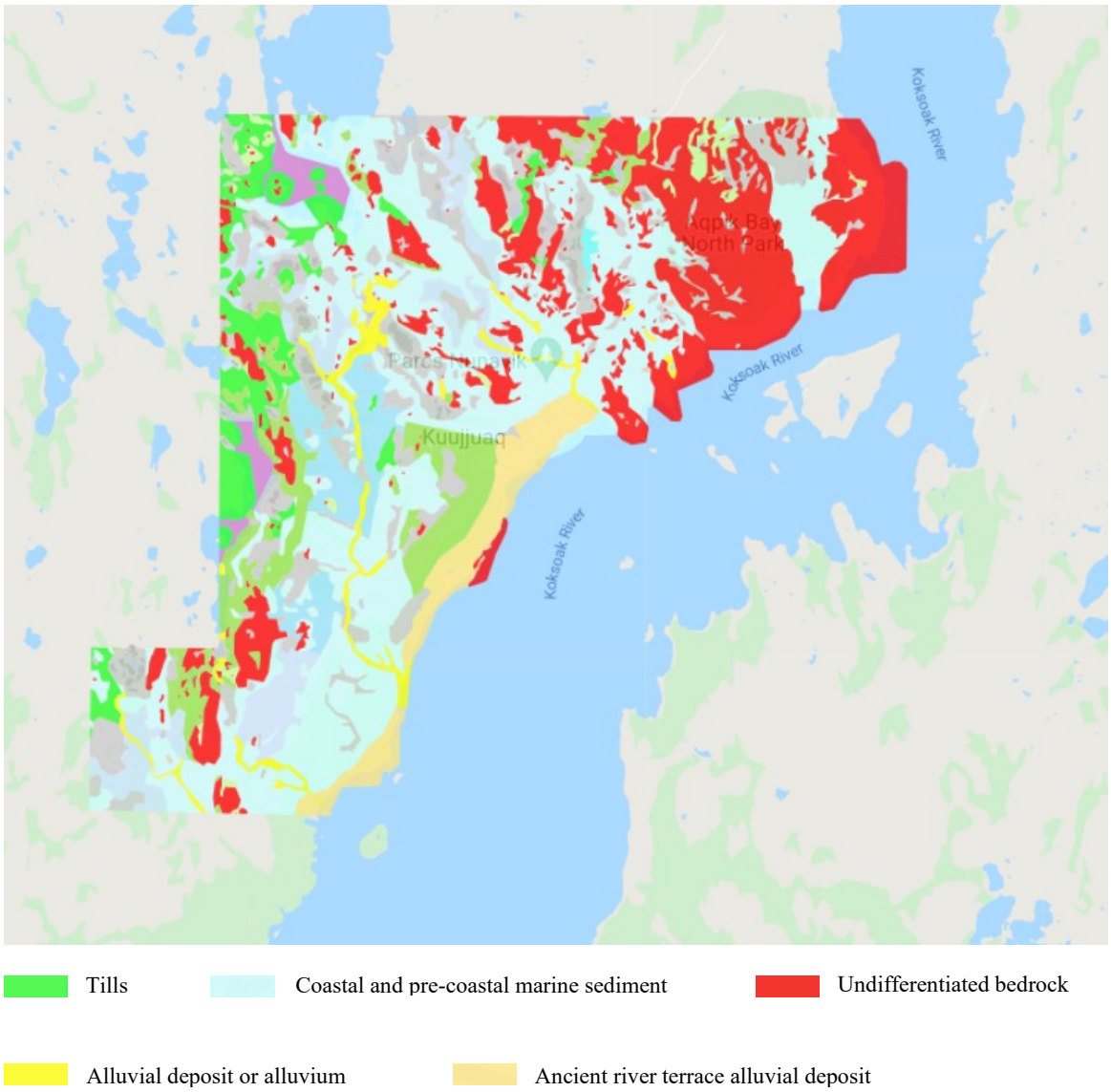

Figure 4.1 Map of unconsolidated deposits in Kuujjuaq (after Fortier, Allard, et al., 2011).

To evaluate the effects of Borehole Thermal Storage (BTES) on glacial till, following assumptions on geological characterizations are proposed in this study:

1. At BTES system site, the water table is at ground level. which means soils are fully saturated. Accordingly, the convection cells (Moradi et al., 2015) are ignored, and heat conduction is the only mechanism for heat transfer in the storage medium.

2. BTES system is constructed in glacial till. The glacial till distributes from the subsurface to 40 m deep underground and is underlain by bedrock.

4.1.2 Geotechnical properties

The geotechnical properties of glacial tills are related to various factors. For instance, glacial till consists usually of clay, silt, sand, gravel, cobbles, and gravels. It is found the plasticity indices are related to clay content (as cited in Watabe et al., 2000). Shear strength is related to gravel content (Liang et al., 2019). In addition to compositions, the stress history is also crucial to analyse glacial till. Stress history of glacial till is complex and is closed related to the glacial process. Glacial till is normally overconsolidated due to the huge preconsolidation pressure in glacial period. Trenter (1999) described the consolidation and swelling processes in Figure 4.2.

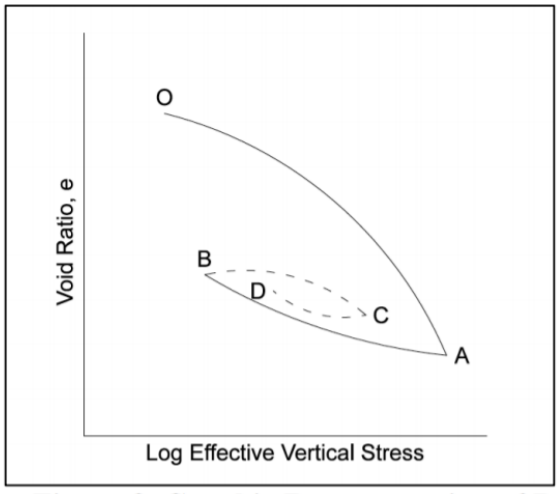

OA: consolidation under the weight of ice.

AB: swelling as ice wastes

BC: consolidation due to the lowering of groundwater

CD: swelling due to the rise of groundwater

Figure 4.2 Graphic representaion of depositional and post-depositional processes for glaciated valley tills (after Trenter, 1999).

The geotechnical properties utilised in this study is shown in Table 4.1. The following sections describe how these parameters are determined.

Table 4.1 Glacial till geotechnical properties.

Expansion coefficient		Thermal coefficient		General					Compressibility	
water α_w, 1/°C	soil particles α_s, 1/°C	Thermal conductivity λ, W/(m*K)	Specific heat capacity C_p, J/(K*kg)	Saturated density ρ, kg/m^3	Permeability k, m/s	Specific gravity G_s	Internal friction angle φ',°	ν	Compression index C_c	Swelling index C_s
$27*10^{-5}$	$3*10^{-5}$	1.57	1359	2200	$1*10^{-10}$	2.71	30	0.3	0.09	0.016

Table 4.2 Physical properties of glacial tills.

Clay fraction	Minerals & deposit compositions	Specific gravity	Dry density ρ_d, kg/m^3	Bulk density ρ, kg/m^3	Saturated density ρ_{sat}, kg/m^3	Water content w_w	Porosity n, %	Degree of saturation S_r	Void ratio	Permeability k, m/s	Compression index C_c	ReCompression index C_s	Angle of internal friction ϕ', °	thermal conductivity λ, W(/m*K)	Specific heat capacity C_v, J/(K*m^3)	K0	Reference	Soil sample location
	Coarse sands and gravels		1260-1800		(1260-1800)+(320-520)	0.14-0.19	32-52	46-81	0.47-1.08					1.08-1.87	2.07-2.66			
	a) well-drained sands and gravels on terraces of fluvioglacial or marine origin b) moderately drained, boulderly sands and silts situated in stony earth circles developed by frost action in glacial tills		1420-2040		(1420-2040)+(230-460)	0.07-0.10	23-46	21-71	0.30-0.85					0.53-2.03	1.62-2.42		J. Gray 1988	Lac Faribault, Ungava, Quebec
1.5%-3.0%	sandy ttll and boulders			2101-2486		6.0%-11.3%											Rosenberg, 1978	Downtown Montreal, Quebec
7.0%-10.0%				2190-2454		5.7%-13.2%												
	a hetergeneous blend of clay, sand, gravel, and boulder in a silt matrix			2300													Thiessen, 2011	Winnipeg
	boulders, glacial lake clay	2.71-2.79		155-158 lb./cu.ft. (2500 kg/m^3)		5.9%-7.0%											Klohn, 1965	southern Saskatchewan, Canada
			1460-2145			9.3%-20.44%			around 0.23		0.10-0.32	0.02-0.11					Saucer, 1993	southern Saskatchewan, Canada
11.7%-17.5%	clay minerals (kaolinite, illite, smectite), Quartz, calcite, traces of amorphous	2.7		2228-2337		9.7%-13.1%				10^{-10}-10^{-5}	0.05-0.08	0.004-0.007	34+-1°			0.2-2.5	Long 2007	Dublin, the Republic of Ireland
	gravelly silty sand	2.69-2.84	2130.5						0.25	1*10^{-9}-1*10^{-6}				1.5-2.3			Pare, 1978	James Bay, Quebec
30%		2.71			2000				0.65	5*10^{-10}			23°				Han, Vana 2016	Saskatchewan, Canada
7%-14%	cohesive till: silty clay till and clayey silt till			1990-2400		7%-22%					0.037-0.101	0.008-0.016	31°-41°				Laifa Cao, 2015	Greater Toronto Area, Ontario
8%-16%	cohesionless till: silty sand till, sand and silt till, and sandy silt till			2230-2380		6%-20%												
	Dense glacial till												35°			0.65	Redhakrisha, 1974	north shore of Lake Ontario
	cohesive glacial till			2030-2420													Geo Regina, 2014	Toronto
	cohesionless glacial till			2100-2510														

Specific gravity, density, void ratio and OCR

Specific gravity is the ratio of the mass of soil solids to the mass of an equal volume of water at 4°C. It is an important index property of soils that is closely linked with mineralogy or chemical composition and also reflects the history of weathering. The specific gravity of sand is generally 2.65-2.67, silty sand 2.67-2.70, inorganic clay 2.70-2.80. In this study, the specific gravity (G_s) value of **2.71** and the **saturated density** (ρ_{sat}) value of **2200 kg/m^3** for soil at 40 meters depth are in general agreement with literatures (Table 4.2).

$$\rho_{sat} = \frac{e_0}{1+e_0}\rho_w + \rho_d = \frac{G_s + e_0}{1+e_0}\rho_w \tag{3.8}$$

Then the **void ratio** (e_0) at 40 meters depth is calculated as 0.42.

Overconsolidation ratio (OCR) varies with depth in glacial till. Due to the formation process of glacial till, as well as the existence of the ice age, glacial till is generally overconsolidated. For a certain depth of overconsolidated glacial till, the part in shallow layer has the largest OCR.

$$OCR = \frac{\sigma'_{zc}}{\sigma'_{z0}} \tag{3.9}$$

σ'_{zc} is preconsolidation pressure, σ'_{z0} is current vertical overburden stress. Preconsolidation pressure is the maximum effective vertical overburden stress that a particular soil sample has sustained in the past.

Heavily overconsolidated soils tend to dilate and experience strain-softening. Normally consolidated and lightly overconsolidated soils tend to compress and strain-

harden when permitted to change volume during shearing. It is not possible to estimate the degree of overconsolidation directly from the geological history of local region. This is because the depositional environment of these tills was complex, and there is a high degree of uncertainty regarding the stress conditions and pore water pressure imposed by past glaciations. Due to the lack of local research on preconsolidation pressure, the author decided to determine the preconsolidation pressure and degree of overconsolidation based on glacial tills in other regions.

Laurentide Ice Sheet (LIS) covered Quebec and Saskatchewan in Ice Age. The preconsolidation pressures of glacial till from Saskatchewan can provide some reference to that of glacial till from northern Quebec. Profiles were remarkably low on the surface of the Laurentide glacier in southern Saskatchewan. Low surface profiles of the Laurentide glacier in western Canada were the result of soft, unfrozen sediments deforming below ice (Mathews, 1974). Quebec locates closer to the ice core than Saskatchewan. A preliminary assumption is the preconsolidation pressures of glacial tills from Quebec is generally higher than that of Saskatchewan considering the ice thickness.

Research on Quaternary deposits in southern Saskatchewan indicates the preconsolidation pressure of glacial tills in various formations (Huang & Sharma, 2008; Sauer et al., 1993b, 1993a; Sauer & Christiansen, 1988; Shaw & Hendry, 1998).

Sauer (1988) and Sauer et al. (1993b, 1993a) reported that, the preconsolidation pressures were calculated using Casagrande (1936) and work per unit volume (Becker

et al. 1987) methods. At 10 sites, the formations are, in ascending order, Battleford FM, Floral FM, Warman FM, Dundurn FM, and Mennon FM. Battleford Formation, which is the youngest, was not overrun by a subsequent glacier. Accordingly, the preconsolidation pressures are lowest in this formation. Among the 10 sites, Battleford Formation was observed at Garson River, Delisle, Goodale farm, and Sutherland overpass, with preconsolidation pressures of 350 to 750 kPa. The mean preconsolidation pressure for pre-Battleford tills and intertill clays at these 10 sites is 1800 ± 200 kPa.

Later in Shaw and Hendry (1998): The sample reveals that glacial till distributes from surficial to a depth of 80 m. The lower till, which was identified as the older Floral Formation, is corrected to be Battleford Formation. The measurements and calculations indicate the preconsolidation pressures range from 400 to 600 kPa.

In addition, in Huang and Sharma (2008): Instead of applying 1-D consolidation theory (Casagrande method), a CCS model which couples the process of consolidation and shearing is proposed by to provide qualitative predictions of the patterns of preconsolidation pressure observed in present-day glaciated soils. They proposed the profiles of preconsolidation pressures versus depth. The results reveal the preconsolidation pressures of Battleford till are also within the range of 400 to 600 kPa with depth from 0 to 50 m.

Due to the lack of information on local formation in northern Quebec, a conservative preconsolidation value of **500 kPa** for glacial till from surficial to the

depth of 40 meters is assumed. Accordingly, for the formation simulated in this study, the OCR of glacial till is about 25 at top, and about 2 at bottom. From surface to the depth 40 meters, the OCR is generally between 2 to 20. This is consistent with the study on glacial till from England (Clarke, 2018).

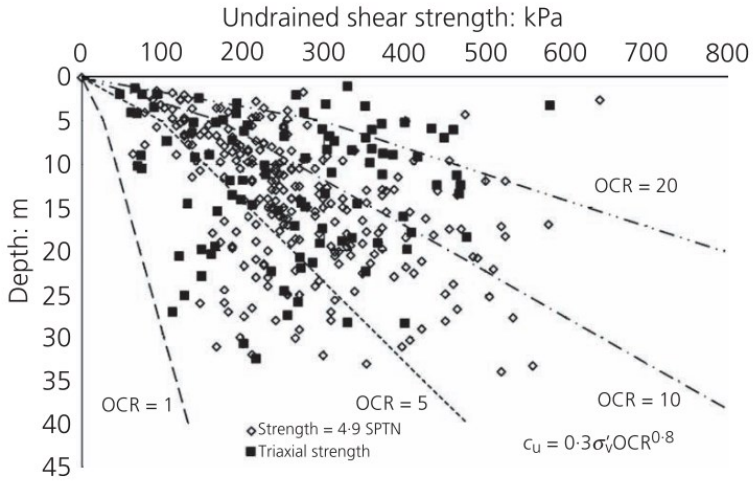

Figure 4.3 Overconsolidation ratio (OCR) and undrained shear stress with depth for an example from England (Clarke, 2018).

Shear strength parameters (φ'), Overconsolidation ratio (OCR) and static earth pressure coefficient (K_0)

The internal friction angle (φ') is related to the stress ratio M as Eq.(3.6). Previous research on shear strength parameters gives a range around 30° for internal friction angle (φ') of glacial till.

Lehane and Simpson (2000) pointed out a mean value of 32° for the critical state friction angle of DBC samples.

Cao et al. (2015) consolidated undrained triaxial tests on cohesive glacial tills showed the effective angle of internal friction ranging (φ') from 31° – 41° with an average value of 34.5° and effective cohesion (c') of 0 to 50 kPa.

Bell (2002) stated "with the exception of the Chalky Boulder Clay, the effective angles of friction for the three other deposits ranged between 25° and 35°."

Han et al. (2016) stated "the angle of internal friction (φ') value of 23° is in general agreement in the literature for the study of IHT."

Clarke (2018) stated "…suggests that the angle of friction of glacial tills would vary between 25° and 35°."

In this study, the internal friction angle (φ'), also called the critical state friction angle is assumed as **30°**.

Static earth pressure coefficient (K_0) is related to soil type, soil density, water content and other factors. For cohesive soil, K_0 also has a lot to do with historical stress state. Comprehensively, the static earth pressure coefficient can vary over a wide range for a certain type of soil (Table 4.3).

Table 4.3 The static earth pressure coefficient for soils.

gravel		0.17
sand	e=0.5	0.23
	e=0.6	0.34
	e=0.7	0.52
	e=0.8	0.6
silt and silty clay	w=15~20%	0.43~0.54
	w=25~30%	0.60~0.75
clay	stiff clay	0.11~0.25
	dense clay	0.33~0.45
	plastic clay	0.61~0.82
peat	high in organic content	0.24~0.37
	low in organic content	0.40~0.65
sandy silt		0.33

In addition, there are empirical equations for estimating static earth pressure (K_0) by internal friction angle (φ') and overconsolidation ratio (OCR).

$$K_0 = 1 - \sin\phi' \tag{3.10}$$

For overconsolidated cohesive soil,

$$(K_0)_{OC} = (K_0)_{NC} * (OCR)^m \tag{3.11}$$

Long and Menkiti (2007) summarized the coefficient of earth pressure at rest (K_0) for tills (Table 4.4).

Table 4.4 Summary of K_0 measurements in till from literature Till (Long & Menkiti, 2007).

Till	Technique	K_0
Iowa, USA	Stepped blade dilatometer	1·3
Cheshire, UK	Hydraulic fracture and packer	0·7–1
Iowa, USA	Dilatometer, spade cell, pressuremeter	3–4 to 4 m depth then decreases to 1
Cowden, UK	As above	As above

Based on the empirical equation and previous work by Long and Menkiti (2007), the static earth pressure coefficient (K_0) of **0.5** is set in this study.

Compressibility

In general, the glacial till in the Edmonton area has been considered an entirely satisfactory foundation material due to their low settlements (Thomson et al., 1982). In northern Quebec, glacial tills have often been used for the construction of earth dams because of their low compressibility (Watabe et al., 2000).

The compression index (C_c) is the slope of the linear portion of void ratio (e) versus logarithm of effective pressure ($\log_{10} p'$) relationship and the swelling index (C_s) represents the slope of the rebound curve of void ratio versus logarithm of effective pressure. Compression index and swelling index are used for the calculation of soil deformation. These two indices are determined by conducting One-Dimensional Compression Test and Swelling Test (Oedometer Test).

One-Dimensional Consolidation Test (Oedometer test) is a complex, time consuming, and expensive test. For soils, there are abundant numbers of empirical expressions available to determine approximate values of compression index (C_c) and swelling index (C_s). Among those expressions, compression index and swelling index are functions to one of parameters including plasticity index, liquid limit, void ratio, clay fraction, particle specific gravity...

The compression index (C_c) value can be predicted in response to the execution of the Atterberg Limit Test (Ibrahim et al., 2012).

Sauer et al. (1993a) studied compression characteristics and index properties of unweathered tills and clays from Saskatchewan. They carried oedometer tests and proposed compression index equation based on test results.

$$C_c = 0.0053 * LL \tag{3.12}$$

Skempton equation (as cited in Sauer et al., 1993a) proposed:

$$C_c = 0.007 * (LL - 10) \tag{3.13}$$

The correlations between C_c and the natural water content appear to be more consistent than the others (Bardet, 1997). They gave three compression index equations and two swelling index equations.

Compression index was estimated using the empirical expression for soft clay suggested by Terzaghi and Peck (cited in Bardet, 1997) as a function of liquid limit of clays:

$$C_c = 0.009 * (LL - 10) \tag{3.14}$$

Wroth and Wood (cited in Bardet, 1997) concluded following expressions for compression index (C_c) and swelling index (C_s):

$$C_c = 0.005 * PI * G_s \tag{3.15}$$

$$C_s = C_c * (1 - \Lambda) \tag{3.16}$$

where Λ is a critical state material constant. For G_s = 2.7 and Λ = 0.8, Eq. (3.15) and Eq. (3.16) become $C_c = \frac{PI}{74}$ and $C_s = \frac{PI}{370}$.

Nadaraj and Srinivasa (1985) (cited in Kaliakin, 2017) proposed:

$$C_c = 0.00234 * LL * G_s \tag{3.17}$$

Gregory and Bell (cited in Trenter, 1999) proposed the following relationships for Belfast tills:

$$C_c = 0.004 * (LL - 5) \tag{3.18}$$

Bell (2002) stated that the compressibility and consolidation characteristics of tills are principally determined by their clay content. The higher liquid limit presumably is due to the higher clay content. The consistency limits of tills are dependent upon moisture content, grain size distribution and the properties of the fine-grained fraction.

For low compressibility tills of low clay content, the empirical expression was suggested by Bernell (cited in Trenter, 1999) as:

$$C_c = 0.0044 * f_s + 0.003 \tag{3.19}$$

Azzouz et al. (1976) (cited in Kaliakin, 2017) proposed a expression related to initial void ratio:

$$C_c = 0.40 * (e_0 - 0.25) \tag{3.20}$$

Işik (2009) summarized two empirical equations for the determination of swelling index.

Nagaraj and Murty proposed (cited in Işik, 2009),

$$C_s = 0.0463 \frac{LL}{100} G_s \tag{3.21}$$

Nakase et al. proposed (cited in Işik, 2009),

$$C_s = 0.00194 * (PI - 4.6) \tag{3.22}$$

According to Işik (2009), Nagaraj's equation generally overestimates the swell index on various undisturbed clay samples from Turkey.

Each empirical expression works best for one kind of soil and may underestimate or overestimate compressibility for other soils. Due to the lack of local soil datum, all the above expressions are adapted to determine the compressibility of glacial till in northern Quebec area.

In addition to compression index (C_c) and swelling index (C_s), the parameters λ and κ are also for estimating compressibility. The slope of the virgin compression line in $e - \ln p'$ space is denoted by λ and the slope of the swell/recompression curve in the space is denoted by κ. The critical state indices λ and κ are related to the compression index (C_c) and swelling index (C_s) in the following manner:

$$\lambda = \frac{C_c}{\ln 10} = \frac{C_c}{2.3} \text{ and } k = \frac{C_s}{\ln 10} = \frac{C_s}{2.3}$$

Klohn (1965) studied glacial till from northern Saskatchewan. It's found average plasticity index as 7%, average liquid limit as 19%, specific gravity as 2.75.

Han et al. (2016) Studied a compacted glacial till from India Head, Saskatchewan. It's found plasticity index as 15.5%, liquid limit as 32.5%, specific gravity as 2.71, clay fraction 30%.

Watabe et al. (2000) studied six tills (LG-2, LG-4, Caniapiscau till, SM-3) from northern Quebec. Clay fraction (<6 um) as 5-20%, plasticity index as 0-6%.

Table 4.5 Calculations on the compressibility parameters of glacial till.

Empirical expressions	Klohn				Han				Watabe			
	input parameter	Cc and Cs	λ and κ		input parameter	Cc and Cs	λ and κ		input parameter	Cc and Cs	λ and κ	
$C_c = 0.0053 * LL$	Gs = 2.75 LL = 19% PI = 7%	0.101	0.044	0.036	Gs = 2.71 LL = 32.5% PI = 15.5% fs = 30%	0.172	0.075	0.072	PI = 6% fs = 15%	-	-	0.033
$C_c = 0.007 * (LL - 10)$		0.063	0.027			0.158	0.068			-	-	
$C_c = 0.009 * (LL - 10)$		0.081	0.035			0.203	0.088			-	-	
$C_c = 0.005 * PI * G_s$		0.096	0.042			0.210	0.091			0.081	0.035	
$C_c = 0.00234 * LL * G_s$		0.122	0.053			0.206	0.090			-	-	
$C_c = 0.004 * (LL - 5)$		0.056	0.024			0.110	0.048			-	-	
$C_c = 0.0044 * f_s + 0.003$		-	-			0.135	0.059			0.069	0.030	
$C_c = 0.4 * (e_0 - 0.25)$		-	-			-	-			-	-	
$C_s = 0.001 * PI * G_s$		0.019	0.008	0.006		0.042	0.018	0.014		0.016	0.007	0.003
$C_s = 0.0463 * \frac{LL}{100} * G_s$		0.024	0.011			0.041	0.018			-	-	
$C_s = 0.00194 * (PI - 4.6)$		0.005	0.002			0.021	0.009			0.003	0.001	

Based on the previous research on glacial tills from Saskatchewan and northern Quebec and the empirical expressions, the values of compression index (C_c) and swelling index (C_s) in this study are assumed to be average value. That is: $C_c = 0.09$, $C_s = 0.016$; $\lambda = 0.04$, $\kappa = 0.007$.

Further work proves the rationality of above assumed value. Lehane and Simpson (2000) studied the glacial till (Dublin Boulder Clay) from the Greater Dublin area in Ireland. After conducting One-Dimensional Compression Test and Swelling Test, they found $\lambda = 0.03$, $\kappa = 0.004$. Atkinson and Little (1988) obtained $\lambda = 0.065$, $\kappa = 0.03$ for a lodgement till from England. Powrie and Li (1991) tested stiff overconsolidated boulder clays from England with $\lambda = 0.155$, $\kappa = 0.016$. Compared with these test results, the calculated values ($\lambda = 0.04$, $\kappa = 0.007$) are reasonable.

Table 4.6 Calculated and collected values of λ and κ values for glacial till.

	λ	κ	Reference
Calculated value	0.04	0.007	
Collected value	0.03	0.004	(Lehane & Simpson, 2000)
	0.065	0.03	(Atkinson & Little, 1988)
	0.155	0.016	(Powrie & Li, 1991)
	(0.10~0.32)/2.3	(0.02~0.11)/2.3	(Sauer et al., 1993a)
	(0.05~0.08)/2.3	(0.004~0.007)/2.3	(Long & Menkiti, 2007)
	(0.037~0.101)/2.3	(0.008~0.016)/2.3	(Cao et al., 2015)

Hydraulic conductivity (k)

Hydraulic conductivity and hydraulic gradient have to be evaluated to account for thermal dispersion. Permeability influences the rate of settlement of a saturated soil under load. According to Darcy's Law, hydraulic conductivity, or coefficient of permeability is a ratio of the rate of fluid flow through the soil matrix to the hydraulic gradient.

According to Darcy's Law, hydraulic conductivity, or coefficient of permeability is a ratio of the rate of fluid flow through the soil matrix to the hydraulic gradient. Hydraulic conductivity influences the rate of settlement of a saturated soil. Common guidelines suggest that borehole thermal energy storage (BTES) systems are constructed on low hydraulic conductivity soils considering the heat losses will increase if ground water flow exists (Catolico et al., 2016; Rad & Fung, 2016). Numerical studies of a porous medium with homogeneous hydraulic properties have shown that a screen to reduce the water flow is required if the ground water flow exceeds 50 mm/day (as cited in Gabrielsson et al., 2000). Glacial tills in northern Quebec have relatively

low hydraulic conductivity (Watabe et al., 2000). Under a certain hydraulic gradient, water flows slowly in a soil with extremely low hydraulic conductivity. Comprehensively, such soil can be regarded as unconsolidated for a certain period of time.

Author summarized the previous research on the hydraulic conductivity of glacial tills in this section. It is found that glacial tills have hydraulic conductivity of a range of 10^{-11} to 10^{-6} m/s. Then, a recommended value is set for this study.

Watabe et al. (2000) carried permeability tests on a glacial till from northern Quebec. It was reported the hydraulic conductivity of glacial till is between 10^{-9} to 10^{-6} m/s and is related to void ratio and compaction degree of saturation of till.

Lehane and Simpson (2000) gave the typical classification index properties for the black till. According to them, the hydraulic conductivity is 10^{-11} to 10^{-8} m/s.

Al-Khazaali, Vanapalli, and Oh (2019) summarized the physical and mechanical soil properties for the India Head till (IHT) and they set saturated hydraulic conductivity (k_{sat}) as $5*10^{-10}$ m/s.

Clarke (2018) concluded the hydraulic conductivity of 10^{-12} to 10^{-9} m/s for matrix-dominated soils, and 10^{-7} to 10^{-5} m/s for clast-dominated soils and the function with void ratio.

It was concluded from the measurements that typical permeability values for the intact cohesive till in the UBkBC and UBrBC formations are in the range 10^{-11} to 10^{-9} m/s (Long & Menkiti, 2007).

As cited in Leroueil et al. (2002), Loiselle studied tills from the Manicouagan and Outardes rivers area, some 1000 km northeast of Montreal, and found hydraulic conductivities varying from $2*10^{-10}$ to $6*10^{-8}$ m/s; Pare tested a till from the LG-3 dam area, about 1000 km northwest of Montreal, and measured hydraulic conductivities of about $5*10^{-6}$ m/s.

From above, the hydraulic conductivity of glacial till is 10^{-11} to 10^{-6} m/s based on different composition, void ratio and degree of saturation. For rationality, the assumed value should be within 10^{-11} to 10^{-6} m/s. In this study, **$1*10^{-10}$ m/s** is set as the hydraulic conductivity of glacial till in the studying site.

4.1.3 Thermal properties

The heat store efficiency and total heat store capacity of Borehole Thermal Energy Storage (BTES) systems are directly related to the thermal properties of storage media. Soils with high thermal conductivity and high heat capacity, which means more heat energy stored in shorter time, are adorable media for BTES systems.

Thermal conductivity: The soil thermal conductivity (λ_t) is the ratio of the magnitude of the conductive heat flux through the soil to the magnitude of temperature gradient (W/(m*K) or W/(m*°C)). It is a measure of the soil's ability to conduct heat, just as the hydraulic conductivity is a measure of the soil's ability to "conduct" water. Soil thermal conductivity is influenced by a wide range of soil characteristics including Air-filled porosity, water content, bulk density, texture, mineralogy, soil structure, soil temperature…

The efficiency of the heat exchange will improve with higher thermal conductivities, but the rate of heat conduction away from the reservoir (hence heat loss) will increase with higher thermal conductivities (Evans et al., 2006).

As cited in Rad and Fung (2016), the best and most efficient BTES is with high thermal conductivity adjacent to the boreholes and pipes and less formation thermal conductivity away from the storage volume with no groundwater flow. Lower formation thermal conductivity away from the storage volume causes less storage heat loss.

Heat capacity: soil volumetric heat capacity (C_v) is the amount of energy required to raise the temperature of a unit volume of soil by one degree ($J/(m^{-3}*°C^{-1})$). Unlike thermal conductivity, volumetric heat capacity increases strictly linearly as soil water content increases. Volumetric heat capacity is also a linear function of bulk density. Specific heat capacity (C_p) is the heat capacity of a sample of the substance divided by the mass of the sample (J/(kg*°C) or J/(kg*K)).

Higher media heat capacity means a smaller volume would be necessary to store the same amount of energy in sedimentary deposits, which means lower drilling costs (Giordano et al., 2017).

Pare et al. (1978) studied glacial tills from the James Bay in northern Quebec. They found thermal conductivity of the tills varied between 1.5 and 2.3 W/(m*°C) ($3.5*10^{-3}$ and $5.5*10^{-3}$ cal*cm/(cm^2*°C)).

As cited in Pare et al. (1978), the volumetric heat capacity (C_v) can be estimated by:

$$C_v = \gamma_d (0.17 - 0.005w) \tag{3.23}$$

where w is water content and γ_d is dry density of soil.

Gray et al. (1988) studied six soils from Ungava in northern Quebec. Thermal conductivity (λ_t) and volumetric heat capacity (C_p) of glacial tills, which were referred to sites 82-4 and 82-5 among six soils, were calculated using the Johansen technique. It was found that thermal conductivities are 0.53-2.03 W/(m*K) for site No.82-4, 1.08-1.87 W/(m*K) for site No. 82-5, 1.62 – 2.42 MJ/(m^3*K) for site No.82-4 and 2.07 – 2.66 MJ/(m^3*K) for site No. 82-5.

$$\lambda_t^{sat} = 0.57^M * k_s^{1-n} \tag{3.24}$$

$$\lambda_t^{dry} = \frac{0.135\rho_d + 65}{2700 - 0.947\rho_d} \tag{3.25}$$

Real conductivity values for the sites fall somewhere in between the values of λ_t^{sat} and λ_t^{dry} can be calculated on the basis of the following final equation:

$$\lambda_t = (\lambda_t^{sat} - \lambda_t^{dry}) K_e + \lambda_t^{dry} \tag{3.26}$$

Volumetric heat capacity (C_v) of the soils was calculated using the following equation:

$$C_v = \rho_d C_p^s + \frac{C_p^w w}{100} \tag{3.27}$$

where C_v volumetric heat capacity; ρ_d dry density; C_p^s specific heat capacity of soil solids; C_p^w specific heat capacity of water; w percentage of water content by dry weight.

According to Hillel (2003), the value of volumetric heat capacity (C_v) can be calculated by addition of the heat capacities of the various constituents, weighted according to their volume fractions, as:

$$C = \sum f_{si} C_{si} + f_w C_w + f_a C_a \tag{3.28}$$

Here, f denotes the volume fraction of each phase: solid (subscripted s), water (w), and air (a).

During a field campaign in summer of 2017, Giordano et al. (2017) focused subsurface geothermal assessments in the northern community of Kuujjuaq, Quebec, Canada. They summarized the thermal conductivity (λ_t) and specific heat capacity (C_p) for unconsolidated sediments. Among these sediments, they found saturated glacial till here has an average thermal conductivity (λ_t) of **1.57 W/(m*K)** and a volumetric heat capacity (C_v) of 2.99 MJ/(m^3*K). Volumetric heat capacity (C_v) and specific heat capacity (C_p) are related to

$$C_{\mathrm{v}} = C_p * \rho \tag{3.29}$$

ρ is 2200 kg/m^3 for glacial till, C_p is therefore **1359** $J/(K*kg)$.

Thermal expansion: Based on the physical law, materials expand upon heating and contract when cooling. The temperature changes regularly in BTES systems in

service period, inducing continuous expansion and contraction within the surrounding soil. To evaluate this thermal induced deformation, thermal expansion coefficient (α) is crucial. Thermal expansion coefficient (α) indicates the extent to which a material expands upon heating. Different substances expand by different amounts. Over small temperature ranges, the thermal expansion of uniform linear objects is proportional to temperature change. In soil mechanics, soil is a mixture of three compositions: solid skeleton, water, air. This study focuses on the BTES systems built on saturated glacial till. The difference between the expansion of solid skeleton and water

As cited in Delage (2013), the thermal expansion of some typical minerals and water are shown as below:

Table 4.7 Thermal expansion coefficients of some typical minerals.

Mineral	Thermal expansion coefficient α, °C^{-1}
Clay	$3.4*10^{-5}$
Quartz	$3.34*10^{-5}$
Calcite	$1.38*10^{-5}$
Felspar	$1.11*10^{-5}$
Water	$\alpha_w = 27*10^{-5}$

Considering there are clay, coarser particles and boulder in glacial till. In this study, the thermal expansion coefficient of glacial till (α_s) and water (α_w) are set as **$3.0*10^{-5}$ °C^{-1}** and **$27*10^{-5}$ °C^{-1}** according to above data and are assumed as constant during the service period of BTES systems. The thermal pore pressure would generate as the fact that the thermal coefficient of pore water is significantly higher than that of the soil particles. The existence of thermal induced pore pressure may aggravate subsurface instability.

Due to the high heat capacity, high thermal conductivity, and low hydraulic conductivity, glacial till is adorable material for BTES storage.

4.2 Finite element modeling

4.2.1 Initial conditions

As discussed in above sections, the problem can be concluded as: A 50-year BTES system with a single borehole of 35 meters in depth is built in glacial till in northern Quebec. Glacial till distributes 40 meters in depth and overlies bedrock. The water table is at the soil surface, the glacial till is regarded as fully saturated with saturated density (ρ_{sat}) of 2200 kg/m^3. The till at 40 meters depth has void ratio of 0.42. The preconsolidation pressure on the top surface is 500 kPa. Considering the practical situation, the construction of BTES system removes topsoil to get reliable subsurface and then place structures like insulation on the glacial till. It is assumed the removed soil applied 20 kPa pressure on the glacial till and the structures will apply 20 kPa pressure on the glacial till.

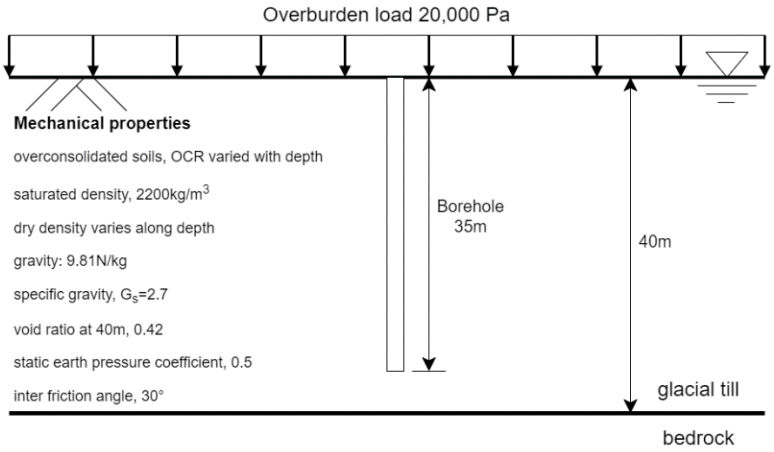

Figure 4.4 Sketch showing the initial boundary conditions.

Initial effective stress state

With this summary, the initial stress state is defined in Figure 4.5.

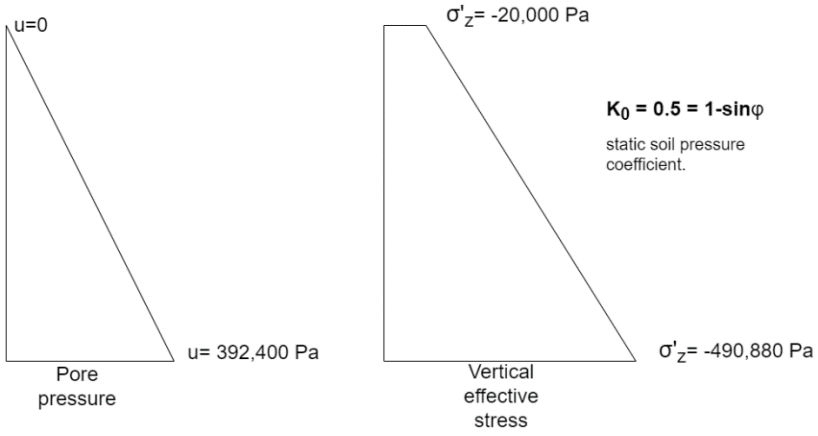

Figure 4.5 Initial pore pressure and vertical effective stress along the studying glacial till formation.

The vertical effective stress is defined:

$$\sigma_z^{'} = 20,000 + 1200 * 9.81 * (40 - Z)$$

where Z is the z value of soil. Z = 0 at the bottom of soil, Z = 40 m at the top of soil.

The horizontal effective stress is defined:

$$\sigma_x^{'} = \sigma_y^{'} = K_0 \sigma_z^{'}$$

where $K_0 = 0.5$

Hence, the mean effective stress: $p_z^{'} = 2/3\sigma_z^{'}$; the deviator shear stress: $q_z = 1/2\sigma_z^{'}$.

Top: $Z = 40m$, $p' = 13,333.33Pa$, $q = 10,000Pa$.

Bot: $Z = 0m$, $p' = 327,523.33Pa$, $q = 245,440Pa$.

Initial pore pressure

Top: $Z = 40m$, $u = 0Pa$

Bot: $Z = 0m$, $u = 392,400Pa$

Initial yield surface size p'_{c-pre}

The glacial till is overconsolidated, the initial yield surface size is calculated based on the maximum stress state in history. As mentioned in previous section, the maximum overburden on the glacial till in the history is 500,000 Pa. Then, the maximum vertical effective stress along depth is given as

$$\sigma'_{z-pre} = 500,000 + 1200 * 9.81 * (40 - Z)$$

According to CCM, the initial yield surface intersects $p' - axis$ at p'_{c-pre}, which is given by equation

$$\frac{M^2 p'^2_{z-pre}}{q_{pre}^2 + M^2 p'^2_{z-pre}} = \frac{p'_{z-pre}}{p'_{cz-pre}} \tag{3.30}$$

hence, $p'_{cz-pre} = (\frac{3}{8*1.44} + \frac{2}{3})\sigma'_{z-pre} = (\frac{9}{16*1.44} + 1)p'_{z-pre}$

Top: $Z = 40m$, $p'_{c-pre} = 463,541.67Pa$

Bot: $Z = 0m$, $p'_{c-pre} = 900,086.67Pa$

In addition, OCR is given by $OCR = \sigma'_{z-pre} / \sigma'_z$, which varies from 25 at top to about 2.0 at the depth of 40 meters.

Initial void ratio (e_0) along depth

Under the assumed overburden and self-weight, the initial stress state of soil at any depth is always within elastic zone. Intial void ratio (e_0) and the void ratio on the normal consolidation line at unit mean effective stress (e_N) are related by the equation

$$e_N = e_0 - \kappa \ln(\frac{p'_{cz-pre}}{p'_z}) + \lambda \ln(p'_{cz-pre}) \tag{3.31}$$

For soil at 40 meters depth, $e_0 = 0.42$. Accordingly, e_N of this glacial till could be calculated, $e_N = 0.96$. The initial void ratio of glacial till decreases along depth as the effective stresses increases along depth. For void ratio along depth

$$e_{0z} = 0.96 + 0.007 \ln(\frac{p'_{cz-pre}}{p'_z}) - 0.04 \ln(p'_{cz-pre})$$

Top: $Z = 40m$, $e_0 = 0.464$

Bot: $Z = 0m$, $e_0 = 0.42$

Initial dry density (ρ_{dry}) along depth

It is assumed the saturated density is constant along depth. According to the phase relationships of soil, the initial dry density could be given

$$\rho_{dry} = \rho_{sat} - \rho_w \frac{e_0}{1+e_0} \tag{3.32}$$

Then, $\rho_{dry} = 2200 - 1000 * \dfrac{e_N + 0.007 \ln(\frac{p'_{cz-pre}}{p'_z}) - 0.04 \ln(p'_{cz-pre})}{1 + e_N + 0.007 \ln(\frac{p'_{cz-pre}}{p'_z}) - 0.04 \ln(p'_{cz-pre})}$

Top: $Z = 40m$, $\rho_{dry} = 1883 kg/m^3$

Bot: $Z = 0m$, $\rho_{dry} = 1904 kg/m^3$

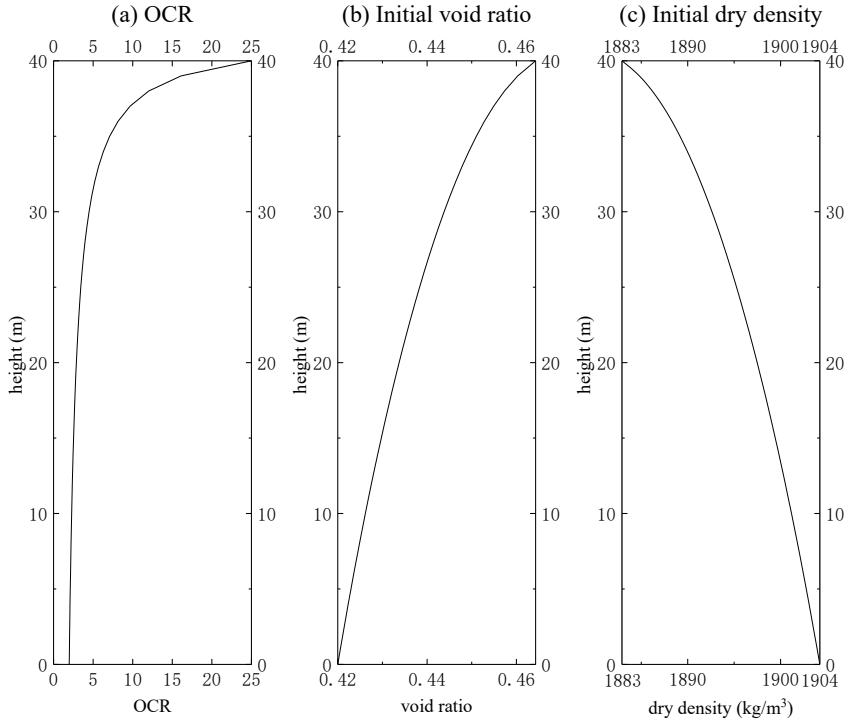

Figure 4.6 Initial conditions along depth: (a) initial OCR, (b) initial void ratio, (c) initial dry density.

4.2.2 ABAQUS Model

ABAQUS is utilized to perform 3D thermal-hydro-mechanical (THM) analysis of the thermally induced deformation problem. For the BTES system with a single borehole (35 meters), this problem is solved using axisymmetric coupled temperature-pore pressure elements. For the purpose of presenting the results, axisymmetric element type CAX4PT is chosen. The finite element model along with the generated mesh is shown in Figure 4.7. To obtain accurate results, a fine mesh is set in the glacial till adjacent to the central borehole, as the dramatical evolution in dependent variables would occur within this region. The further away from the central borehole, the less dense the mesh becomes. 336 nodes and 300 elements in CAX4PT type are generated in total.

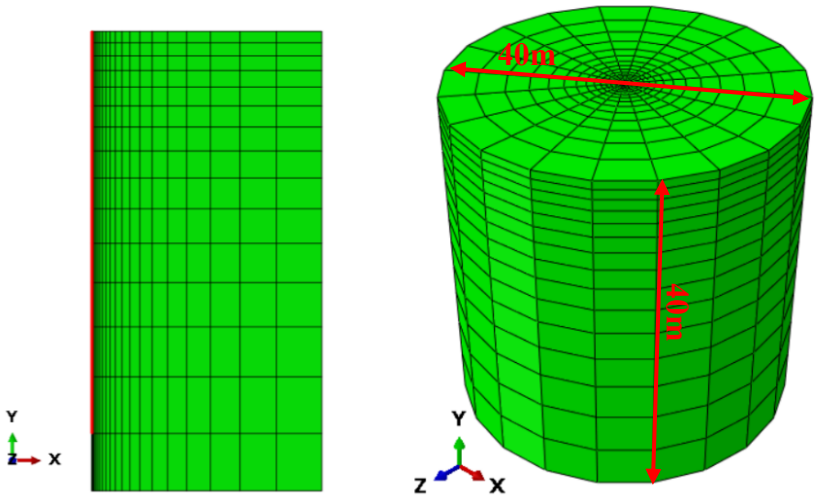

Figure 4.7 The finite-element model along with generated mesh for single borehole system (left: original mesh; right: sweep from 0 to 360°).

The response of the glacial till is assumed to be elastoplastic, with following Modified Cam-Clay Model parameter (Table 4.9).

The first step of such analysis involving an initial stress state should be a geostatic step. In this step the geostatic external loads (the pore pressure, overburden pressure and gravity) is specified. Abaqus will then check whether the initial stress state is in equilibrium with these loads. The next step is consolidation step with time period of 1.5768e9 seconds (50 years), where the storage temperature evolves continuously.

The normal (vertical) component of displacement is constrained at the base of the glacial till, while displacement in the two lateral directions is prevented by constraining the side surfaces. The structure over glacial till is assumed to allow draining freely throughout the operation to prevent hydraulic failure between insulation and till layer. This is specified by fixing the pore pressure at zero on the top edge of the mesh. The pore pressure is assumed to be fixed at initial value on the side surfaces because it is far from temperature influenced zone. For the same reason, the temperature

is assumed to be fixed at 1°C on the bottom and side surfaces. The heat source (the single borehole) is specified as a column with periodic temperature evolution (Figure 4.8). A BTES system is abounded above by an insulation layer to prevent heat exchange between storage medium and air. For simplicity, this thermal insulation layer extends across the entire top of the model. As a result, the temperature on the top surface would evolve under the influence of the central borehole.

For detailed study, dependent variables including PEEQ, NT, POR, S, U, VOIDR, and SAT are requested for the results. Table 4.8 gives the basic units adopted in Abaqus simulation.

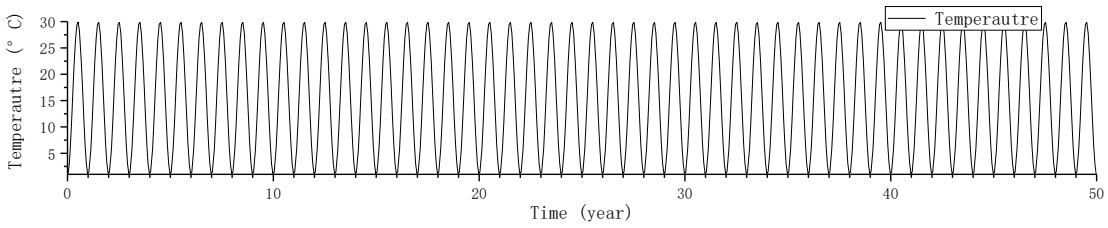

(a)

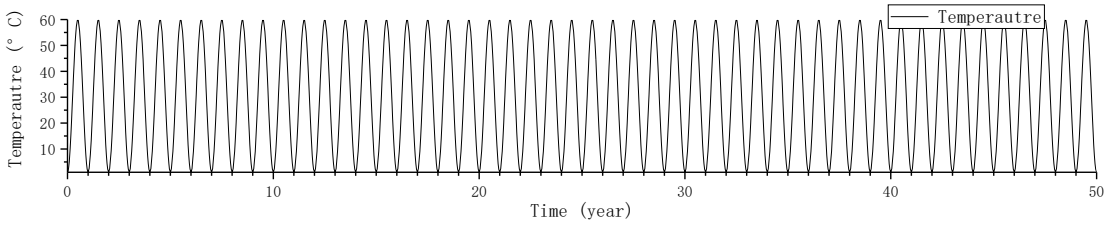

(b)

Figure 4.8 Storage temperature evolution (at the outer surface of the borheole): (a) 30°C; (b) extreme scenario: highest temperature 60°C.

Table 4.8 Basic unit adopted in Abaqus simulation.

Energy	Weight	Length	Time	Force	Stress
Joule (J)	kg	m	s	N	Pa

Table 4.9 Cam-Clay model parameters.

General		Plasticity	
ρ_{sat}, kg/m^3	2200	λ	0.04
k, m/s	1*10^{-10}	Stress ratio, M	1.2
γ_w, kN/m^3	9.81	Initial yield surface size, a_0	e
G_s	2.71	Wet yield surface size, β	1
φ',°	30		
Elastic			
ν	0.3		
κ	0.007	Flow stress rate, K	1
Thermal			
α_w, 1/°C	27*10^{-5}		
α_s, 1/°C	3*10^{-5}		
λ_t, W/(m*K)	1.57		
C_p, J/(K*kg)	1359		

4.2.3 Results

The thermal operation of a BTES system with a single borehole, whose temperature evolves periodically between 1°C and 30°C, has limited impact on surrounding glacial till. Seasonal temperature evolution was observed in the surrounding soil within thermally influenced zone. And such impact on surrounding glacial till decreases rapidly with the distance to the central borehole. From out surface of borehole to a distance of 10 meters, the highest temperature reached by soil decreases dramatically from 30°C to around 2.7°C. The thermally influenced zone is in a shape of half prolate spheroid, whose top surface is a circle with a radius of around 10 meters. Deformation and stress state evolution are most severe in the region adjacent to the central borehole. The ultimate settlement is about only 7 millimetres at the center of top surface. At the same location, the annual vertical displacement induced by thermal expansion and contraction is about 1 centimeter. The further from the borehole, the less

is the amplitude of annual vertical displacement evolution. As a whole, the annual evolution of vertical displacement is negligible, indicating the limited impact of a single borehole. In addition to the deformation, the pore pressure also evolves with the operation of the single-borehole BTES system. The pore pressure in adjacent region fluctuated over 50 years as the temperature raised and fell, generally showing an increasing trend at the beginning and a decreasing trend in the following years. The annual change in pore pressure is below 70 kPa. During the operation, a maximum pore pressure of 426.9 kPa is reached at the center of bottom surface.

Temperature evolution

Results of 50-year run BTES system shows that the whole thermal influenced zone is approximately in a shape of half prolate spheroid, whose top surface is a circle with a radius of around 10 meters. Figure 4.9 shows the temperature contour plot at the end of heat injection phase in the 50^{th} year.

Due to the radiative transfer pattern of heat energy in the glacial till, the temperature of soil near the boreholes changes the most rapidly because heat is transferred to this part of soil immediately. While the soil far away from boreholes receives less heat at a lower rate. Heat energy transfers from borehole to surrounding soil when in “summer time”, accordingly the soil near the single borehole can obtain more heat than soil at far distance. Figure 4.10 presents the evolution process of surrounding soil at three different locations on the top surface. Within distance of 2 meters, the highest temperature soil can reach drops rapidly from 30°C to slightly lower than 10°C. From 2 to 10 meters, the highest temperature continuously decreases to

2.7°C. At the depth of 20 and 10 meters, the highest temperature also drops with distance to the central borehole following the same rule (Figure 4.11). Also, it can be found that it usually takes nearly 10 years for soil not adjacent to the borehole to reach "balanced state", where the peak and trough value are equal to those of the last year and the next year (Figure 4.12). The closer to the central borehole, the temperature evolves more consistent with that of the borehole: the soil at distance of 0.16 m can reach 25°C in the first year of operation, while seven years are needed for soil at distance of 2 m to reach the highest temperature, about 9°C. Further away, the rate of temperature evolution gets lower, indicating less thermal influence. During the first ten years, the annual highest temperature climbs rapidly in the first several years. Such climbing state in soil temperature found in the result is in good agreement with the report of (Giordano & Raymond, 2019; Rad et al., 2017; Reuss et al., 1997).

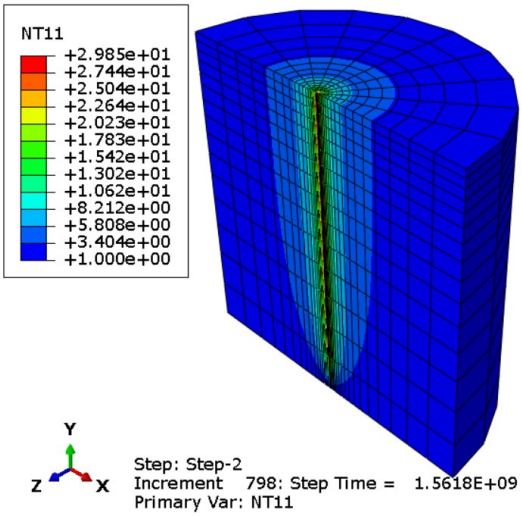

Figure 4.9 Storage temperature profile at a the end of the 50th heat injection phase (unit = °C).

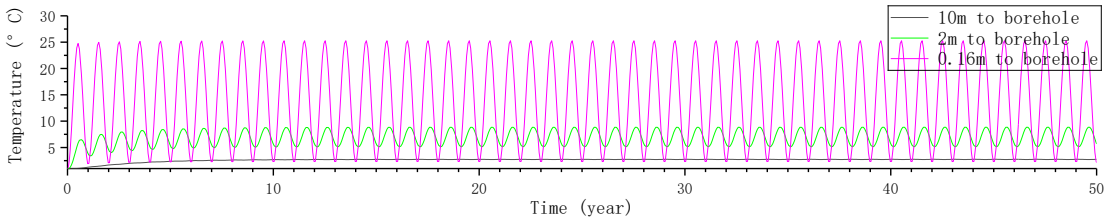

Figure 4.10 Soil temperature evolution at different distance to the central borehole on the top surface.

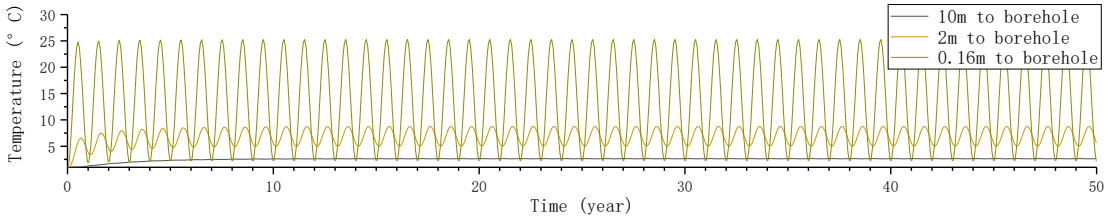

(a)

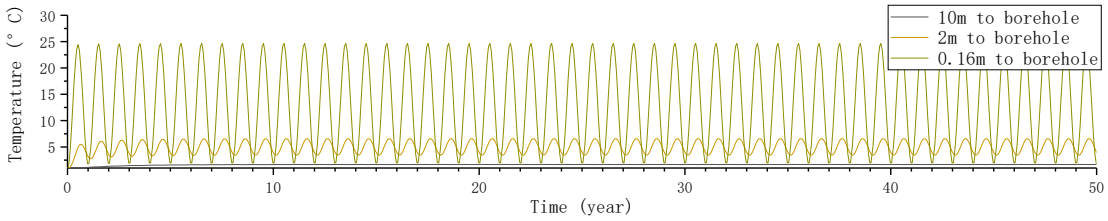

(b)

Figure 4.11 Soil Temperature evolution at different distance to the central borehole: (a) at depth of 20 m; (b) at depth of 35 m.

The influenced shape is half a prolate spheroid, rather than a cylinder, indicating the difference in temperature along depth. Figure 4.12 shows the temperature evolution of three points locate 2 meters to the central borehole. It can be concluded that due to the stable temperature in bedrock, the temperature of soil at 35-meter depth evolves sightly rapidly than that at top surface and 20-m depth.

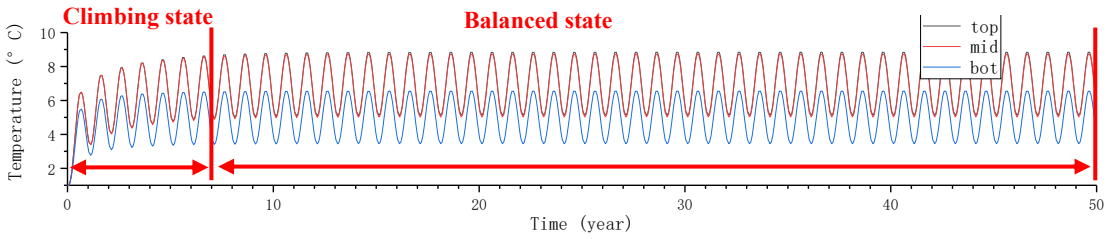

Figure 4.12 Soil temperature evolution at different depth at distance of 2 meters.

As the temperature of soil near the boreholes changes the most rapidly because heat is transferred to this part of soil immediately. While the soil far away from boreholes receives less heat at a lower rate. It takes longer for soil in far region to warm up or cool down. At the beginning of heat extraction period, the temperature of boreholes and glacial till adjacent to boreholes starts to decrease because heat energy is extracted in the region adjacent to boreholes. While the temperature in the far region is still increasing because it remains receiving heat from the region adjacent to boreholes (Figure 4.13). The temperature in far region will starts to fall after the temperature of the region adjacent to boreholes falls equal to the far region. This is the thermal retention effect in surrounding soil. Residual temperature was found in the surrounding soil, as a result of thermal retention effect. The lowest temperature in "balanced state" at a distance of 2 meters is higher than that of 0.16 meters and 5 meters.

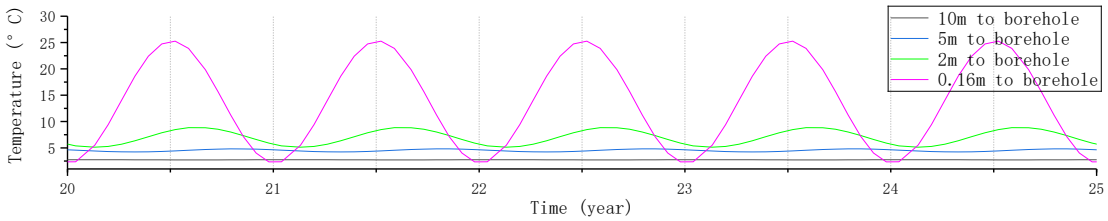

Figure 4.13 Soil temperature evolution from 21st to 25th year.

Because of the radiative transfer pattern, the highest temperature drops with distance to the central borehole in a certain year. While the lowest temperature increases slightly with the distance due to the thermal retention effect within a certain distance and falls back a little till the edge of the influenced zone.

Table 4.10 Highest and lowest soil temperature with different distance to the central borehole.

Distance to the central boreheole	Highest temperature in balanced state	Lowest temperature in balanced statee
close	Max.	Min.
mid-distance	Mid.	Max.
far	Min.	Mid.

The result of temperature evolution of a single borehole system reveals that:

1. The temperature evolution indicates this ABAQUS model can reasonably and accurately simulates the practical temperature evolution.

2. The thermal operation of a BTES system with a single borehole has limited impact on surrounding glacial till.

3. The temperature of surrounding soil usually climbs with fluctuation for the first ten years before reaching balanced state. Highest storage temperature drops rapidly with distance to the central borehole. Lowest temperature in balanced state firstly increases slightly with distance within a limited distance to the central borehole and then decreases with distance till the edge of influenced zone. Indicating more severe thermal influence in adjacent region. Along depth, less rapidly temperature is found in the bottom region.

Pore pressure evolution

Pore pressure fluctuates with the heat injection and extraction process over 50 years. As a result of the periodic change of the borehole temperature, pore pressure fluctuates seasonally in the surrounding soil. In addition, due to the uneven rise of the

underground temperature and dissipation, the pore pressure fluctuates with rising trend at first and then downward till fluctuating over the initial value. The pore pressure in a half prolate spheroid undergoes seasonal evolution due to the underground temperature changing in the same region. The highest increment in a single year is around 70 kPa found at 30-meter depth adjacent to the central borehole. Similar to temperature evolution, the thermally induced pore pressure decays rapidly with distance to the central borehole. Figure 4.14 shows the pore pressure contour plot at the end of heat injection phase in the 50th year. Additionally, the average pore pressure would exceed initial value over the first 15 years. After that, the pore pressure falls back till reaching balanced sate: where the pore pressure fluctuates around a certain value, which is the initial pore pressure, as shown in Figure 4.15.

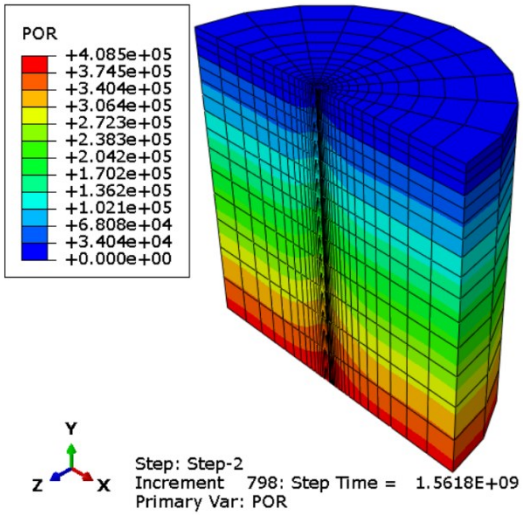

Figure 4.14 Pore pressure contour plot for the whole formation at the end of the 50th heat injection phase (unit = Pa).

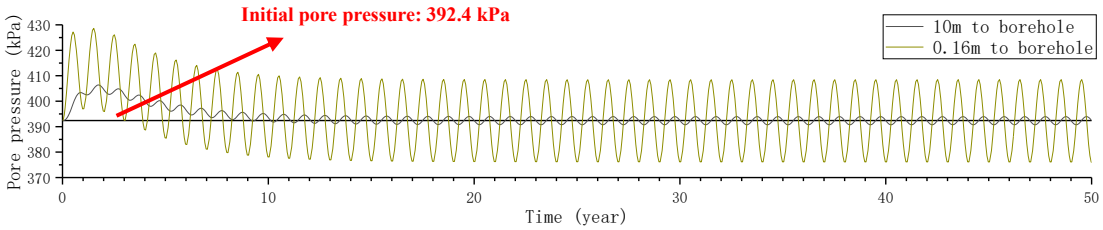

Figure 4.15 Pore pressure evolution at two locations at depth of 40 meters.

Soil is composed of soil skeleton, pore water, and air. In saturated glacial till, pore water takes all the voids. When heated, the soil skeleton and pore water expand. Due to the high thermal expansion coefficient of water and low hydraulic conductivity of glacial till, high thermally induced pore pressure would develop rapidly. The extend to which pore pressure evolves depends on the increment of temperature and the rate of increase. As stated in last section, the closer to the central borehole, both in horizontal and vertical direction, the temperature evolves more rapidly each year. Accordingly, more severe pore pressure evolution could be induced in such region.

In the first heat injection period, the underground temperature gradually increases, inducing higher pore pressure. In the adjacent region, the underground temperature increases more rapidly than far region. Accordingly, pore pressure increases at a higher rate in the adjacent region. At the start of the first heat extraction period, the underground temperature at different distance to the central borehole shows different evolution rule: in adjacent region, underground temperature starts decreasing, consistent with the borehole temperature; while as the underground temperature in far region is lower than adjacent region, heat keeps flowing to far region. As a result, the pore pressure in far region would remain increasing for a while at the beginning of the first heat extraction period. The further away from the central borehole, the longer

would this increasing trend lasts. In the first ten years, the overall underground temperature was rising, despite the temperature would fall in every heat extraction period. Due to the overall temperature rising, the overall pore pressure also increases for a certain time. After underground temperature reached its balanced state, the pore pressure evolution would gradually get stable.

From 0.16 meters to 10 meters away from the central borehole, the highest underground temperature drops rapidly from 25°C to 2.7°C under the thermal operation. Comprehensively, the amplitude of pore pressure evolution adjacent to the borehole is much more significant than that far away. For example, Figure 4.16 shows the pore pressure evolution at three locations on the plane at a depth of 35 meters. At the distance of 0.16 meters, the magnitude of annual amplitude is approximately 50 kPa. From 0.16 meters to 2 meters, the magnitude decreases to about 40 kPa. At the distance of 10 meters, it is near 10 kPa. On the same horizontal plane, the magnitude of annual amplitude decreases with distance to the central borehole.

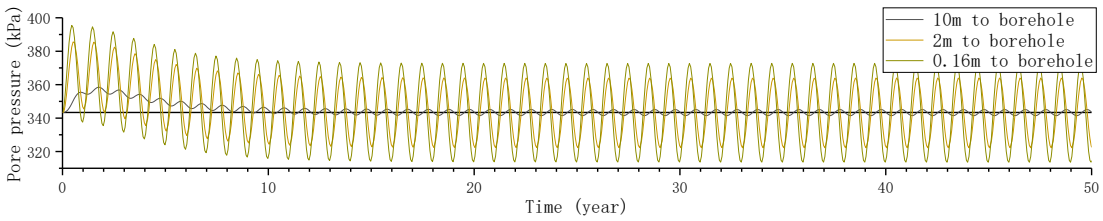

Figure 4.16 Pore pressure evolution at three locations on the plane at a depth of 35 meters (initial pore pressure: 343.35 kPa).

The initial static pore pressure distributes linearly with depth from 0 to 40 meters. The existence of a single borehole (35 meters) induces severe pore pressure evolution in underground, especially in adjacent region. During 50-year thermal

operation, the pore pressure no longer remains linearly with depth. The results reveal that the when the borehole temperature fluctuates from 1 to 30°C every year, the maximum annual amplitude of pore pressure is 70 kPa, located at the depth of 30 meters and 0.16 meters from the central borehole (Figure 4.18 (a)). As for depth of 40 meters, the underground temperature evolves less significantly than upper layer (Figure 4.18 (b)). As a result, the pore pressure fluctuates slightly less dramatically. As for soil near the top surface, where initial pore pressure is small, the pore pressure could increase by a factor of 2 during thermal operation (Figure 4.18 (c)).

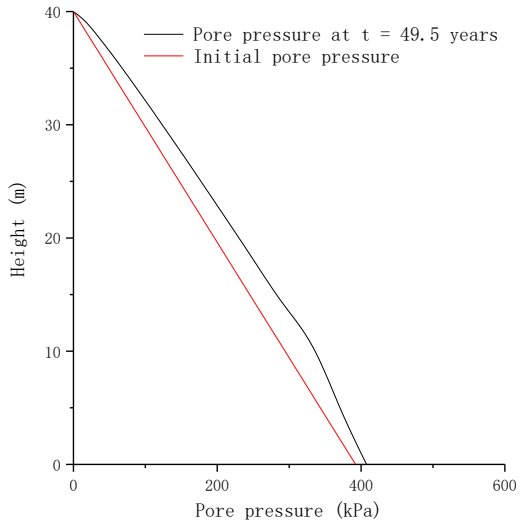

Figure 4.17 Pore pressure along depth at a moment in the 50th year (distance to the borehole: 0.16 meters).

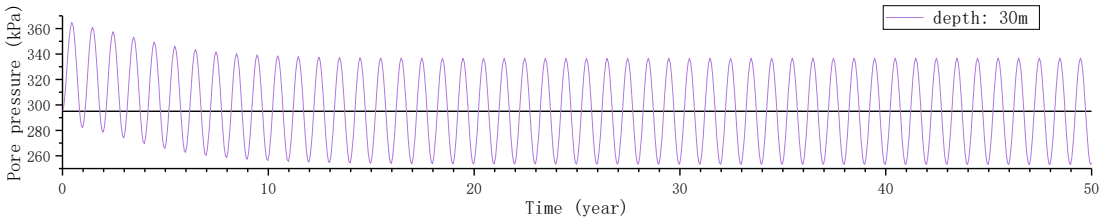

(a)

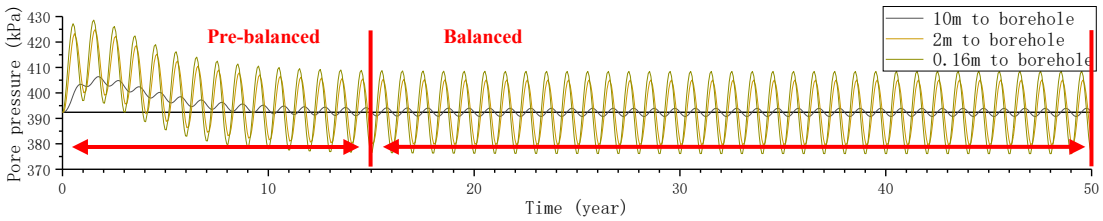

(b)

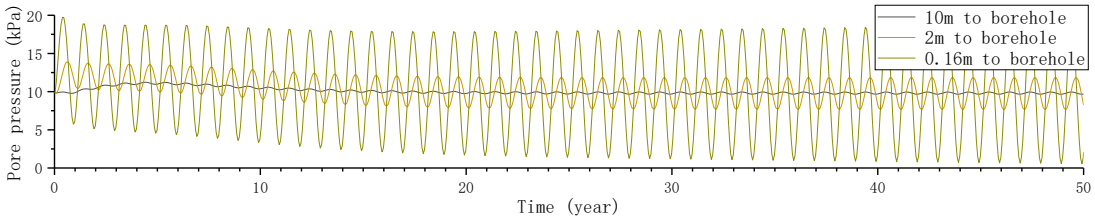

(c)

Figure 4.18 Pore pressure evolution at different depth: (a) at depth of 30 meters (initial pore pressure: 295.05 kPa), (b) at depth of 40 meters (initial pore pressure: 392.4 kPa), (c) at depth of 1 meter (initial pore pressure: 9.81 kPa).

From above pore pressure evolution figures, the pore pressure evolution process can be divided into two phases: pre-balanced phase and balanced state. During the first 15 years, the average pore pressure is always beyond the initial value: pore pressure fluctuating with increasing trend and then falls back. When the pore pressure increases as temperature goes high, it would finally dissipate. After dissipating for years, the increment of pore pressure would be lower when heated to the same temperature. After pre-balanced phase, the pore pressure reaches balanced state: it fluctuates around a certain value, which is identical to the initial pore pressure. For instance, at the depth of 40 meters (Figure 4.18 (b)), the pore pressure increases from initial value (392.4 kPa)

to 427 kPa during the first heat injection period. After falling back towards initial value during the first heat extraction period, the pore pressure increases to near 430 kPa, which is the highest pore pressure over the 50 years. Such climbing phenomenon of annual highest pore pressure is in consistent with the climbing of annual highest temperature. As mentioned in previous section, the annual highest temperature climbs at a decreasing rate and the underground temperature would reach its balanced state after the first ten years. Additionally, the excess pore pressure would finally dissipate, despite at a low rate in glacial till. Accordingly, the annual highest pore pressure would then start to fall till reaching its balanced state. In the balanced state, the pore pressure fluctuates the same for every period and the average pore pressure is identical the initial pore pressure. The pore pressure in balanced state is more stable and predictable than in pre-balanced state.

The result of temperature evolution of a single borehole system reveals that:

1. The influenced zone reflected by pore pressure is in consistent with that by underground temperature.

2. The pore pressure evolution is closely related to the temperature evolution. Before reaching balanced state, the average pore pressure is evidently higher than the initial value. In balanced state, the pore pressure fluctuates perfectly over the initial value. A single borehole has limited impact on the surrounding soil. The largest magnitude of the amplitude of pore pressure evolution curve is 70 kPa at distance of 0.16 meters to the central borehole

on the plane at the depth of 30 meters. The influence on pore pressure decreases with distance to the borehole.

Effective stresses evolution and stress path

Similar to pore pressure, effective stresses in the shape of half prolate spheroid also evolve with fluctuation over the 50-year operation. While The influence on stress state is limited as the stress paths are always within the initial yield surface (Figure 4.22). However, the overall underground effective stresses are all increased in the influenced zone after thermal operation. With borehole temperature fluctuates between 1°C and 30°C, the maximum magnitude of induced vertical effective stress is around 30 kPa, located at the depth of 30 meters from 0.16 meters to the borehole. From top surface to the depth of 15 meters, the vertical effective fluctuated with negligible amplitude. The evolution of two horizontal effective stresses less significant compared to the vertical effective stress.

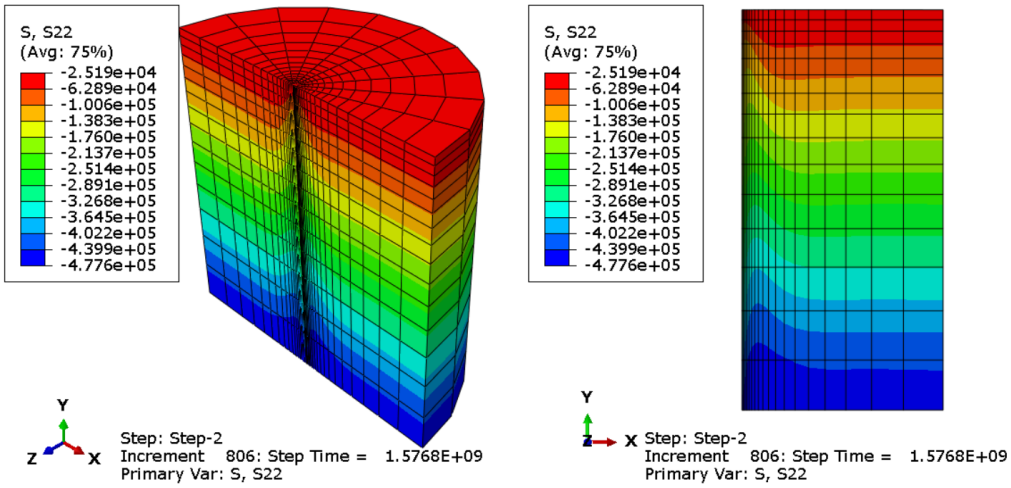

Figure 4.19 Vertical effective stress state contour plot for the whole formation at the end of the 50th heat injection phase (unit = Pa).

Figure 4.20 shows the vertical effective stress evolution at three locations on the bottom surface. With thermal operation, the vertical effective stress in the whole formation would gradually exceed the initial stress, despite with annual fluctuation. That is to say, consolidation occured over years with the operation of a BTES system with a single borehole.

It was found that in region adjacent to the borehole, the vertical effective stress and pore pressure both increased in the heat injection phases (Figure 4.20). While in far region (within 2 meters to the borehole), the vertical effective stress decreased in the heat injection phases and increased in the heat extraction phases. In heat injection phase, the whole underground temperature would increase. While in adjacent region, as the temperature evolves dramatically, the soil particles and pore water both expand significantly. In addition to pore pressure increment, the soil particles squeeze each other harder in vertical direction, inducing effective stress increasing. As a result, the total stress in vertical direction increased. While in far region, the total stress increment was much smaller (Figure 4.21) due to the less significant temperature evolution. The induced pore pressure took part of effective stress. As a result, the total vertical stress and pore pressure increased, and effective stress decreased in heat injection phases. While in heat extraction phases, the situation is reversed.

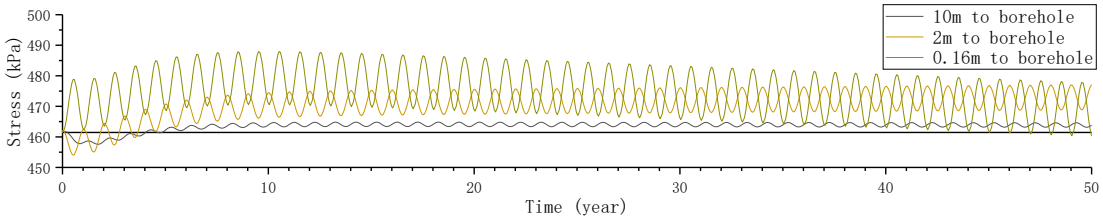

Figure 4.20 Vertical effective stress ($\sigma_1^{'}$) evolution at depth of 40 meters.

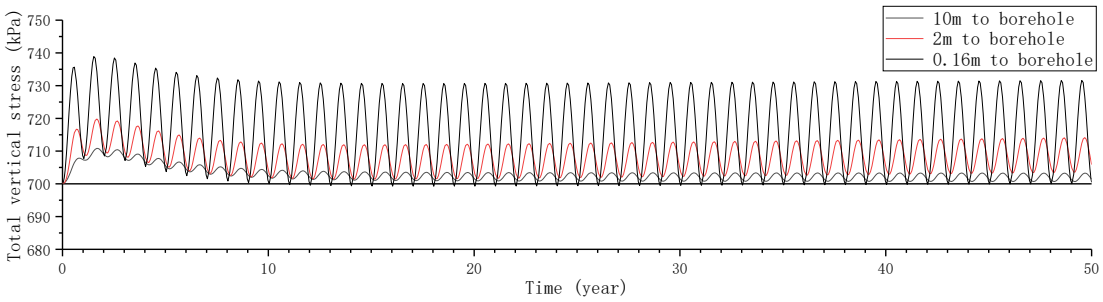

Figure 4.21 Total vertical stress (σ_1) evolution at depth of 40 meters.

From the results, it was found the PEEQ remained the same over 50 years, which is equal to half the preconsolidation pressure ($p_c^{'}/2$), that is to say, yield surface never expanded (hardening) or contracted (softening). As shown in Figure 4.22, the stress paths never intersected CSL or initial yield surface. The glacial till was always in elastic zone under the thermal operation of a BTES system with a single borehole.

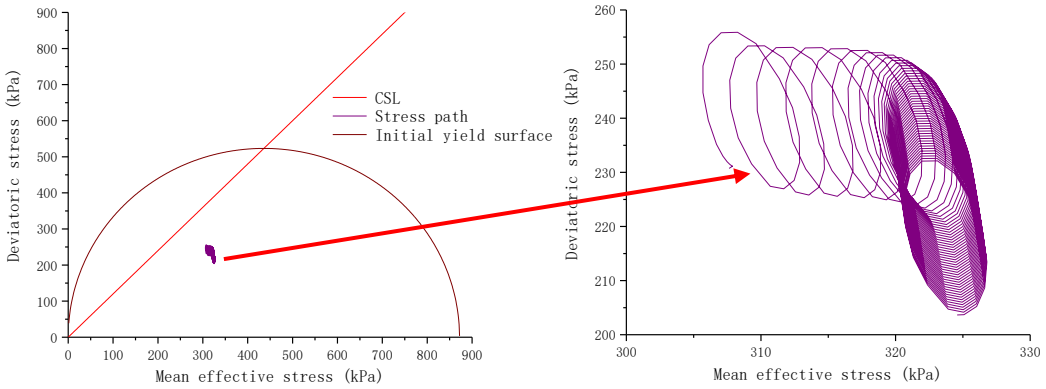

(a)

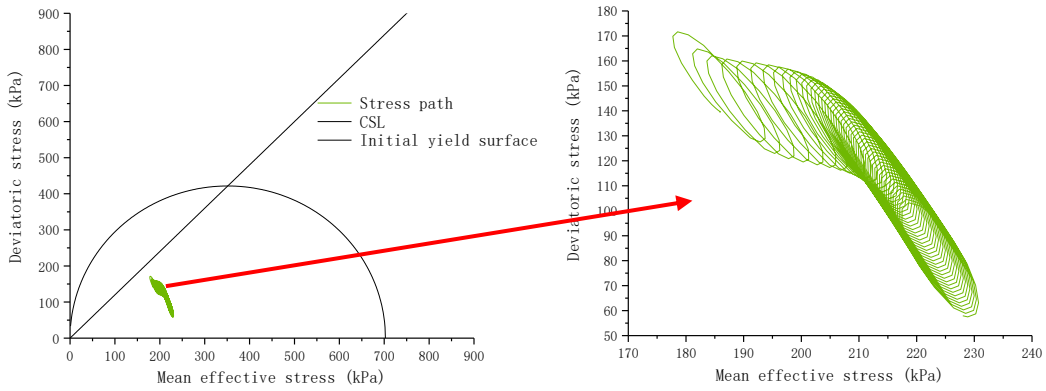

(b)

Figure 4.22 Results of simulated stress paths in the $p'-q$ plot at monitoring points located 0.16 meters from central borehole: (a) at depth of 40 meters; (b) at depth of 20 meters.

The result of temperature evolution of a single borehole system reveals that:

1. The results of effective stresses evolution and stress paths are in consistent with that of pore pressure and temperature.

2. Although the thermally influence of a BTES system with a single borehole is limited, the vertical effective stress within depth 15 to 40 meters and within distance of 2 meters to the borehole showed evident fluctuation over 50 years.

3. In heat injection phases, both pore pressure and vertical effective stress increased as severe thermal expansion happen in both soil particles and pore water in adjacent region.

4. Consolidation occurred over 50 years as the vertical effective stress eventually increased to a certain extend in the influenced zone.

Displacement evolution

With the thermal operation of a BTES system with a single borehole, the surrounding soil would undergo periodical expansion and contraction in both vertical and horizontal direction. In heat injection phases, the surrounding soil expanded. And to what extend it expand depends on the distance to the borehole. The closer to the borehole, the higher the amplitude of expansion. In heat extraction phases, the surrounding soil contracted as the temperature went down. In addition to the thermal expansion and contraction, the consolidation also plays a crucial part in vertical displacement evolution. However, the thermally induced displacement is negligible, as all the deformation is within ± 2 cm.

As shown in Figure 4.23, surrounding soil shows settlement near the borehole and expansion at a distance to the borehole in the top region at the end of 50 years. The effective vertical stress fluctuated dramatically with increasing trend in adjacent region, leading to most significant consolidation settlement (ultimate is 7 mm) within the formation. While the underground temperature raised the most in far region (Figure 4.11), the thermal expansion occurred in this region.

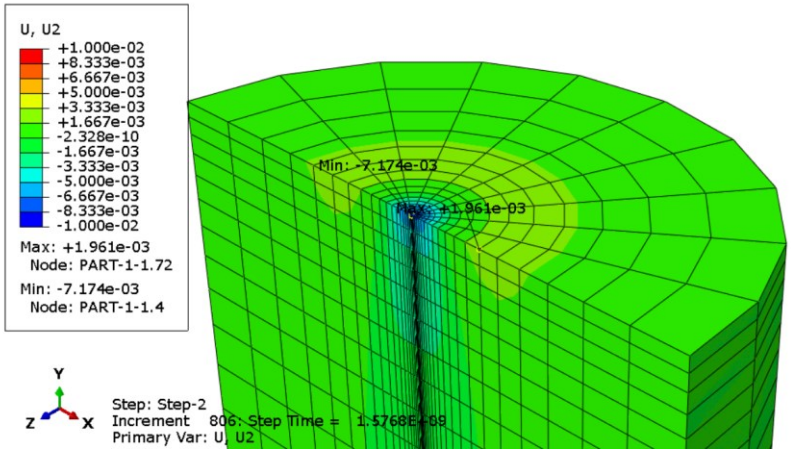

(a)

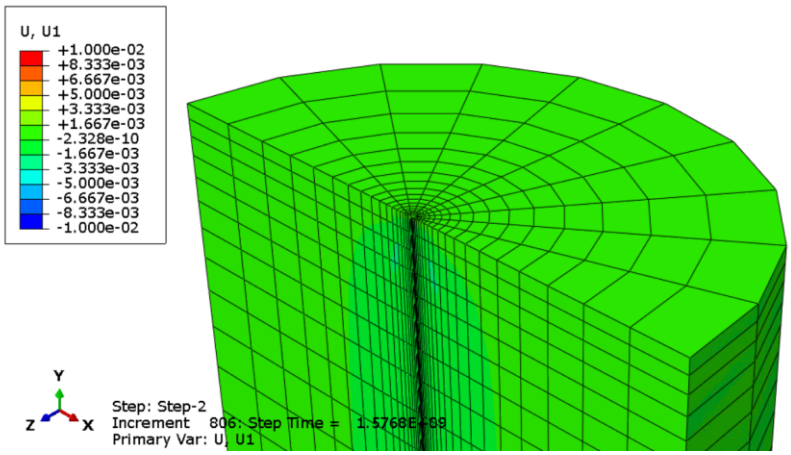

(b)

Figure 4.23 Displacement contour plot in both vertical and horizontal directions at the end of 50 years: (a) vertical displacement; (b) horizontal displacement (unit = m).

During the 50 years, the surrounding soil underwent thermal expansion and contraction, and consolidation. Figure 4.24 shows the displacement evolution at two locations on the top surface. In the first several years, the underground heaved more than the last year as the highest temperature climbed. The maximum vertical expansion occurred in the 3rd to 5th year at the two locations, 13 mm and 10 mm, respectively. Consolidation occurred over 50 years, resulting in the settlement. Theis result is in good agreement with the prediction of Gabrielsson et al. (2000), as shown in Figure 4.25. In

adjacent region, the settlement was more significant because effective vertical stress evolved dramatically. As for horizontal displacement, it expanded in heat injection phases and contracted in heat extraction phases. While the magnitude of amplitude in adjacent region is much less than that in far region. This is because the temperature gradient between the right and left side of soil particles in adjacent is smaller than that in far region.

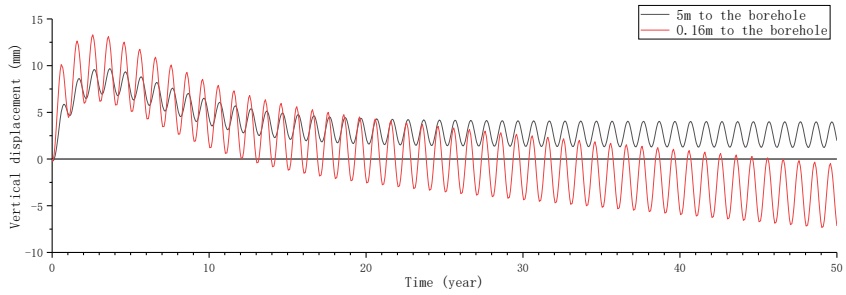

(a)

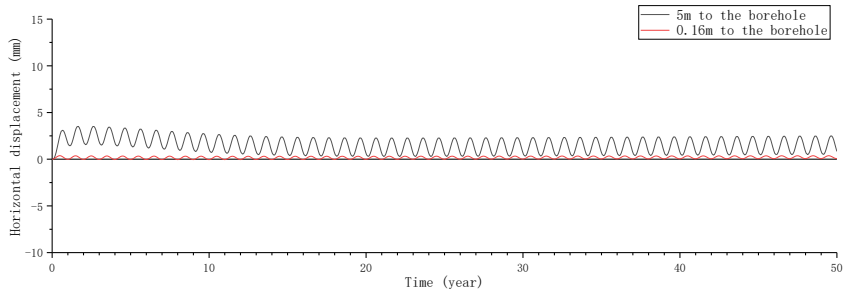

(b)

Figure 4.24 Displacement evolution at two locations on the top surface: (a) vertical displacement; (b) horizontal displacement.

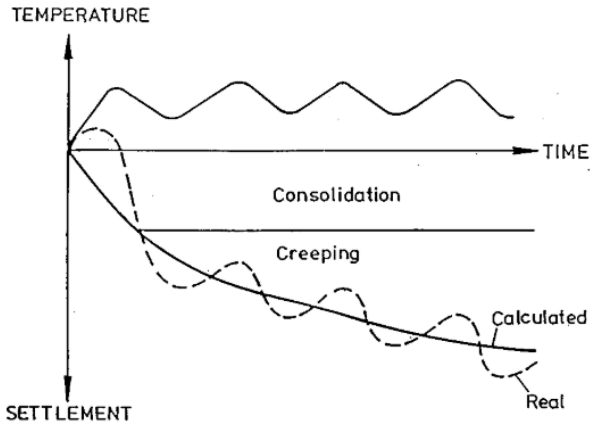

Figure 4.25 Outline of settlements in a heat store in soft clay at cyclic temperature (Gabrielsson et al., 2000).

The result of temperature evolution of a single borehole system reveals that:

1. The influence of a single-borehole BTES system on the deformation is limited and negligible. The maximum vertical expansion is 15 mm in adjacent region on the top surface. An ultimate settlement of about 7 mm occurred in the same region.

2. In consistent with pore pressure and effective stresses, the displacements also fluctuated with the thermal operation over 50 years.

Extreme scenario (60°C)

In this extreme scenario, the temperature of the central borehole would rise to 60°C after a heat injection period. The underground temperature, pore pressure, effective stresses, and deformation evolve following the same rule with the 30°C scenario. The influenced zone expands outwards a little compared to 30°C scenario. The highest temperature soil can reach drops rapidly to 10°C from adjacent region to the distance of 5 meters. And at distance of 10 meters, the glacial till temperature raised by 4°C (Figure 4.26). The maximum increment of pore pressure in a single year was

130 kPa, located at distance of 0.16 meters to the central borehole on the plane of depth of 30 meters (Figure 4.27). The stress path at a monitoring point is shown in Figure 4.28, it locates a little bit to the right side of the stress path of 30°C scenario. However, the PEEQ still remained the same over 50 years. From the view of deformation, there would be an ultimate settlement of 3 centimeters in the adjacent region and an ultimate vertical expansion of 5 millimeters on the top surface. In addition, there would be a maximum vertical expansion of 2.6 centimeters, happened in the 3rd year in the adjacent region. Above all, the influence of a single-borehole BTES system is limited, both for 30°C and 60°C scenarios.

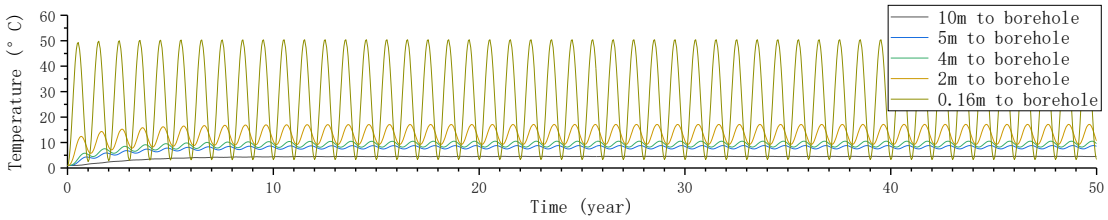

Figure 4.26 Underground temperature evolution at different distance to the central borehole on the top surface.

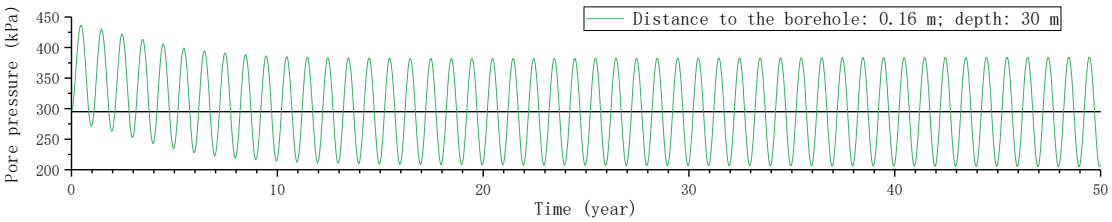

Figure 4.27 Pore pressure evolution at distance of 0.16 meters to the borehole on the plane of depth of 30 meters.

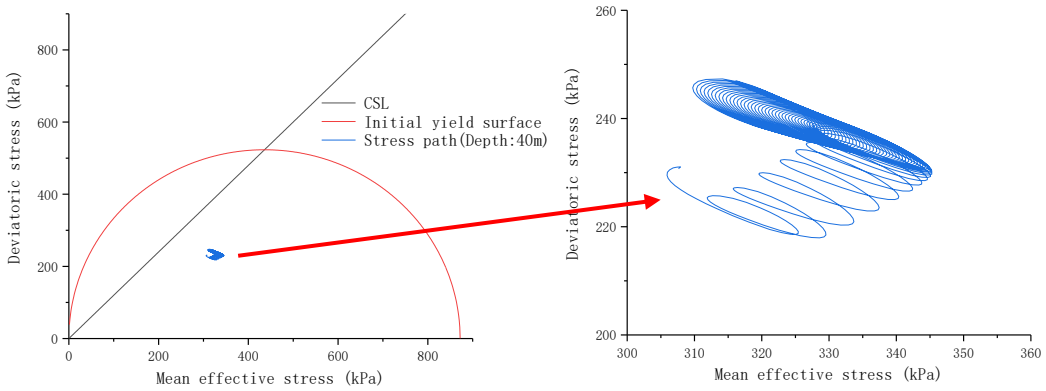

Figure 4.28 Results of simulated stress paths in the $p'-q$ plot at a monitoring point located 0.16 meters from central borehole on the bottom surface.

5 Numerical modeling of borehole groups

A major part of the heat injected via the borehole quickly dissipated into the surrounding soil in a single borehole storage system. Such dissipation was much insignificant in a three-borehole system. Therefore, a single borehole is less efficient for storage than a borehole group (Lanini et al., 2014).

The efficiency of the geothermal borehole thermal energy storage (BTES) systems decreases with the increases of distance between boreholes (Lanini et al., 2014).

Arrays with smaller borehole spacings permit more concentrated storage of heat at higher temperatures (Baser & McCartney, 2015). Heat energy harvested by solar collectors are the same in both single-borehole and borehole-group systems. Multiple boreholes provide much wider contact surface, through which heat conduction happens, with underground soil than a single borehole. That is to say, a single borehole system concentrates heat in the center area, while a borehole group system stores heat in a wider area. Accordingly, borehole group systems are more likely to reach a lower temperature in a larger volume than a single borehole under the same conditions.

The ABAQUS simulation results of a single borehole BTES system indicates that the thermally induced deformation is minimal. While the deformation evolution and stress state evolution are much more severe in multi-borehole systems.

5.1 Five-Borehole in triangular array

By adding boreholes and solar collectors, more heat energy could be stored in BTES system. To evaluate the effect of borehole groups on the glacial till, five-borehole BTES system and 100-borehole BTES system are modelled in this chapter.

5.1.1 ABAQUS model

The configuration of boreholes in five-borehole BTES system is referred to Baser and McCartney (2015). The five boreholes of 35 meters in depth are in a triangular array with spacing of 2 meters, as shown in Figure 5.1. The finite element model along with the generated mesh is illustrated in Figure 5.2. On the basis of the single-borehole model, the size of the five-borehole model is broadened. This is to take into account the entire influenced area, considering the five-borehole could induce more severe temperature, stress, and deformation evolution in a wider zone. The diameter of the modeled region is 100 meters, with a thickness of 40 meters. A total of 19888 nodes and 18480 elements (C3D8PT type) were generated. The boreholes and glacial till formation treated as a continuous body, where the dislocation behaviour among different parts cannot be modeled in this study.

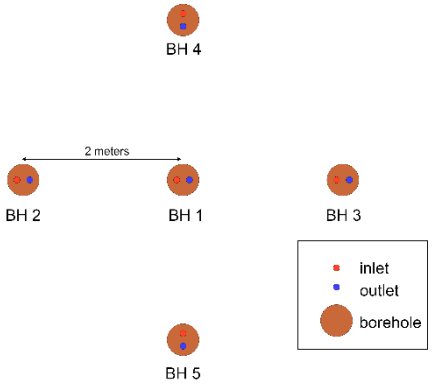

Figure 5.1 Sketch of boreholes arrangement on the top surface.

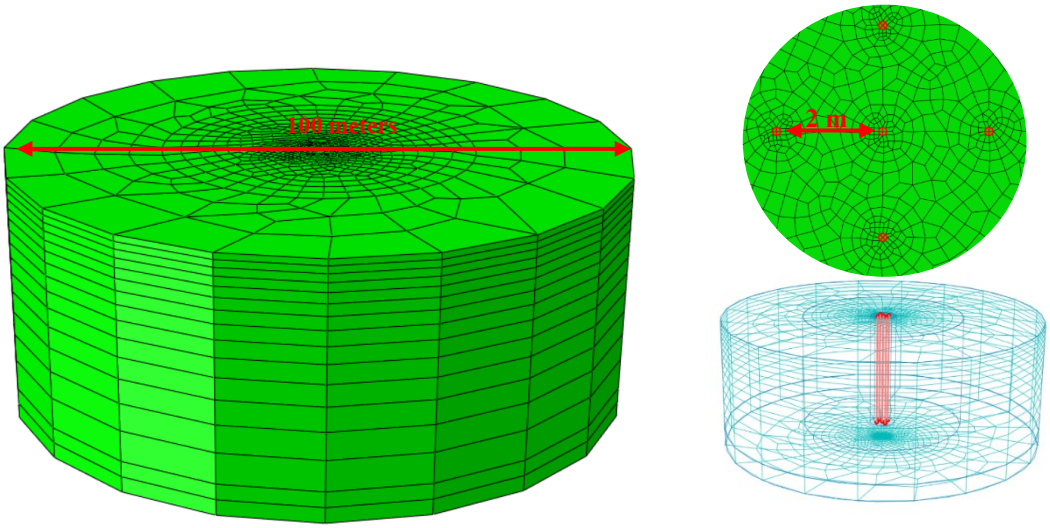

Figure 5.2 The 3D finite-element model along with generated mesh for a five-borehole BTES system.

5.1.2 Results

The thermal operation of a BTES system with five boreholes, whose temperature evolves periodically between 1°C and 30°C, has a certain impact on surrounding glacial till. Similar to the Single-borehole model, the thermally influenced region is also in a shape of half prolate spheroid, whose top surface is a circle with a radius of about 30 meters. The whole region is divided into three zones based on the degree of thermal influence. Zone 1 is a cylinder with diameter of 8 meters in the center of the formation. In Zone 1, underground temperature, pore pressure, effective stresses, and deformation evolves the most dramatically. Zone 2 is an annular cylinder next to Zone 1, with outer diameter of 60 meters. And Zone 3 is the rest of the formation, where there is barely no thermal impact.

Within the influenced zone, seasonal underground temperature evolution was observed. And such impact on surrounding glacial till weakens rapidly with distance to the boreholes.

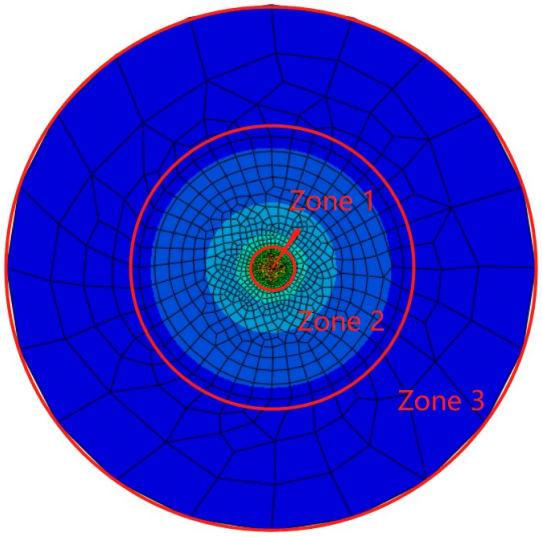

Figure 5.3 The schematic view of three zones.

Temperature evolution

Results of 50-year run BTES system shows that the whole thermal influenced zone is approximately in a shape of half prolate spheroid, whose top surface is a circle with a radius of around 30 meters. Figure 5.4 shows the temperature contour plot at the end of heat injection phase in the 50th year.

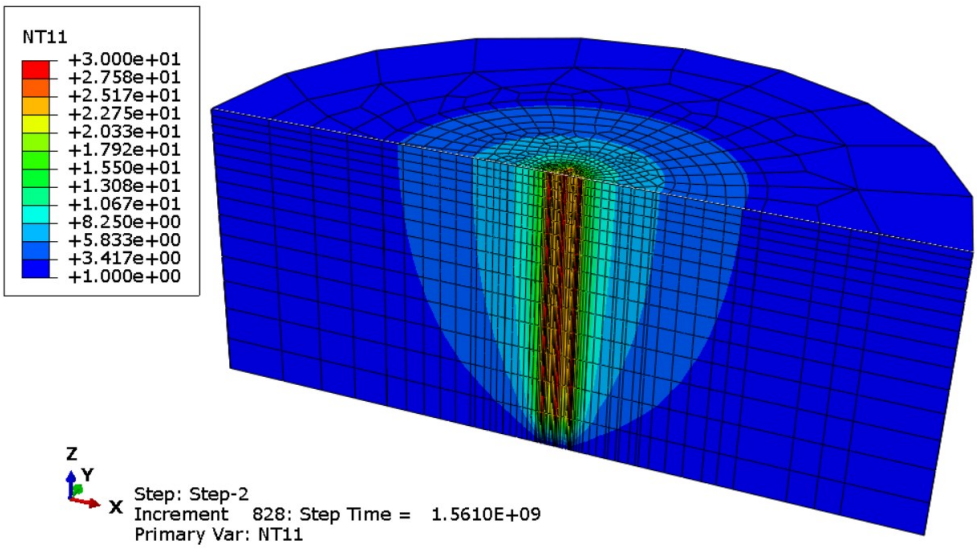

Figure 5.4 Underground temperature profile at the end heat injection phase in the 50th year (unit = °C).

The temperature evolution is similar to that of Single-borehole system. The highest temperature drops with distance to the central borehole. The highest temperature increment in a single year is 27°C, at the distance of 0.16 meters to the central borehole in Zone 1 (Figure 5.5 a), which is higher than at the same location in single-borehole system. This is because the surrounding four other boreholes allow more heat to be stored in the central area (Zone 1). The closer to the boreholes, the higher is the highest temperature. The annual temperature increment was higher than 10°C in the whole Zone 1, and a large part of it was over 20°C. In Five-borehole system, the temperature evolutions at two locations, which are at distance of 0.8 and 1.2 meters to the central borehole along x-axis, respectively, are nearly the same, which are slightly lower than that at distance of 1.8 meters (Figure 5.5 b). Because it is closer to one of the boreholes at the distance of 1.8 meters. In general, a high temperature could be reached, and the overall underground temperature evolves the most dramatically in Zone 1. The farthest point that can reach 10°C is 6 meters from the center (2 meters for Single-borehole system). In Zone 2, the highest temperature drops rapidly with distance. As shown in Figure 5.5 a, the temperature evolution at distance of 8 meters barely fluctuates over 50 years, despite it could reach 8°C after years. When the distance increased to 25 meters, the ultimate temperature is only near 3°C. This is to say, the thermal influence is most severe in Zone 1, and it weakens rapidly in Zone 2. In heat injection phases, Zone 1 is heated the most. In heat extraction phases, temperature in Zone 1 could drops below that in Zone 2 shortly, allowing heat transfers from Zone 2 to Zone 1 (Figure 5.7).

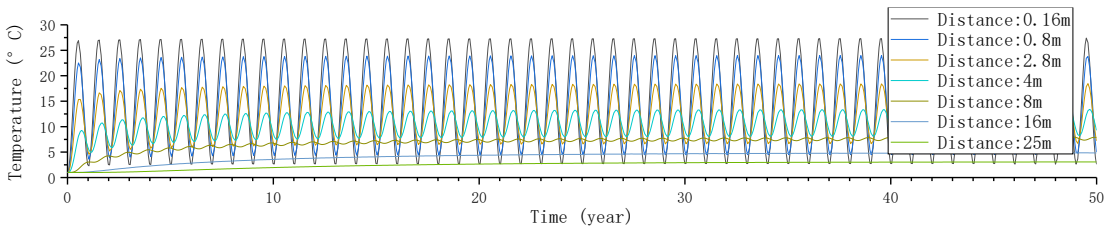

(a)

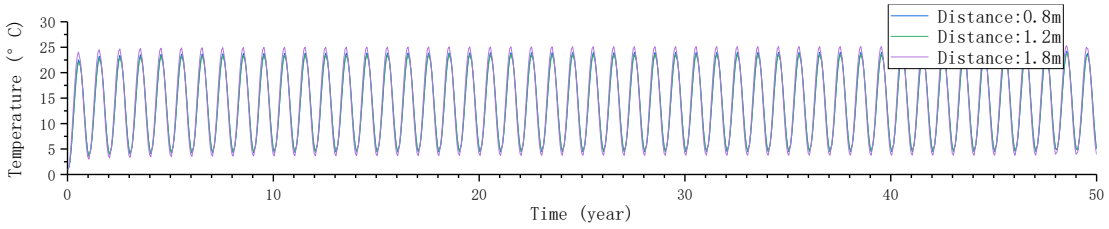

(b)

Figure 5.5 Underground temperature evolution at different locations on the top surface.

Figure 5.6 shows the underground temperature evolution along depth. The underground temperature evolved nearly the same from top surface to depth of 20 meters. The temperature decreases gradually along depth from 20 to 40 meters. This is in consistent with the result of single-borehole system.

The temperature evolution curve includes two phases: climbing state and balanced state. The closer to the boreholes, the closer to the borehole temperature is the till temperature, the shorter is the climbing state, the larger is the annual amplitude of temperature evolution. As shown in Figure 5.6 a, the underground temperature at distance of 4 meters to the central borehole on the top surface approached to 10°C after the first heat injection phase. While it got higher in the next heat injection phase. After 10 years, it finally climbed to 13°C. The climbing state indicates the extension of influenced region: the underground temperature increased to near 10°C at the distance of 4 meters after the first heat injection phase. It could not reach 27°C as that at the

distance of 0.16 meters because it received less heat energy. However, 10°C is not the cap. Years after years, the highest temperature at distance of 4 meters got higher, and so did soil at further distance. Accordingly, the influenced region got wider.

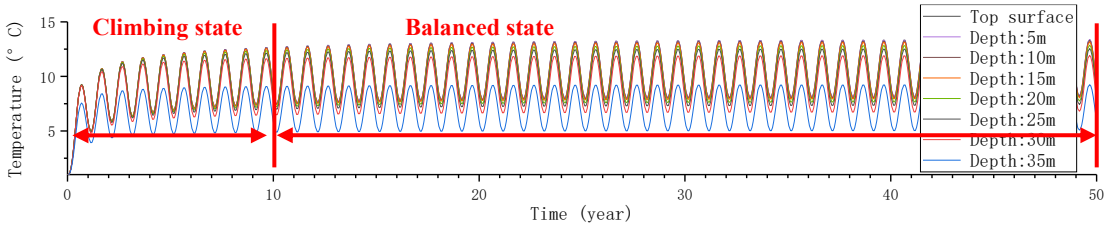

(a)

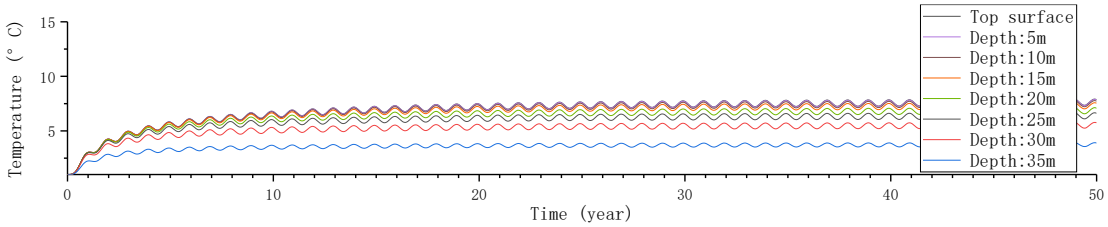

(b)

Figure 5.6 Underground temperature evolution along depth: (a) at the distance of 4 meters to the central borehole; (b) at the distance of 8 meters.

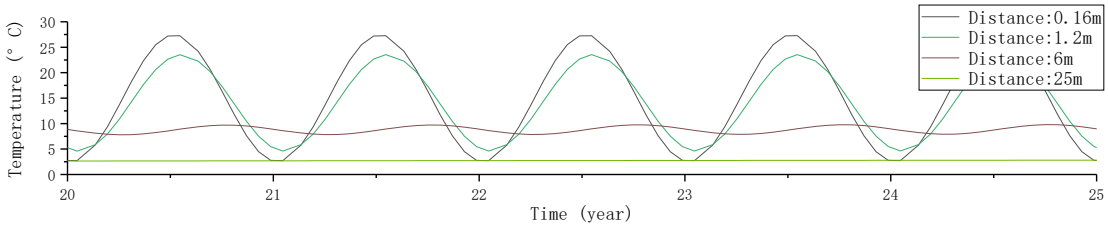

Figure 5.7 Underground evolution from 21st to 25th year.

The result of temperature evolution of five-borehole system reveals that:

1. The shape of influenced region is half prolate spheroid, similar to that of a single-borehole system. However, the area of influenced region and the degree of influence are larger than that of single-borehole system. The evolution rule is similar to that of a single-borehole system.

2. Zone 1 suffers severe thermal influence; Zone 3 is out of thermal influence.

Pore pressure evolution

Glacial till in Zone 1 and Zone 2 suffered periodical pore pressure changing. The evolution rule is similar to that of a single borehole system, but more severe. The annual pore pressure increment is over 180 kPa over 50 years at depth of 30 meters in the center area of Zone 1.

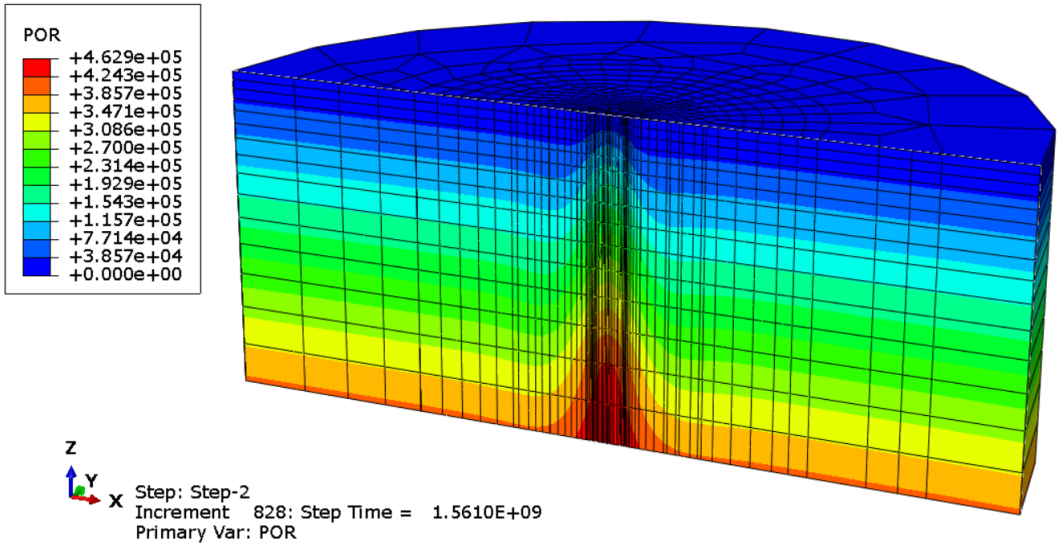

Figure 5.8 Pore pressure contour plot at the end of heat injection phase in the 50th year (unit = Pa).

The increment of pore pressure is nonlinearly along depth. The largest increment appeared at the depth of around 30 meters. This is because the borehole is 35 meters long, the bottom 5 meters layer would receive less heat energy in heat injection phase. As for soil near the top surface, where initial pore pressure is small, the impact is the same severe at the upper layer, the pore pressure could increase by a factor of 2 during thermal operation (Figure 5.9).

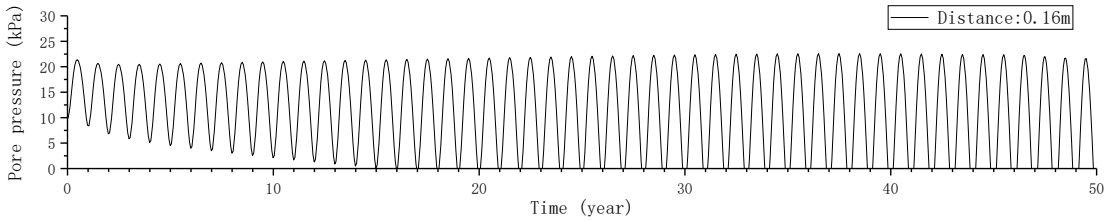

Figure 5.9 Underground pore pressure evolution at distance of 0.16 meters to the central borehole at depth of 1 meter.

The thermal influence on pore pressure drops with distance to the boreholes. Figure 5.10 shows the pore pressure evolution over 50 years at four locations on the plane of depth of 30 meters. In five-borehole system, annual increment of over180 kPa in pore pressure was observed at the distance of 0.16 meters to the central borehole at the depth of 30 meters. Also, the pore pressure evolution is nearly the same for till at distance of 0.16, 0.8, and 1.2 meters. That is to say, the pore pressure evolved dramatically in a large part of Zone 1. At distance of 6 meters, the annual increment is 70 kPa, which is equal to the annual increment at distance of 0.16 meters in a single borehole BTES system. The increment at distance of 30 meter is always lower than 10 kPa, indicating the edge of thermal influence.

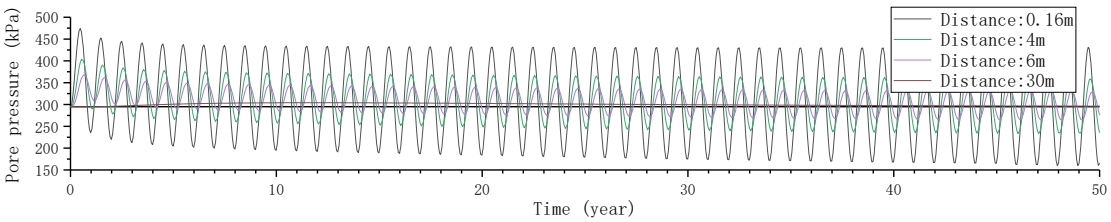

Figure 5.10 Underground pore pressure evolution over 50 years at four locations on the plane of depth of 30 meters.

Effective stress evolution and stress path

In five-borehole scenario, vertical effective stress decreased with the heat injected into underground and increased with the underground temperature got lower.

The vertical effective stress within influenced region fluctuated with increasing trend over 50 years. And the ultimate increment in the vertical effective stress could reach 300 kPa over 50 years, locates at the distance of 0.16 meters to the central borehole on the plane of depth of 20 meters (Figure 5.11).

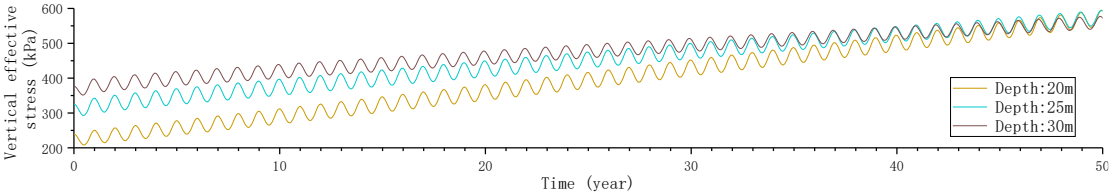

Figure 5.11 Vertical effective stress evolution in adjacent region at different depth.

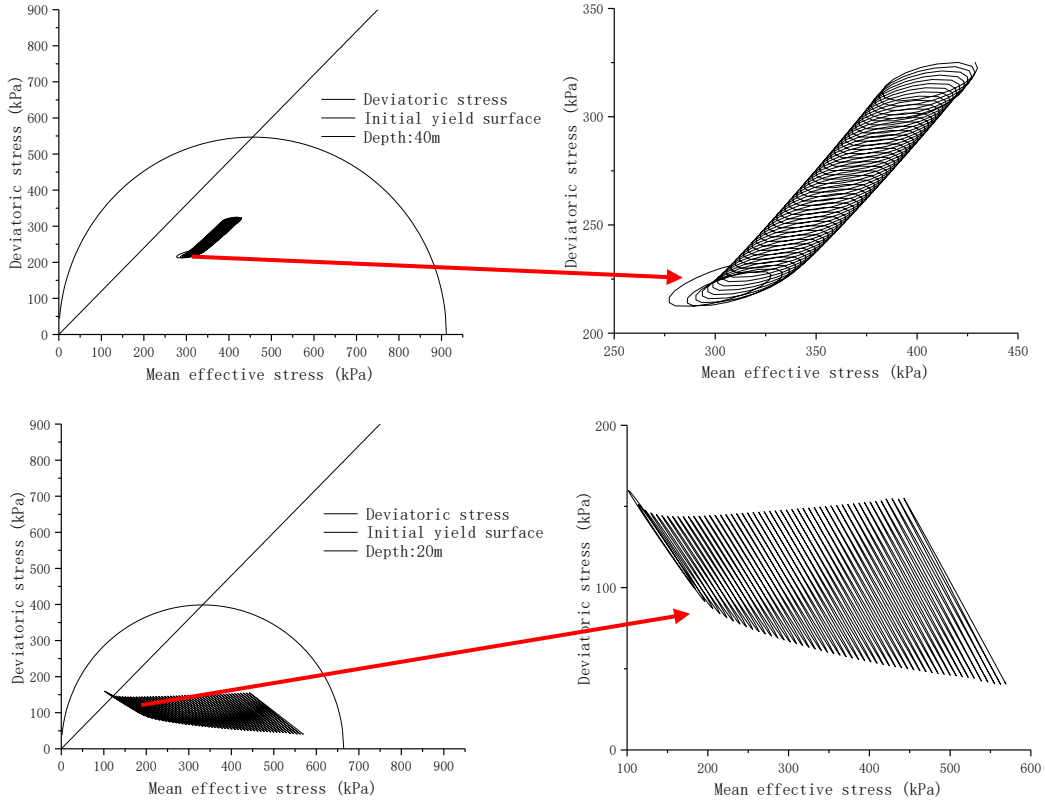

Figure 5.12 Results of simulated stress paths in the $p'-q$ plot at monitoring points located 0.16 meters from central borehole: (a) at depth of 40 meters; (b) at depth of 20 meters.

Although the results indicates that the PEEQ never changed over 50 years, the stress paths were more violent than that of a single borehole BTES system. Figure 5.12 shows the stress paths at distance of 0.16 meters to the central borehole at different

depths. From depth of 20 meters to 40 meters, the magnitude of amplitude of pore pressure and effective stresses are the hugest within the whole influenced region. The stress paths of these two reference points were always within the initial yield surface, indicating the elastic mechanical response over 50-year thermal operation. Nevertheless, things are different for 60°C scenario.

Displacement

The deformation is similar to that of a single borehole. As shown in Figure 5.13, an ultimate settlement in the center of top surface and ultimate heave in Zone 2. The ultimate settlement is 3.7 centimeters in the center of top surface. And there are the maximum annual thermal vertical expansion and maximum vertical expansion over 50 years at the same locations: 2.3 cm and 2.8 cm, respectively (Figure 5.13). There would be approximately 1 cm vertical expansion on the top surface in Zone 2.

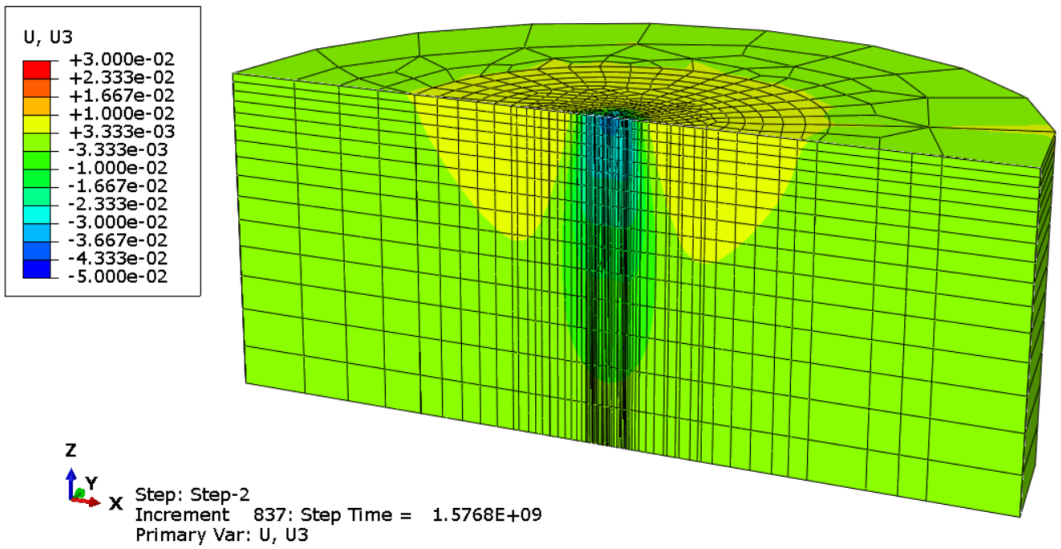

Figure 5.13 Vertical displacement contour plot at the end of 50 years (unit = m).

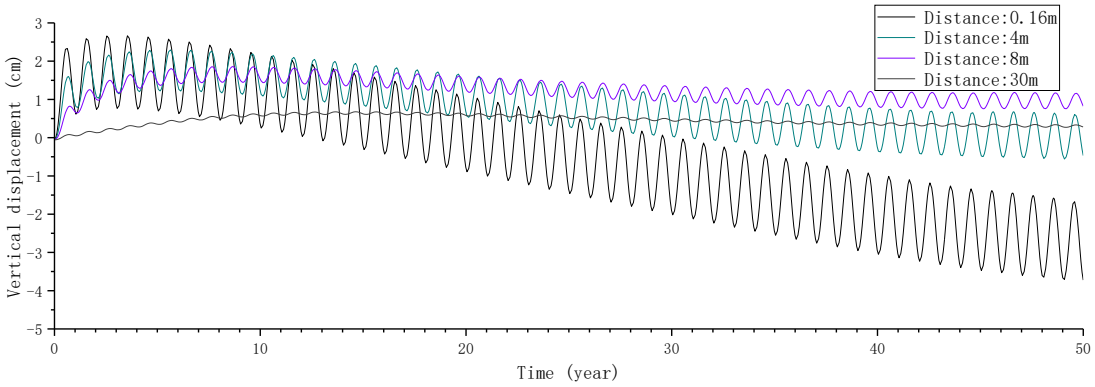

Figure 5.14 Vertical displacement evolution at four locations on the top surface over 50 years.

As shown in Figure 5.15, the horizontal expansion is less significant compared to vertical expansion. In addition, the existence of a horizontal contraction region within depth of 5 to 30 meters in Zone 1 indicates the boreholes could be compressed by surrounding glacial till. The contraction aggravated over years since it appeared in around the 10^{th} year. Figure shows the vertical displacement evolution of the point, where there is the most severe vertical contraction. At the end of 50 year, the ultimate vertical contraction was 0.5 cm. Although horizontal displacement is unimpressive in five-borehole BTES system, the horizontal contraction inside of the formation and horizontal expansion on the top surface could be severe in a 100-borehole BTES system.

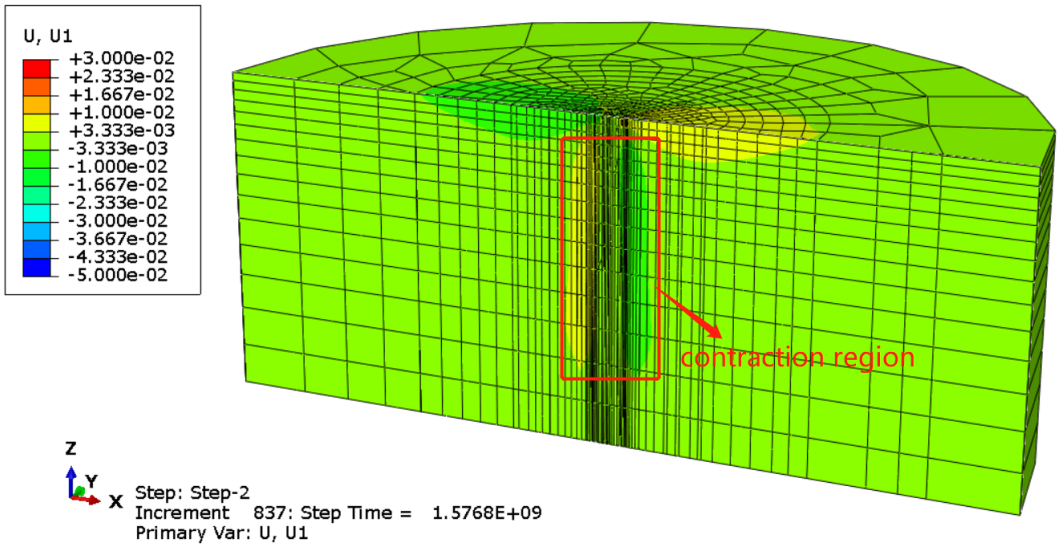

Figure 5.15 Horizontal displacement contour plot at the end of 50 years (unit = m).

5.1.3 Extreme scenario (60°C)

In this extreme scenario, the temperature of the five boreholes would rise to 60°C after each heat injection period and fall back to 1°C after each heat extraction phase. The underground temperature, pore pressure, effective stresses, and deformation evolve following the same rule with the 30°C scenario. However, the result of PEEQ indicates the existence of plastic strain within Zone 1 after 10-year operation in extreme scenario.

As shown in Figure 5.16, the influenced region and the magnitude of the displacement was close to that of the 30°C scenario. In contraction region mentioned in displacement section, there was vertical contraction for 60°C scenario. That is to say, the contraction in the contraction region is aggravated as the borehole temperature is increased from 30°C to 60°C. The contraction region distributes within depth of 2 meter to 20 meters in Zone 1, with maximum vertical contraction of 6.5 cm at the depth of 10 meters. While the ultimate settlement on top surface in zone 1 is 1~4 cm, and the

ultimate vertical expansion on top surface in Zone 2 is around 3 cm. In addition, the annual vertical thermal expansion is around 5 cm in Zone 1.

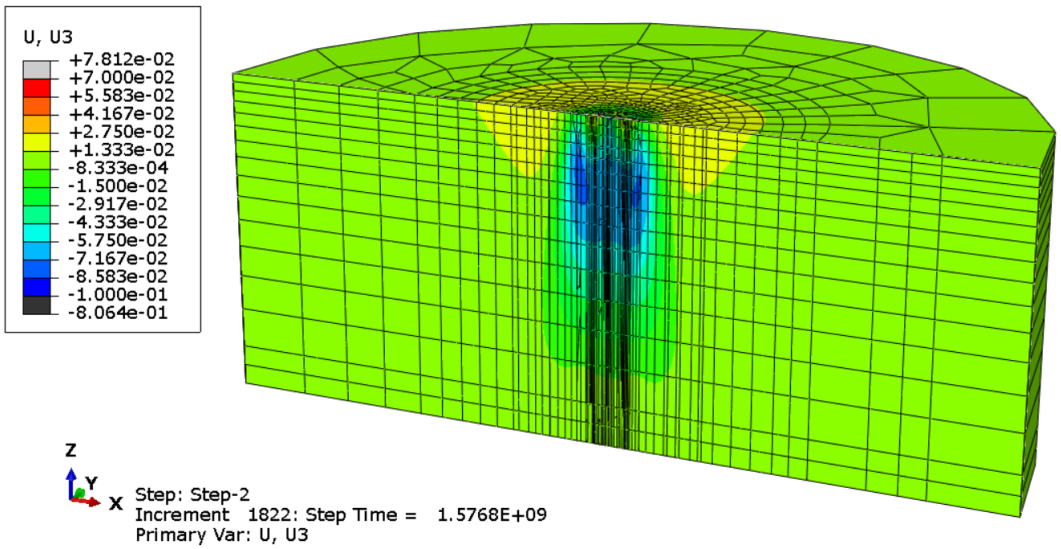

Figure 5.16 Vertical displacement in contour plot at the end of 50 years (unit = m).

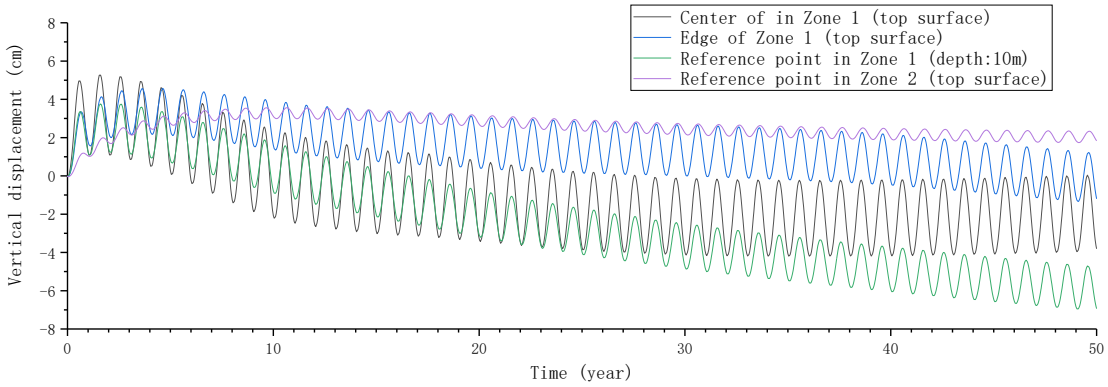

Figure 5.17 Vertical displacement evolution at four reference points.

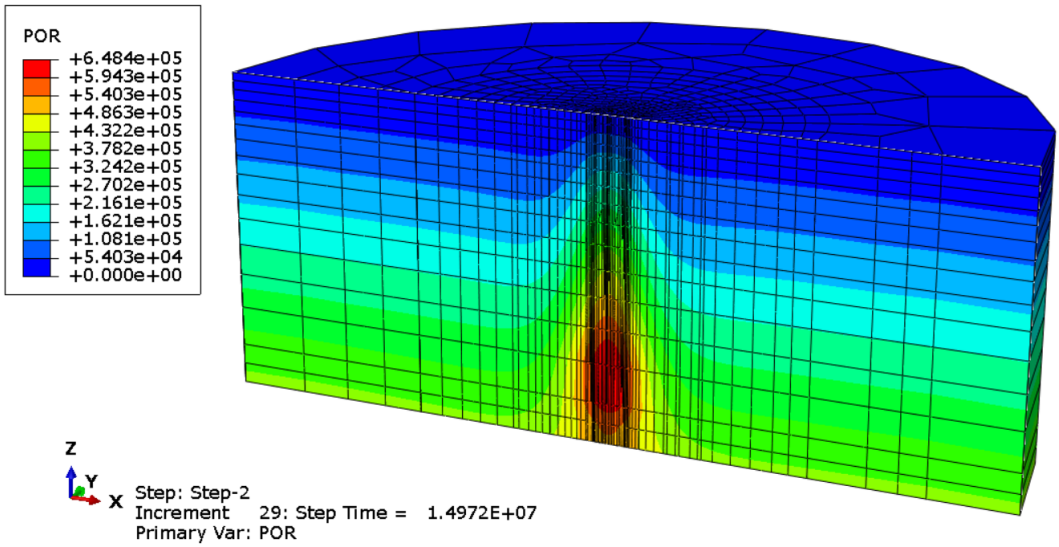

Figure 5.18 Pore pressure contour plot at the moment maximum value appeared (the end of the first heat injection phase) (unit = Pa).

However, severe impact on stresses appeared in the 60°C scenario. Pore pressure contour plot is shown in Figure 5.18. Pore pressure on the plane of depth of 30 meters could reach a maximum value of 650 kPa. The increment in pore pressure for the first year was about 350 kPa under extreme scenario. In addition, the horizontal effective stresses and vertical effective stresses evolved dramatically as temperature and pore pressure evolved. Similar to that of 30°C scenario, vertical effective stresses in influenced region fluctuated with increasing trend over 50 years. Interestingly, in 60°C scenario, horizontal effective stresses could exceed beyond vertical effective stresses in a large region during thermal operation. For example, the horizontal effective stresses eventually exceeded vertical effective stress at the location from 0.16 meters to the central borehole on the plane of depth of 10 meters. This results in the complexity of deformation in vertical and horizontal directions.

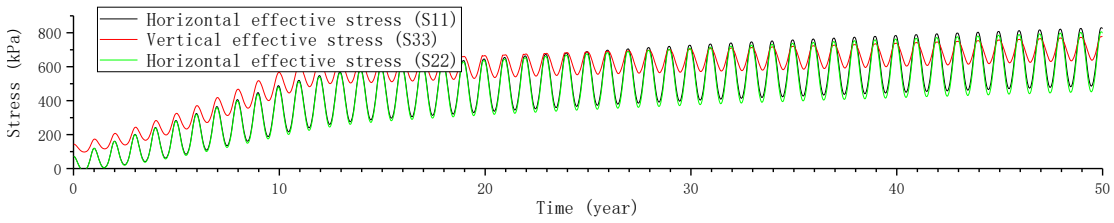

Figure 5.19 Effective stress evolution at the location from 0.16 meters to the central borehole at depth of 10 meters.

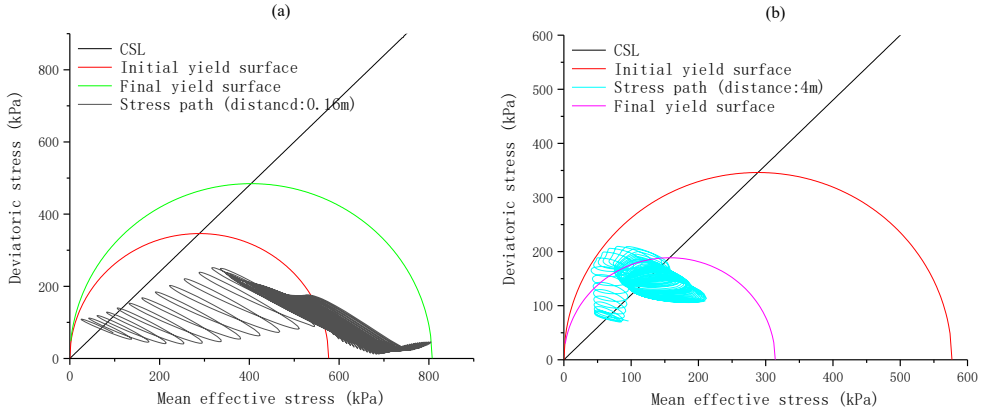

Figure 5.20 Results of simulated stress paths in the $p'-q$ plot at monitoring points located 0.16 meters and 4 meters from central borehole on the plane of depth of 10 meters.

It was found that the glacial till would suffer strain hardening or strain softening with the borehole temperature raised and fell periodically between 1°C and 60°C. Figure 5.20 describes the stress paths of two locations on the plane of depth of 10 meters in Zone 1. The overconsolidation ratio (OCR) is 4.5 on this Plane. The stress path of the point from 0.16 meters to the central borehole evolved tortuously and violently. After it touched the initial yield surface to the right of the CSL, the yield surface started to expand (strain hardening), causing plastic strains. As shown in Figure 5.20 a, after touching the initial yield surface, the stress path kept moving forward until the end of 50^{th} heat cycle. Accordingly, the glacial till at this location would keep getting denser during the thermal operation. As for glacial till a little further away, for example at

distance of 4 meters, the stress path showed the opposite rule: strain softening. The stress path evolved tortuously with less span in mean effective stress, as the stresses evolved less significantly than at distance of 0.16 meters. The stress path traversed the CSL within the initial yield surface and then touched the initial yield surface to the left, during which the soil sustained elastic strains. After then, the yield surface started to contract, and the stress path started to move towards CSL until failure. When the depth exceeds 30 meters, the PEEQ no longer decreases whatever the distance to the central borehole (Figure 5.23). That is to say, strain softening didn't happen within ten meters of the bottom. The results also revealed that the region where strain softening happened is approximately identical to the contraction region.

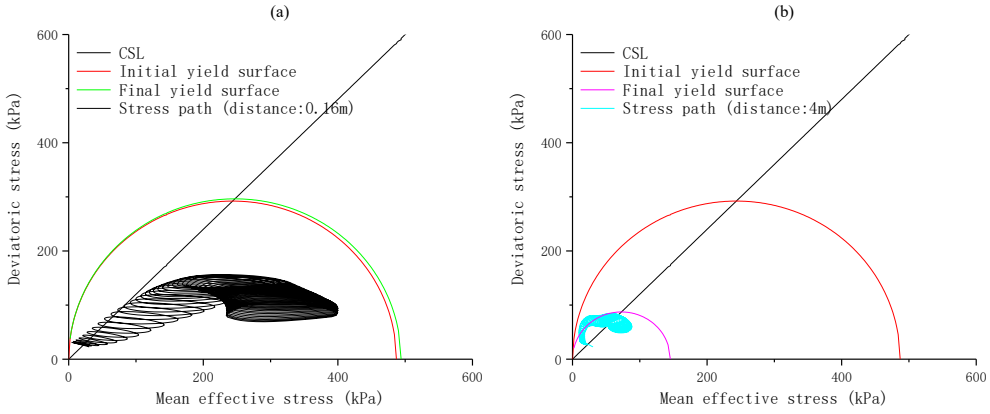

Figure 5.21 Results of simulated stress paths in the $p'-q$ plot at monitoring points located 0.16 meters and 4 meters from central borehole at depth of 2 meters.

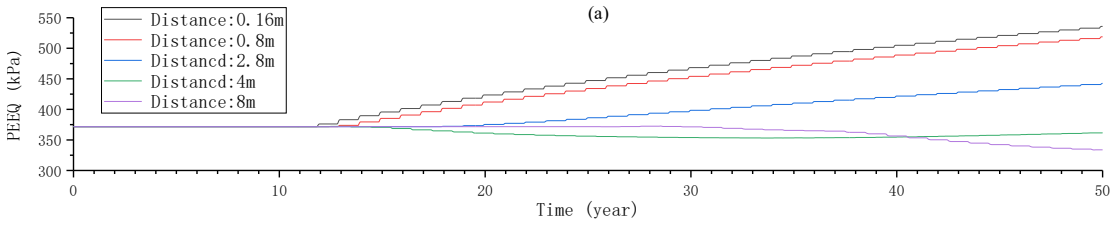

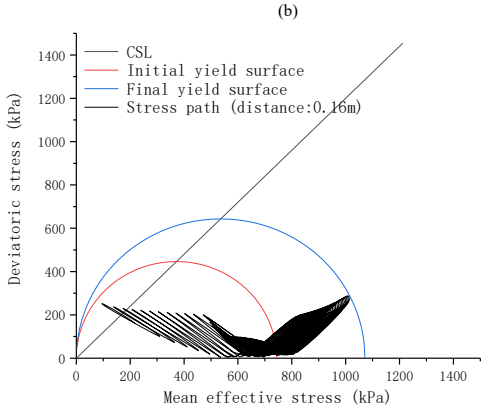

Figure 5.22 Results of PEEQ and simulated stress paths in the $p'-q$ plot at monitoring points on the plane of depth of 25 meters.

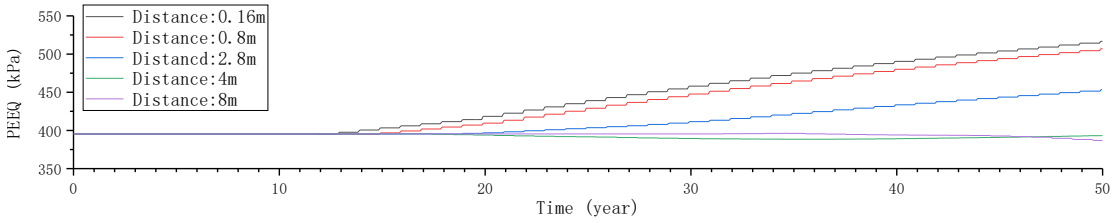

Figure 5.23 PEEQ evolution on the plane of depth of 30 meters.

In addition, the maximum increment in PEEQ, 150 kPa, appeared at distance of 0.16 meters to the central borehole within depth of 25 to 30 meters (Figure 5.22 and Figure 5.23).

Table 5.1 Strain summary of Model 1 and Model 2.

Model		Boreholes	Space room	Highest temperature	Strain
Model 1	a	1	-	30°C	Elastic
	b	1	-	60°C	Elastic
Model 2	a	5	2m	30°C	Elastic
	b	5	2m	60°C	Elastic and Plastic (hardening, softening)

5.2 100-Borehole in a different array

A 100-borehole BTES system is capable for the demand of a community. The configuration of the 100-borehole BTES systems is referred to Giordano and Raymond (2019). The borehole temperature is set as the same for all the five boreholes in a five-borehole BTES system. While temperature gradient between boreholes is not neglectable in a 100-borheole system. In a large storage system, the path of fluid in the tubes are long enough to induce large different temperature at inlet and outlet. A gradient of 5°C is set for 100-borehole systems. Giordano and Raymond (2019) concluded in their report that when the spacing room is 1.9 meters in circular array, the center could reach a higher temperature. While the spacing room increases to 3.8, the heat loss would be less. In addition, a BTES system with boreholes in square array has the least heat loss, leading to a relatively homogeneous underground temperature within the storage. Accordingly, a total of three models with different configuration array are studied (Table 5.2). The highest borehole temperature is set as 35°C for Model 3. The borehole temperature gradient is 5°C between central 20 boreholes and outer 40 borheoles

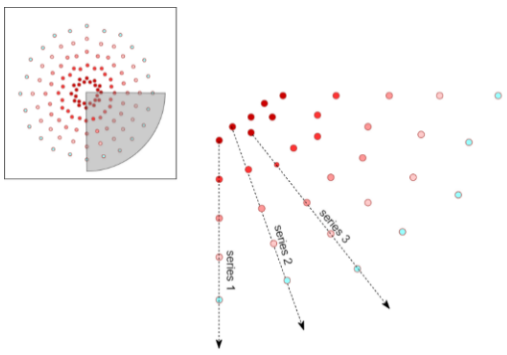

Figure 5.24 Storage shape and boreholes arrangement on the top surface (after Giordano & Raymond, 2019).

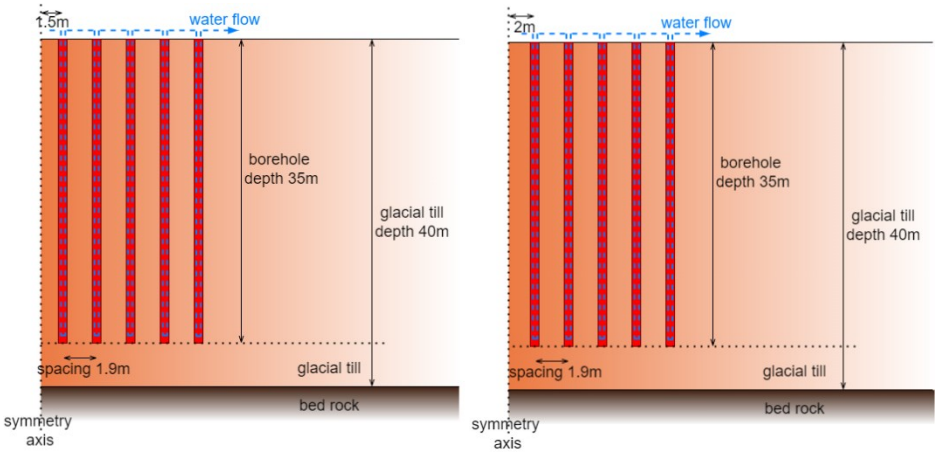

Figure 5.25 Longitudinal cross section views of series 1 (right) and series 2 (left).

Table 5.2 Group setting for 100-Borehole BTES system.

Group		Boreholes	Space room	Highest temperature		
				Central 20 boreholes	Middle 40 boreholes	Outer 40 boreholes
Model 3	a	100	1.9	35°C	32.5°C	30°C
	b	100	1.9	60°C	57.5°C	55°C
Model 4		100	3.8	30°C	27.5°C	25°C
Model 5		100	2.9	30°C	29°C	28°C

5.2.1 ABAQUS model

To simulate the 100-borheole BTES systems using ABAQUS, a large dimension in $x-y$ plane is defined. The diameter of the formation is 400 meters. This is to take account the whole influenced zone. The finite element model along with the generated mesh is illustrated in Figure 5.26. Boundary conditions are defined the same with the single borehole system and the five-borehole system, except the temperature on the bottom surface is no longer fixed at initial value (1°C).

Based on the research of Giordano and Raymond (2019), three models in different configuration array are studied.

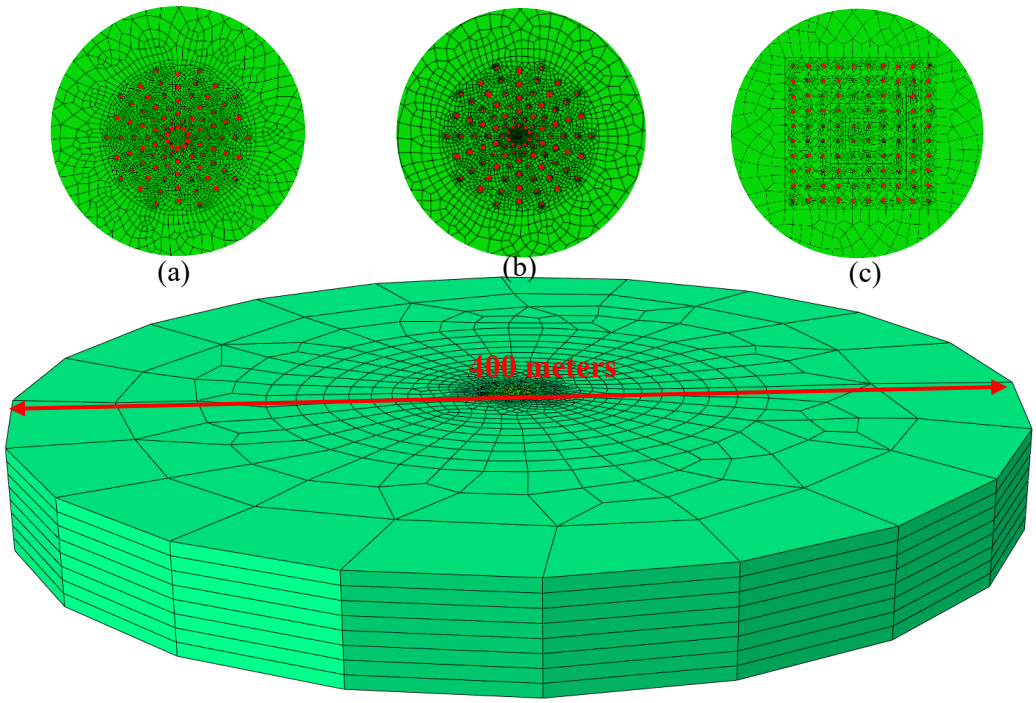

Figure 5.26 The finite element model along with the generated mesh: (a) Model 3, the circular array with spacing room of 1.9 m; (b) Model 4, the circular array with spacing room of 3.8 m; (c) Model 5, the square array with spacing room of 2.9 m.

Model 3

As shown in Figure 5.26, a total of 42930 nodes and 38072 elements (C3D8PT type) were generated. The boreholes and glacial till formation treated as a continuous body, where the dislocation behaviour among different parts cannot be modeled in this study.

Model 4

This model includes 100 boreholes in cylinder array, with space room of 3.8 meters. The center 20 borehole could reach a highest temperature of 30°C, the outer 40

boreholes could reach a highest temperature of 25°C after each heat injection phase. A total of 38835 nodes and 34432 elements, (C3D8PT type) were generated.

Model 5

The model includes 100 boreholes in square array, with space room of 2.9 meters. The center 20 boreholes could reach a highest temperature of 30°C, the outer 40 boreholes could reach a highest temperature of 28°C after each heat injection phase. A total of 44307 nodes and 39296 elements (C3D8PT type) were generated.

5.2.2 Results

The model is divided into 5 zones according to the distance from the central axis (Figure 5.27). Zone 1 is the center region with diameter of 6 meters, other four zones are annular cylinders next to the last one. The outer radius of Zone 2 is 7 meters. The outer radius of Zone 3 is 11 meters. The outer radius of Zone 4 is 50 meters.

Within Zone 1, 2, 3, and 4, seasonal underground temperature evolution was observed. The results indicate that the thermally influenced zone is a cylinder with diameter of 100 meters under the operation of a 100-borehole system with borehole temperature varies periodically from 1°C to 35°C. Zone 1 can generally reach over 34°C after every thermal injection phase.

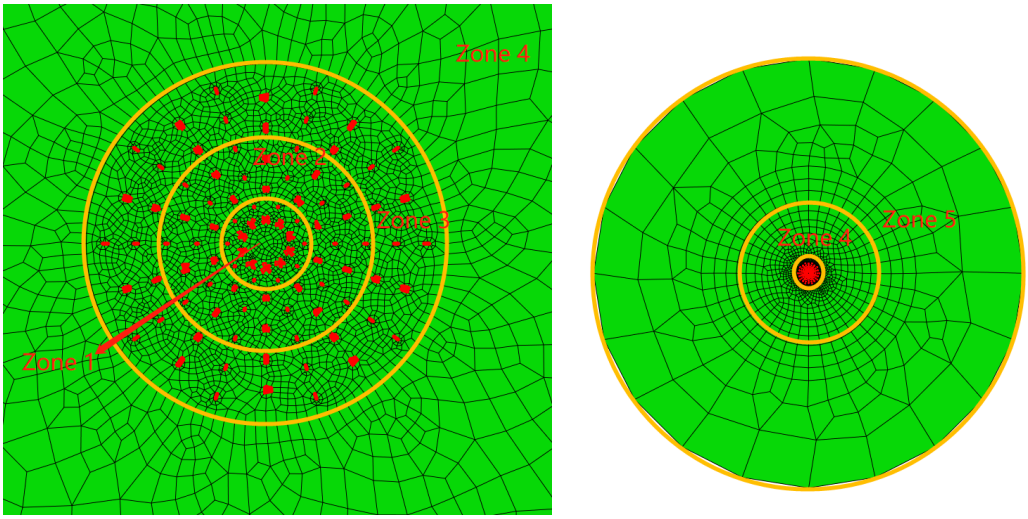

Figure 5.27 The schematic view of five zones for Model 3.

Temperature evolution

The temperature contour plot shows the influenced zone is a cylinder with a diameter of 100 meters in the 100-borehole BTES system. In other smaller BTES systems as described in previous sections, the influenced zone is a half prolate spheroid. This indicates that the impact of a 100-borehole BTES system is widespread.

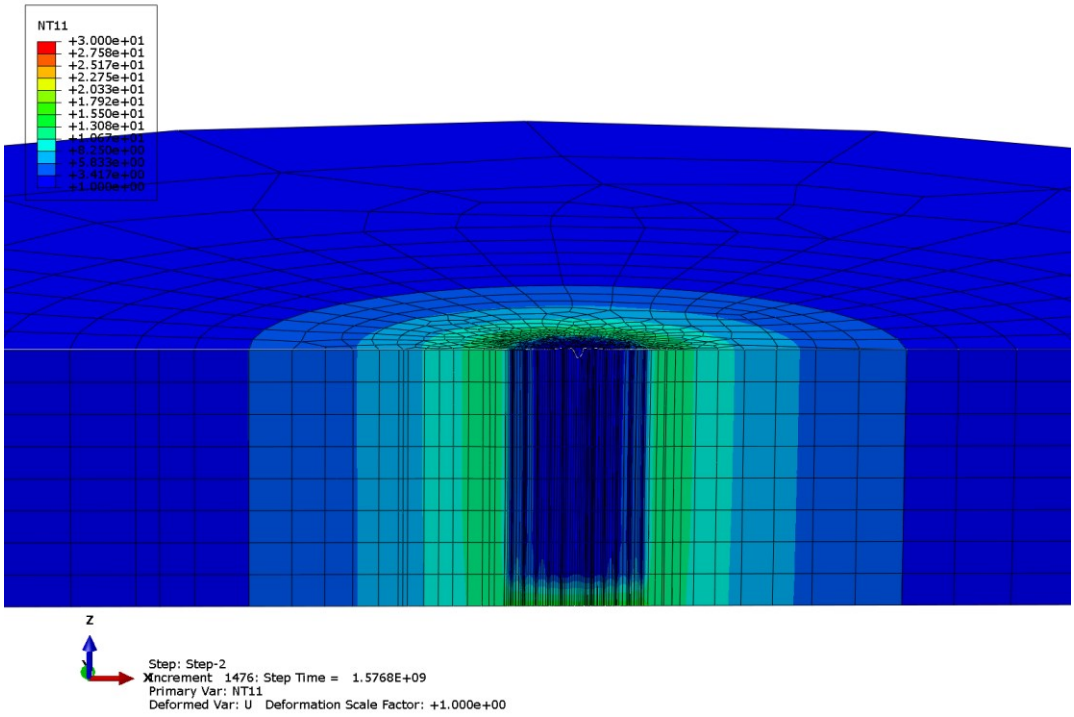

Figure 5.28 Underground temperature profile at the end of 50 years (unit = °C).

In zone 1, the temperature is homogenous in every moment from top surface to the depth of 35 meters. The temperature in Zone 1 could reach over 34°C after each heat injection phase. In Zone 2, glacial till could reach over 30°C in every operation cycle. The highest annual temperature in Zone 3 drops from 28°C to 20°C with the distance to the center from 7 to 11 meters. When the distance reaches 50 meters, there is nearly no temperature increment.

The temperature evolution rule is similar to the single borehole system and five-borehole system. As shown in Figure 5.29, thermal retention effect appeared at locations far from the boreholes in the whole influenced region. Temperature climbing state and balanced state is evident in Zone 3 and Zone 4 (Figure 5.30).

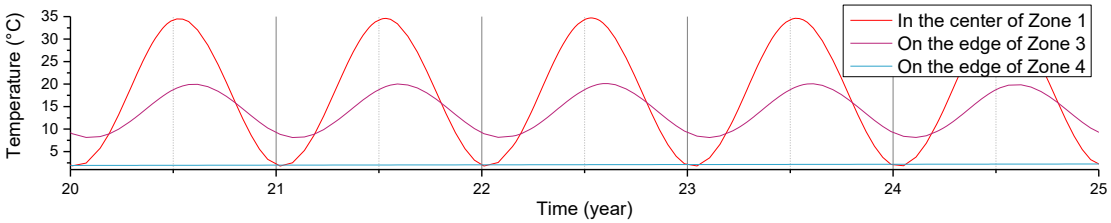

Figure 5.29 Underground temperature evolution at reference points on the top surface in Zone 1, 3, and 4 during 20th to 25th years.

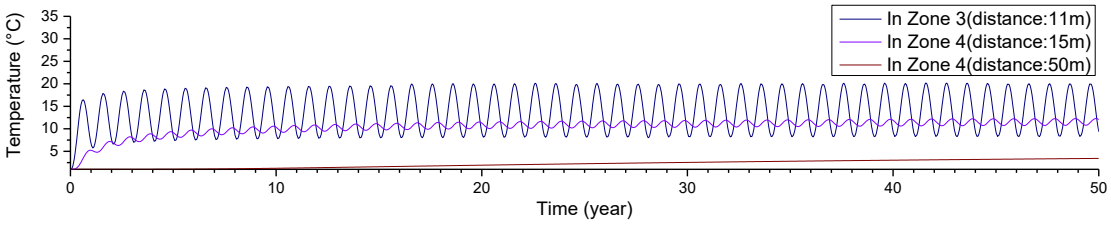

Figure 5.30 Underground temperature evolution at reference points on the top surface in Zone 3, and 4 on over 50 years.

As the boreholes distribute in 35 meters in depth. The underground temperature in the bottom layer of five meters evolved less significantly than the upper layer.

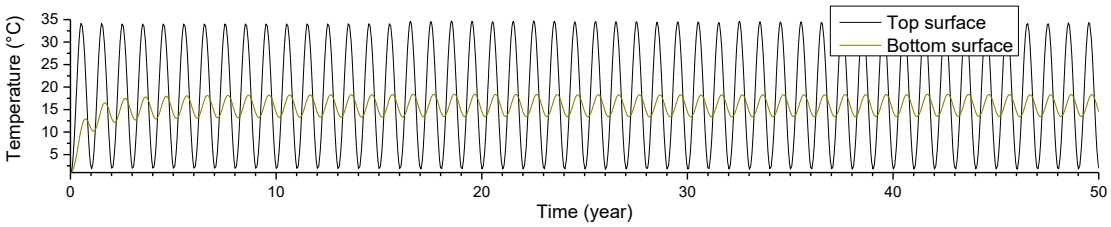

Figure 5.31 Underground temperature evolution in the center of Zone 1 on top surface and bottom surface.

Pore pressure evolution

The pore pressure under the thermal operation of a 100-borheole system evolved the much more dramatically than previous models. In whole influenced region, the pore pressure fluctuated following the same rule with a single borehole system. The highest pore pressure (861 kPa, depth of 30 meters) and largest negative pore pressure (-366 kPa, depth of 25 meters) appeared in the core of the whole formation over 50 years. Figure 5.32 shows the pore pressure at the moment where the highest pore pressure and largest negative pore pressure occurred.

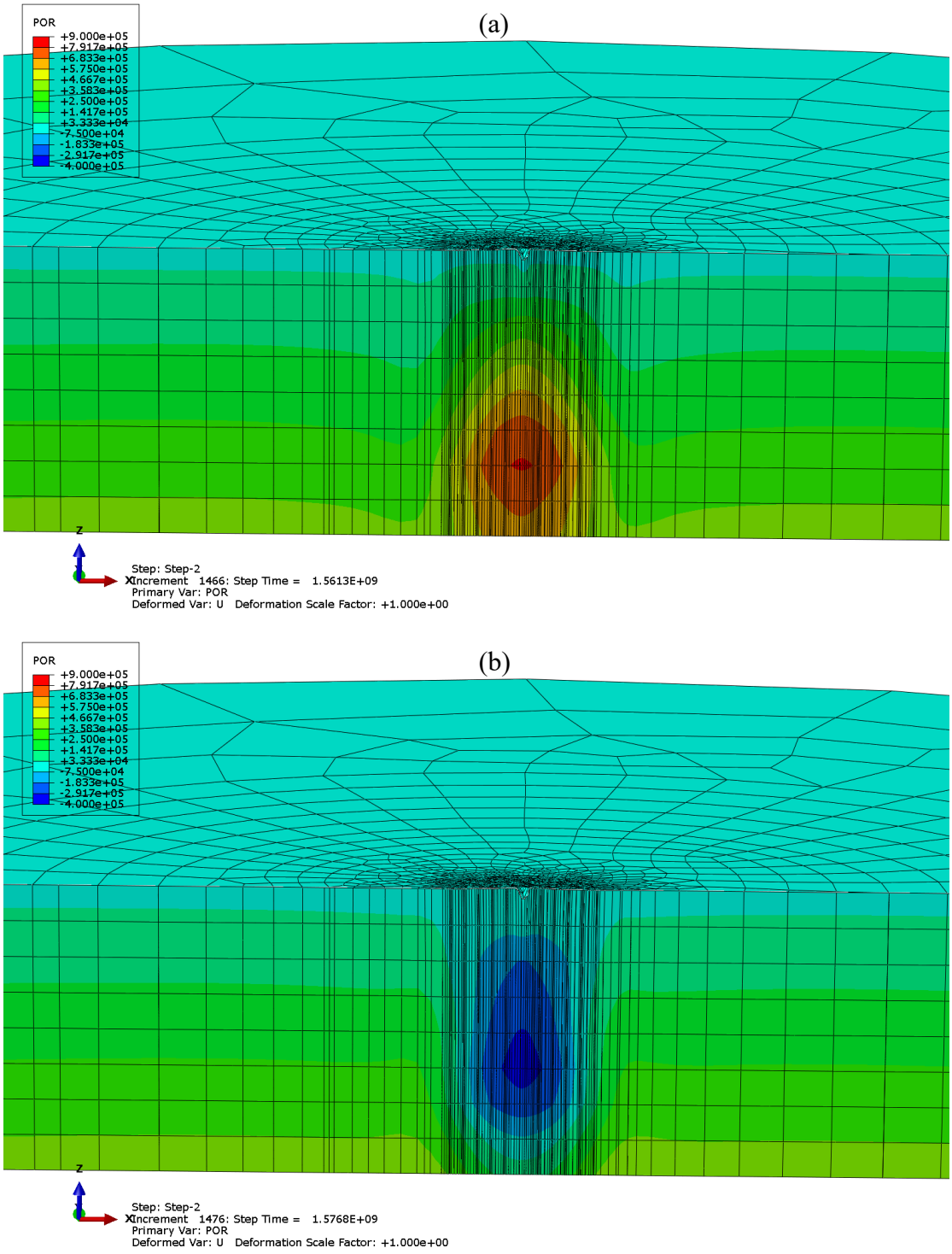

Figure 5.32 Pore pressure contour plot at two moments in the 50th year: (a) the end of the heat injection phase, (b) the end of the heat extraction phase (unit = Pa).

In the first heat injection phase, the pore pressure in the bottom layer raised the most rapidly. After falling back towards the initial value during the next heat extraction phase, the pore pressure raised again towards a higher value. Years by years, the annual

highest pore pressure got increased. And such increment in annual highest pore pressure is more significant in the first 10 years. In addition, the magnitude of annual amplitude increased evidently with time. The negative pore pressure occurred after 10 years, indicating the complexity of the impact of a 100-borehole system.

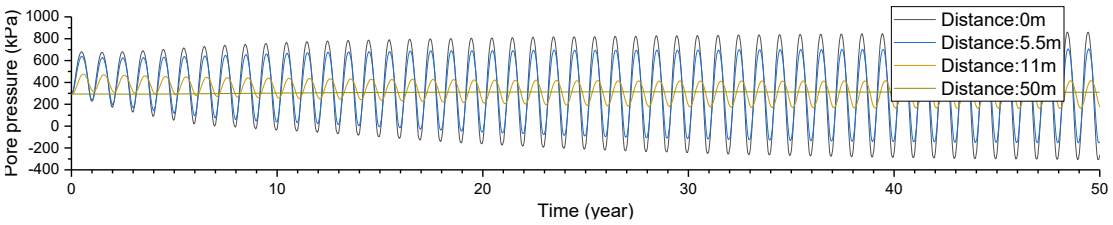

Figure 5.33 Pore pressure evolution at locations with different distance to the center on the plane of depth of 30 meters.

Similar to previous models, the influence on pore pressure drops with the distance to the boreholes. The maximum pore pressure increment on the inner edge of Zone 4 was 200 kPa, and it decreased rapidly to zero on the outer edge of Zone 5.

As shown in Figure 5.33, the maximum increment in pore pressure and highest pore pressure appeared at the depth of 30 meters in the core of the whole formation. The initial pore pressure is 294.3 kPa at depth of 30 meters. While the annual highest pore pressure increased gradually from 700 kPa to 861 kPa over 50 years.

Effective stress evolution and stress path

The effective stresses fluctuated rapidly with generally increasing trend over 50 years within the most part of influenced region (Figure 5.34). In the inner region of Zone 4, the vertical effective stress fluctuated with slightly decreasing trend. In the core of the whole formation where pore pressure evolved most rapidly happened the most violent effective stresses evolution. During 50-year thermal operation, the vertical

effective stress within depth of 20 to 30 meters in the center of Zone 1 could reach over 1800 kPa. In the same region, maximum increment in PEEQ (from 368 kPa to 818 kPa) occurred, indicating strain hardening behaviour. The maximum horizontal effective stress, which was near 1700 kPa, also occurred in this region.

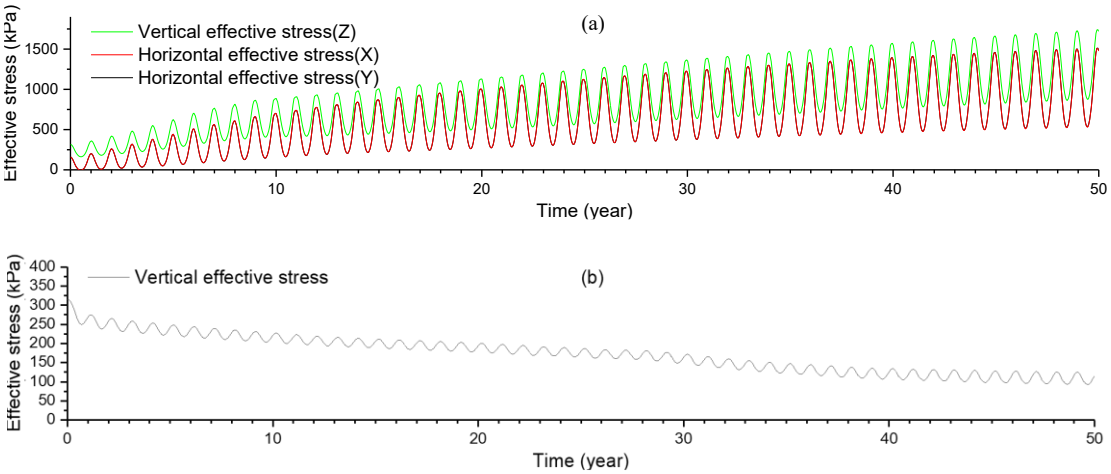

Figure 5.34 Vertical and horizontal effective stresses evolution over 50 years at 25 meters depth in the center: (a) in the center; (b) in the inner region of Zone 4.

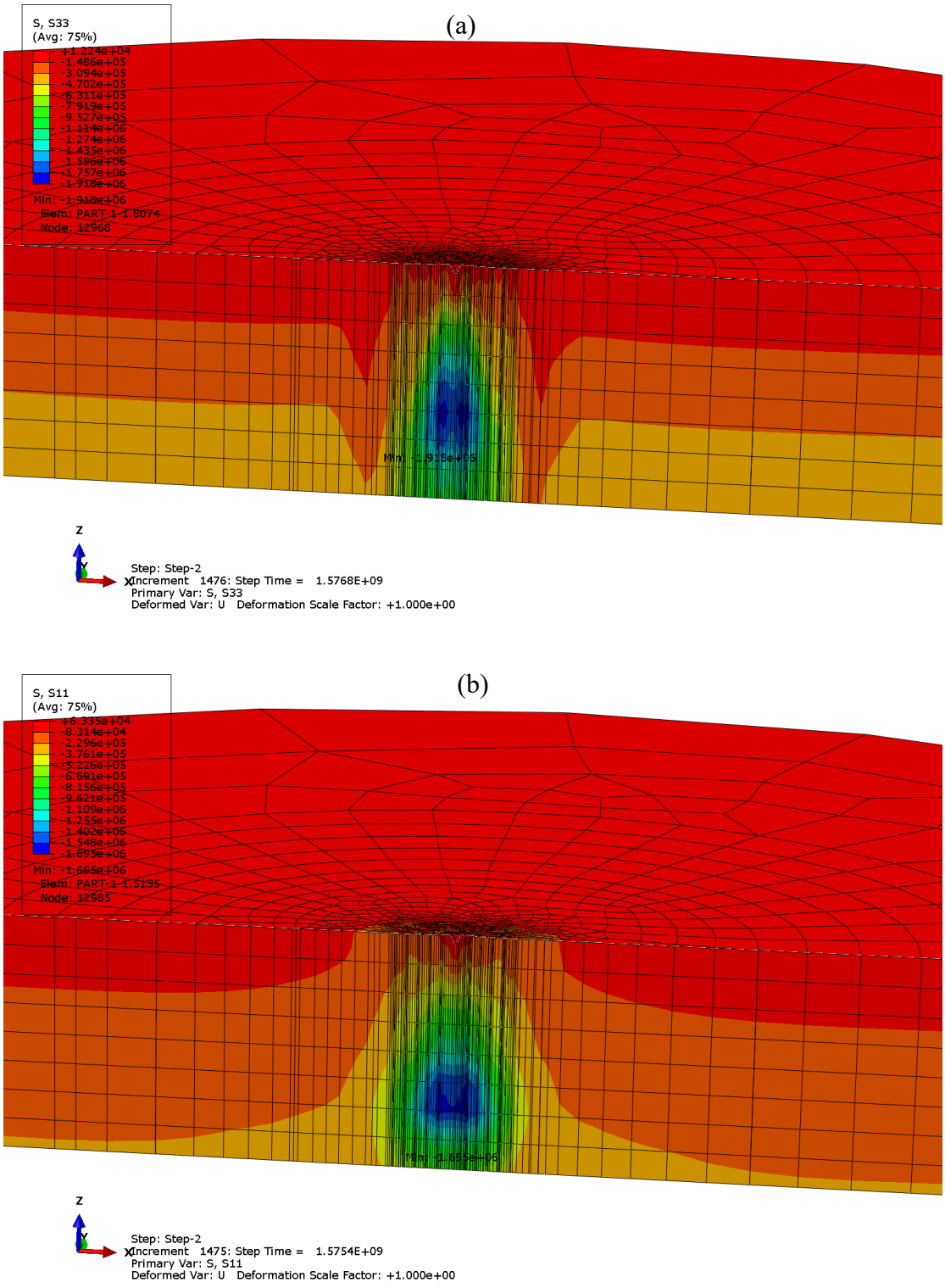

Figure 5.35 Effective stress contour plots at the moment the maximum value occurred: (a) maximum vertical effective stress; (b) maximum horizontal effective stress (unit = Pa).

In the core region, both horizontal and horizontal effective stresses evolved violently. Similar to the five-borehole model under extreme scenario, the horizontal stresses could eventually reach vertical effective stress in a certain region. Accordingly, it would result in violent deformation.

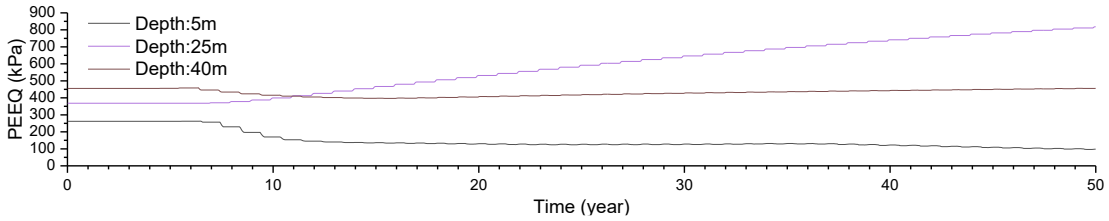

Figure 5.36 PEEQ evolution at different depth in the center.

The results of PEEQ indicate that the glacial till would suffer strain hardening or strain softening in Zone 1, 2, 3, and inner region of Zone 4. As the upper layer has high OCR, the upper layer is prone to suffer strain softening and the lower layer is prone to suffer strain hardening. Despite the PEEQ at the bottom remained unchanged as boreholes only reach 35m in depth. In addition, the results also reveal that evolution of PEEQ is related to the distance to the center. As the distance increased, the glacial till is prone to suffer strain softening. As shown in Figure 5.37, the glacial till on the plane of depth of 5 meters in Zone 1, 2, 3, and inner region of Zone 4 all suffered strain softening. While the glacial till on the plane of depth of 25 meters showed strain hardening behaviour within Zone 1, 2, and inner region of Zone 3, and showed strain softening behaviour when the distance is over 9 meters.

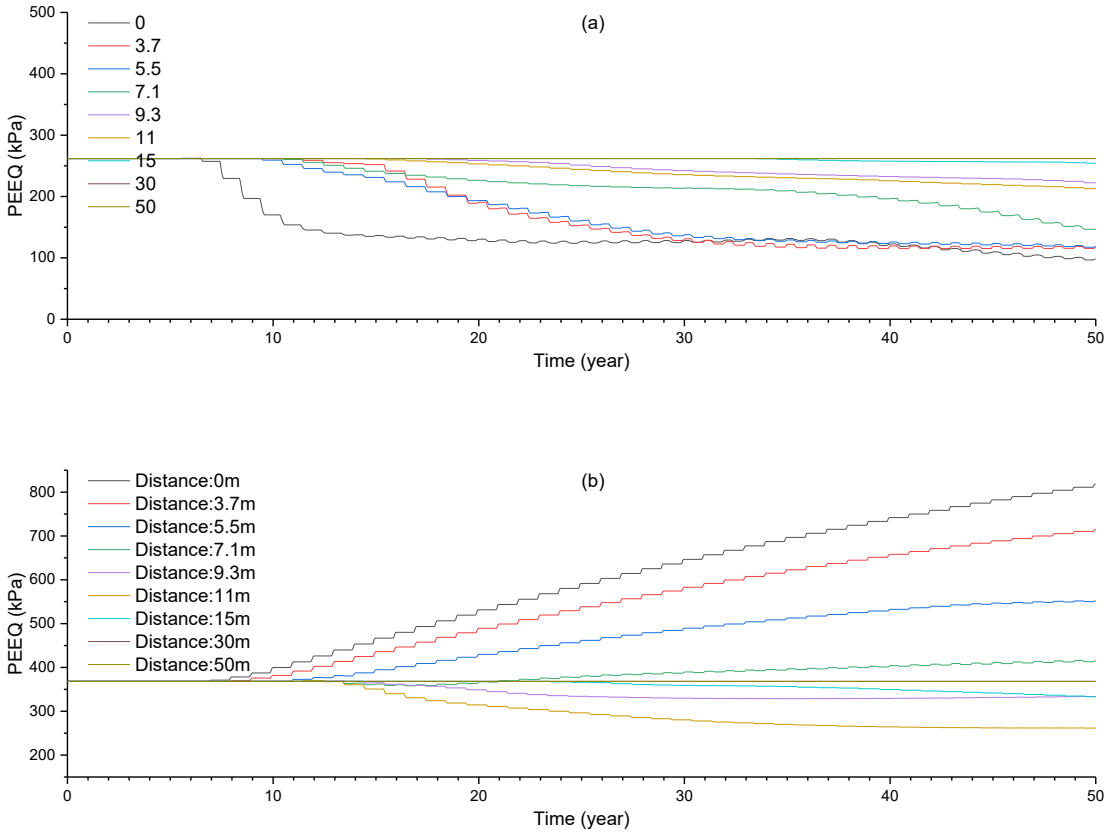

Figure 5.37 PEEQ evolution at the depth of 25 meters.

The results of simulated stress paths in the $p'-q$ plot at monitoring points proved the plastic behaviour. The initial stress state is (209.533, 157.150) in the plot at the location in the center of the plane of depth of 25 meters (Figure 5.38). The stress path began from (209.533, 157.150) and moved tortuously towards a larger p' value till it reached (1557.816, 244.022). The stress path at this point traversed CSL at the beginning and then intersected the initial yield surface to the right. Later, the yield surface and the plastic strain kept increasing for the rest of the operation period, during which the stress path never touched CSL again. The glacial till whose stress path followed the same rule showed strain hardening behaviour and would become denser with the thermal operation. The initial stress state is (52.573, 39.430) in the plot at the location in the center of the plane of depth of 5 meters Figure 5.39. The stress path

firstly traversed the CSL and then touched the initial yield surface to the left. After then, the yield surface started to contract. Later, the stress path traversed CSL again and again when moving tortuously towards the end. Finally, the stress state ended at (121.935, 38.167). The glacial till whose stress path followed the similar rule showed strain softening behaviour and would suffer "failure" during the thermal operation.

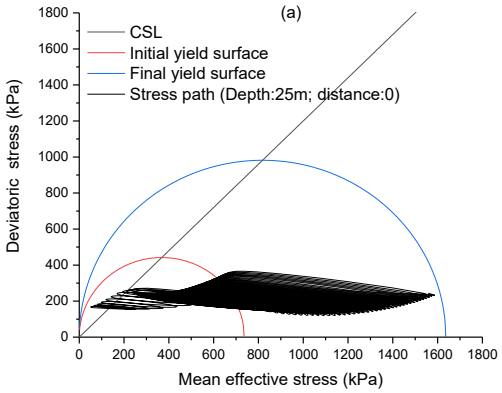

Figure 5.38 Stress path at the location where the most severe effective stress occurred (in the center of plane of depth of 25 meters).

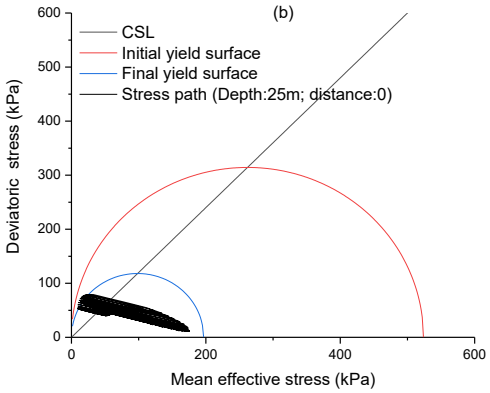

Figure 5.39 Stress path at the location in the center of the plane of depth of 5 meters.

Displacement

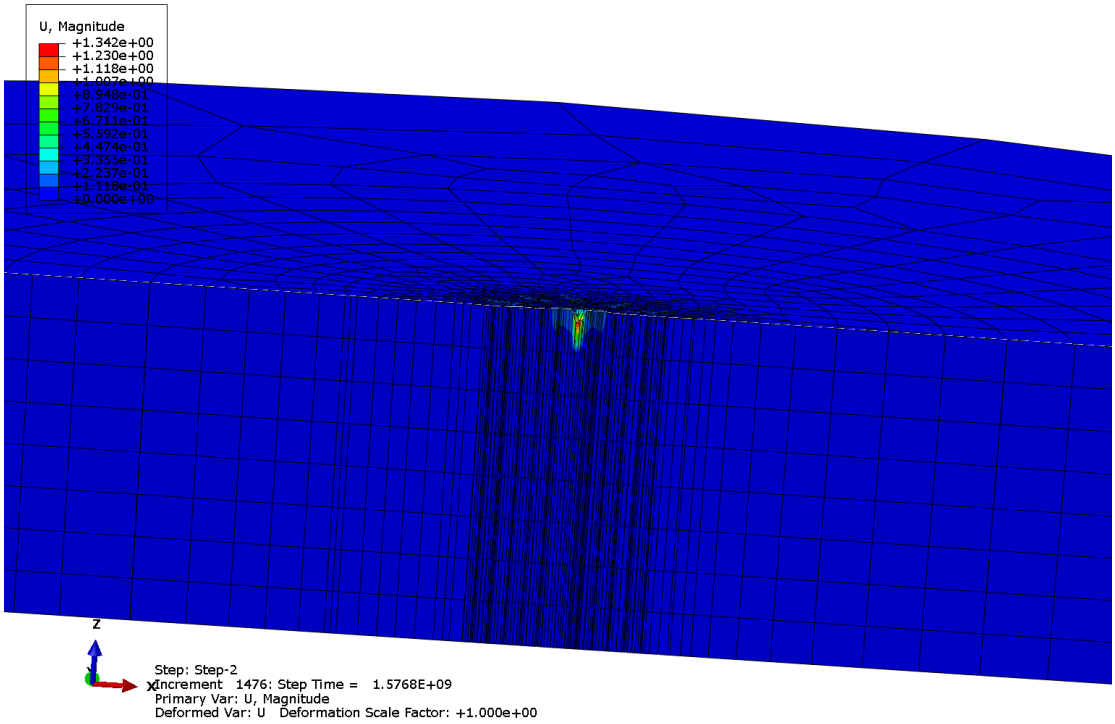

Figure 5.40 Displacement at the end of 50 years (unit = m).

Seasonal expansion and contraction happened in the influenced region with the operation of a 100-borehole BTES system. After the first heat injection phase, the glacial till within the radius of 30 meters heaved unevenly, decreasing with the distance to the center. The vertical expansion was 10 cm in Zone 1 and 2. The top surface contracted towards the initial level during the next heat extraction period. After the first heat extraction period, there was residual vertical displacement, over 1 cm in Zone 1, 2 and 3. In the next thermal cycle, the top layer heaved and contracted again. The maximum vertical expansion was 10 cm in Zone 1 and 2, 7 cm in Zone 3, 5cm in the inner region of Zone 4. In addition to the periodical thermal expansion and contraction, settlement would occur in Zone 1, 2, and 3 under the thermal operation of a 100-borehole BTES system. The closer to the center, the more settlement would happen. As shown in Figure 5.41, in the center, the glacial till began to settle from the 7th year. Beginning from the 22nd year, the settlement became dramatical till the end of thermal

operation, with vertical displacement from -4cm to -135cm. At a reference point in Zone2 and Zone 3, the glacial till began to settle from the 7th year and ended in the 20th year, where the vertical displacements were -4cm and -2.5cm for the two locations. Beginning from the 20th year, the glacial till in the top layer of Zone 2 and Zone 3 began to fluctuate vertically with a rising trend.

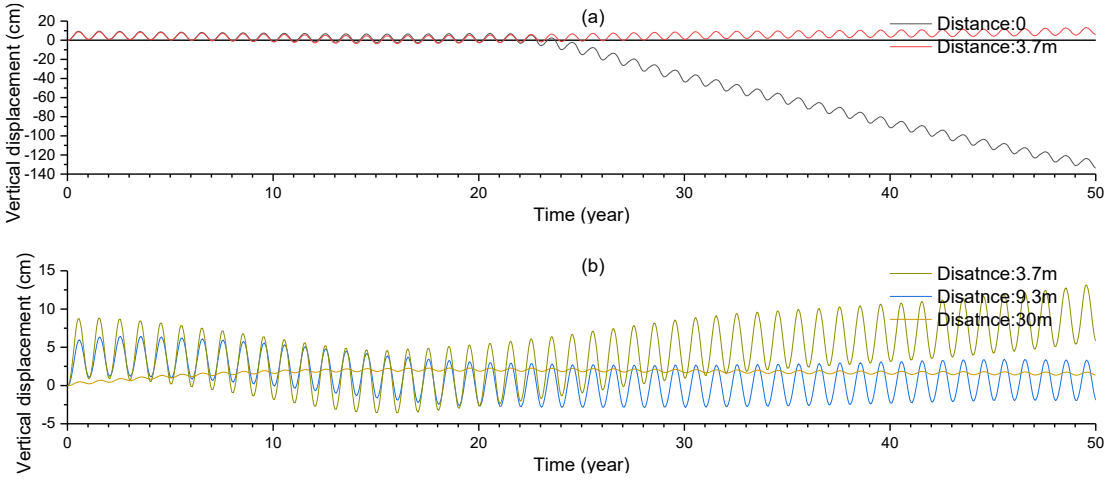

Figure 5.41 Vertical displacement evolution at reference points on the top surface: (a) in Zone 1 and 2; (b) in Zone 2, 3, and 4.

(Below the top layer) the settlement in glacial till within Zone 1, 2, 3, and inner region of Zone 4 dominated the deformation in the middle height (Figure 5.43). Figure 5.42 shows the vertical displacement at reference points on the plane of depth of 25 meters. This could be explained by the strain hardening behaviour happened in the region.

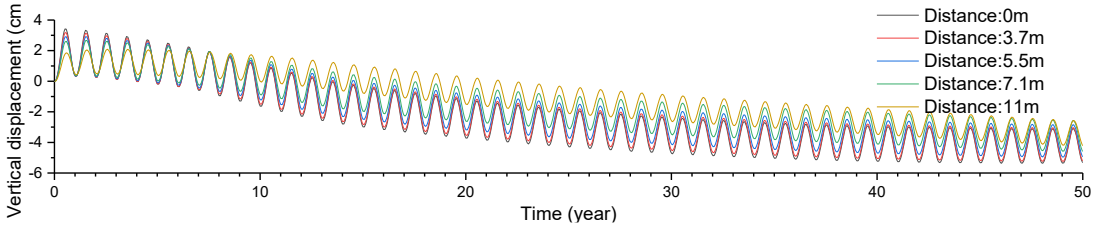

Figure 5.42 Vertical displacement at reference points on the plane of depth of 25 meters.

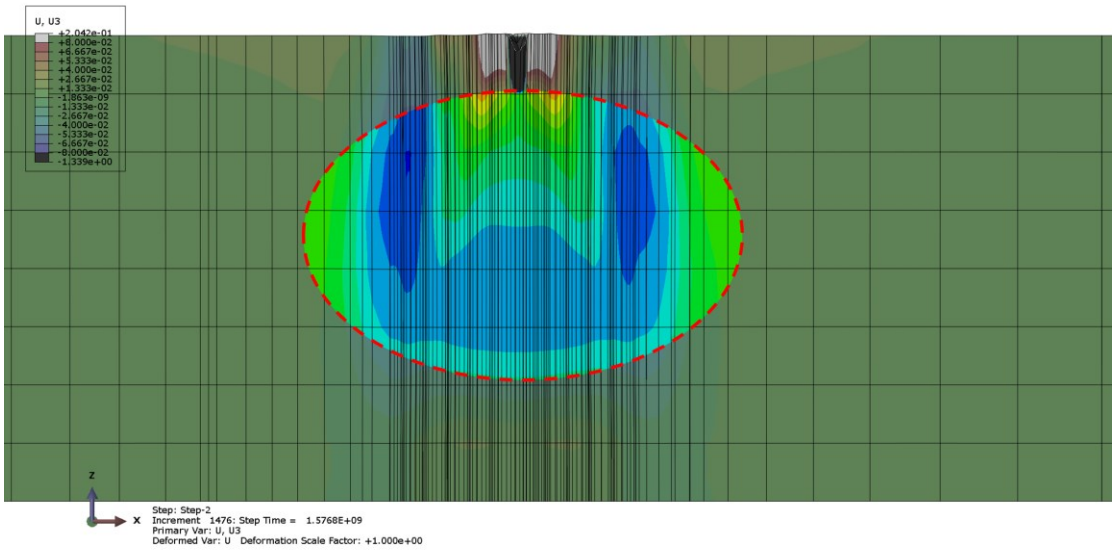

Figure 5.43 Vertical displacement contour plot in the middle height of the formation (unit = m).

In addition, the horizontal expansion and contraction induced by thermal operation is the same significant to the vertical displacement in Zone 2, 3. The glacial till in the top region would suffer horizontal thermal expansion, with horizontal displacement of 9cm, during the first heat injection phase and began to contract towards initial state in the next heat extraction phase. In the first 20 years, the periodical thermal expansion and contraction was in a balanced state, as the residual horizontal displacement was small after every cycle. Beginning from the 20th year, the horizontal displacement in top region aggravated. At reference points in Zone 2 and 3, the horizontal displacement would reach maximum value of 14cm and 6cm over 50-year operation, respectively (Figure 5.44).

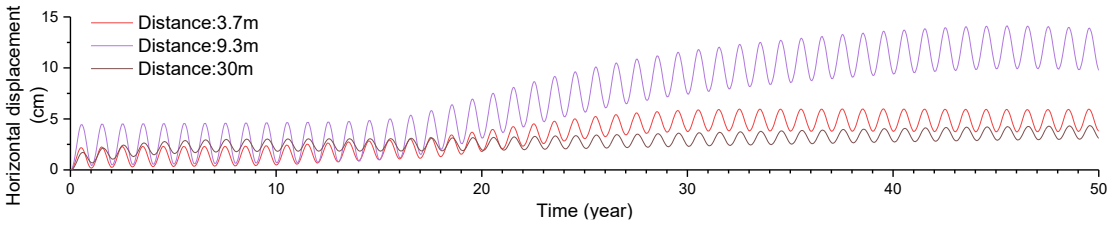

Figure 5.44 Horizontal displacement at reference points in Zone 2 and 3.

In the five-borehole BTES system under 60°C scenario, the horizontal contraction region was mentioned. The horizontal contraction region is more evident in the 100-borehole BTES system. Horizontal contraction area locates within depth of 10 to 35 meters in Zone 2 and 3 in the 100-borheole system under 35°C scenario (Figure 5.45).

In horizontal contraction region, the glacial till suffered horizontal expansion after the first heat injection phase and horizontal contraction in the next heat extraction phase, From the results of reference points, it can be found that the horizontal contraction was slightly larger than the expansion in every cycle. More movement in the negative direction would be accumulated over 50 years, where the ultimate maximum horizontal displacement is -6.4cm.

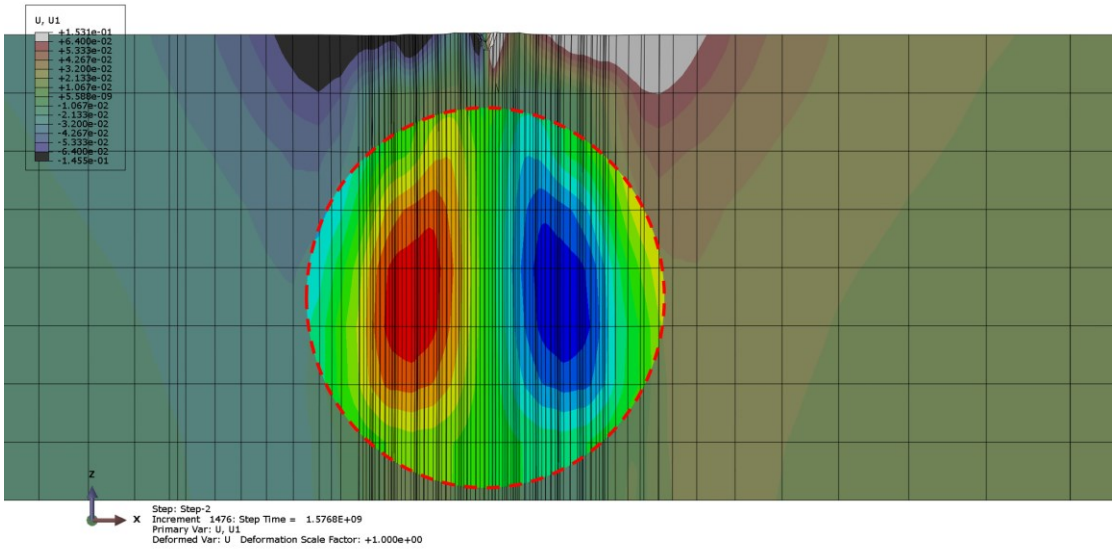

Figure 5.45 Contraction region (unit = m).

5.2.3 Analysis

In this section, the author is going to analyze the relationship between deformation and effective stress evolution. In effective stress evolution and stress path,

it is pointed out that the glacial till would suffer strain hardening or strain softening behaviour during the 50-year thermal operation. Detailed stress evolution at two representative points (one suffered strain hardening, the other suffered strain softening) are provided in this section. They are two points at depth of 25 meters and 5 meters in the center of the formation.

Strain hardening and glacial till deformation (Figure 5.47): $p'-t$ plot shows that the mean effective stress (p') would decrease in the first half year (heat injection period) and increase in the second half year (heat extraction period). $PEEQ-t$ plot indicates that the initial yield surface would begin to expand from the end of the 7th year, where the stress path touched the initial yield surface to the right. Then the corresponding mean effective stress could be located on the $p'-t$ plot. Accordingly, the projection of p' value on the $e-p'$ plot could be located. Then it is found that the glacial till at this representative point sustained elastic strain before the end of 7th year. For example, in the first heat injection phase, the void ratio increased from 0.43 to 0.44. Then it decreased to 0.428 after the first heat extraction phase. After the first thermal operation cycle, the glacial till became denser than initial state with elastic strain happening.In the first half of 7th year, the void ratio (e) increased from 0.424 to 0.432, with glacial till expansion. In the second half of 7th year, the void ratio would decrease to 0.422 before the stress path touched the initial yield surface. When the stress path exceeded the initial yield surface, small plastic strain occurred. Glacial till tends to get denser as strain hardening happens. As a result, the increment of void ratio in the heat injection phases tends to shrink and the reduction in heat extraction phases tends to

increase. Comprehensively, beginning from the 8th year, the void ratio decreased more dramatically. With time, new plastic strain would be accumulated (glacial till would get denser and denser). Till the middle of the 50th year, which is the end of the 50th heat injection phase, the glacial till at this point suffered sustainable plastic strain, with void ratio changing to 0.396. After the 50th heat extraction phase, where void ratio changed from 0.396 to 0.39, new elastic and plastic strain occurred as p' increased. In conclusion, the detailed stress plots indicate that the glacial till locates at depth of 25 meters in the center would sustain elastic and strain hardening behaviour. The volume would increase in the heat injection phase and decrease in the next heat extraction phase. The glacial till at the location with similar stress path would become dense eventually.

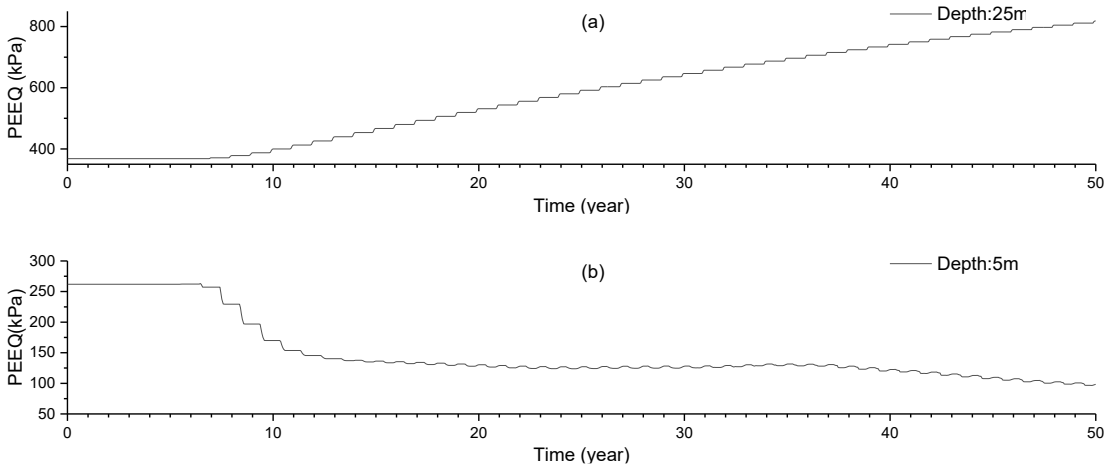

Figure 5.46 PEEQ evolution at depth of 25 and 5 meters in the center.

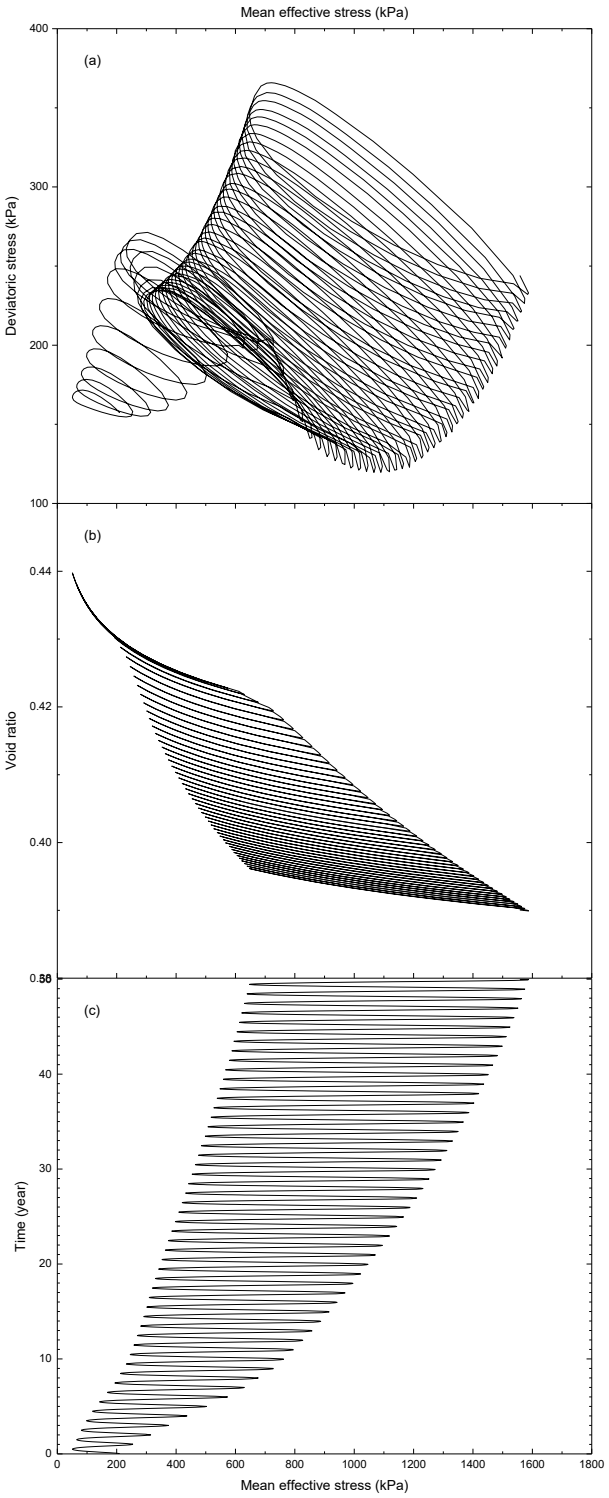

Figure 5.47 Mean effective stress at the center of the plane of depth of 25 meters: (a) $p'-q$ plot; (b) $e-p'$ plot; (c) $p'-t$ plot.

Strain softening and glacial till deformation (Figure 5.48): $PEEQ-t$ plot shows that the stress path touched the initial yield surface to the left of CSL at a moment

in the first half of the 7th year, when p' was decreasing. That is to say, the deformation at this point was all elastic before this moment, with void ratio from 0.451 to 0.465. When the stress path touched the initial yield surface, the yield surface started to contraction (glacial till softening). With strain softening behaviour, glacial till is prone to dilate. p' increased again towards the CSL in the second half of the 7th year. Meanwhile, the void ratio decreased from 0.466 to 0.452, as shown in $e-p'$ plot. Glacial till at this point would sustain both elastic and plastic strain. According to the $p'-q$ and $e-p'$ plot, the stress path would travers CSL in this second half of 7th year. That indicates the failure in the glacial till at this point. In the first half of 8th year, glacial till would sustain more plastic than last year as the p' decreased and void ratio increased. While the void ratio would be restored partly in the second half of 8th year. Accordingly, the volume of glacial till at this point increased dramatically with time. As shown in $e-p'$ plot, the void ratio reached the maximum value of 0.53 in the mid of 24th year, at which moment the till was the most loosen. Then the void ratio would fluctuate towards a smaller value in the rest time. This is consistent with the dramatical settlement in the top layer as shown in Figure 5.41 a. In the second half of 24th year, the void ratio decreased from 0.53 to 0.50. The glacial till became denser than last year. With time, the void ratio eventually became 0.498 at the end of 50 years. In conclusion, the detailed stress plots indicate that the glacial till locates at depth of 5 meters in the center would sustain elastic and strain softening behaviour. The volume would increase in the heat injection phase and decrease in the next heat extraction phase. Overall, the

glacial till at the location with similar stress path would become loosen at first and then changing towards dense.

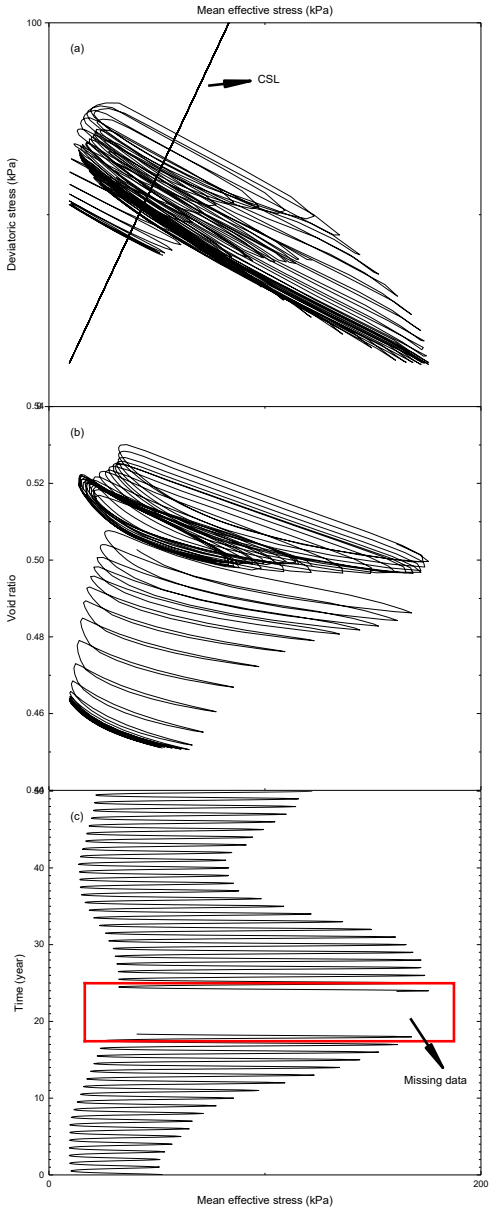

Figure 5.48 Mean effective stress at the center of the plane of depth of 5 meters: (a) $p'-q$ plot; (b) $e-p'$ plot; (c) $p'-t$ plot.

5.2.4 Other models

Extreme scenario

The influenced zone and the rule of pore pressure, effective stresses, and deformation under extreme scenario is the same with that of 35°C scenario. In this scenario, the influenced zone is a cylinder with a radius of 50 meters. And the deformation in Zone 1, 2, 3, and 4 evolved followed the same pattern. However, the impact of the periodical thermal operation is significantly more severe in this scenario. In the influenced zone, pore pressure, effective stresses and deformation evolved dramatically.

The maximum vertical expansion was 79 cm, occurred at the end of the 35th heat injection phase. After 36 years, the model would fail. The maximum vertical settlement was 69 cm, occurred at the end of 35th year. This vertical settlement is much large than that in 30°C scenario at the same time.

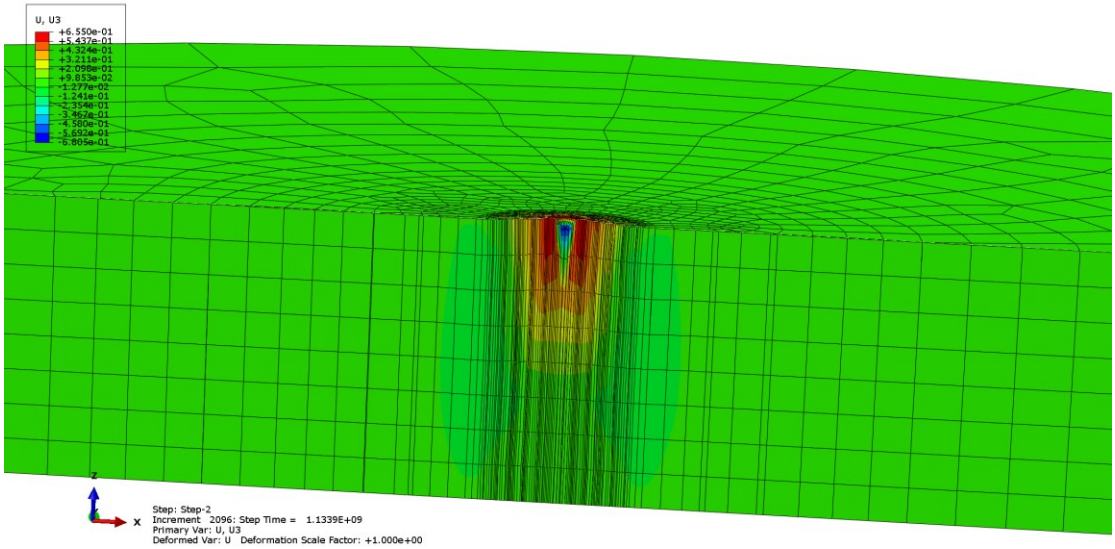

Figure 5.49 Vertical displacement at the end of 35th year for Model 3 under extreme scenario (unit = m).

The most severe effective stresses occurred in the core of whole formation, where the effective stresses fluctuated with increasing trend. The maximum vertical effective stress is near 2740 kPa, occurred at the depth 25 meters in the center of Zone 1 at the end of the 35th year. The maximum horizontal effective stresses are near 2700 kPa, occurred at the depth of 30 meters at the end of the 35th year. Maximum pore pressure over 1200 kPa, maximum negative pore pressure -800 kPa, occurred at the depth of 30 meters.

Model 4

The influenced zone is a cylinder with a radius of 50 meters. Dramatic pore pressure and effective stress evolution and severe deformation happen in glacial till in the influenced zone. To describe the result, the influenced zone is divided into 4 groups: Zone 1, Zone 2, Zone 3, and Zone 4. Zone 1 is a cylinder in the center of the formation, with a radius of 5.8 meters. The other four zones are annular cylinders next to the last one. The outer radius of Zone 2 is 13.3 meters. The outer radius of Zone 3 is 22 meters. The outer radius of Zone 4 is 50 meters.

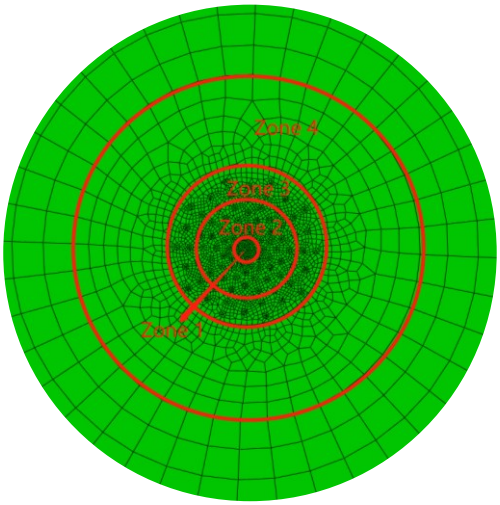

Figure 5.50 The schematic view of five zones for Model 4.

The glacial till in influenced zone expanded vertically in heat injection phase and contracted vertically in heat extraction phase. The maximum vertical expansion was 24cm, occurred at the end of 41st heat injection phase. In the center of the Zone 1, glacial till sustained vertical expansion in the first 20 years and then began to settle with fluctuating for the rest of the time. In the top layer of the whole influenced zone, glacial till generally showed heave over 41 years. The ultimate settlement in the center of Zone 1 was 2.5 meters at the end of 41 years. After 41 years, the model would fail.

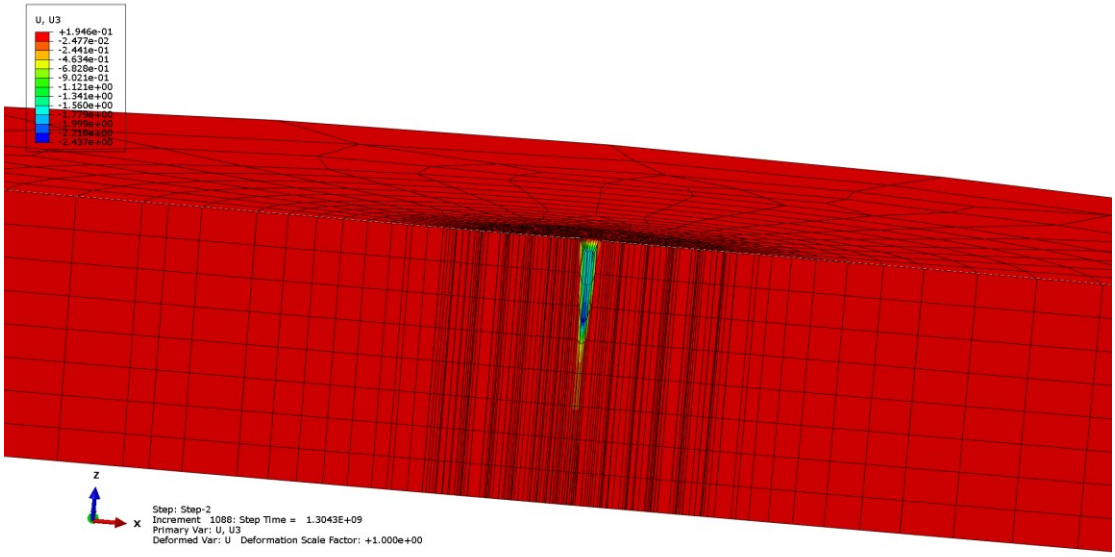

Figure 5.51 Vertical displacement contour plot at the end of 41st year for Model 4 (unit = m).

In the bottom of Zone 1, the whole Zone 2 and Zone 3, effective stress fluctuated with increasing trend (decreased when heat injection increased when heat extraction). In upper layer of Zone 1, effective stress fluctuated with decreasing trend.

Maximum vertical effective stress, 1350 kPa, at end of the 41 years at depth of 25 meters in Zone 1, where the initial value is 310 kPa. At the same location, occurred the maximum horizontal effective stress, 1200 kPa.

Pore pressure evolved following the same pattern with Model 3. While the maximum negative pore pressure is only -140 kPa.

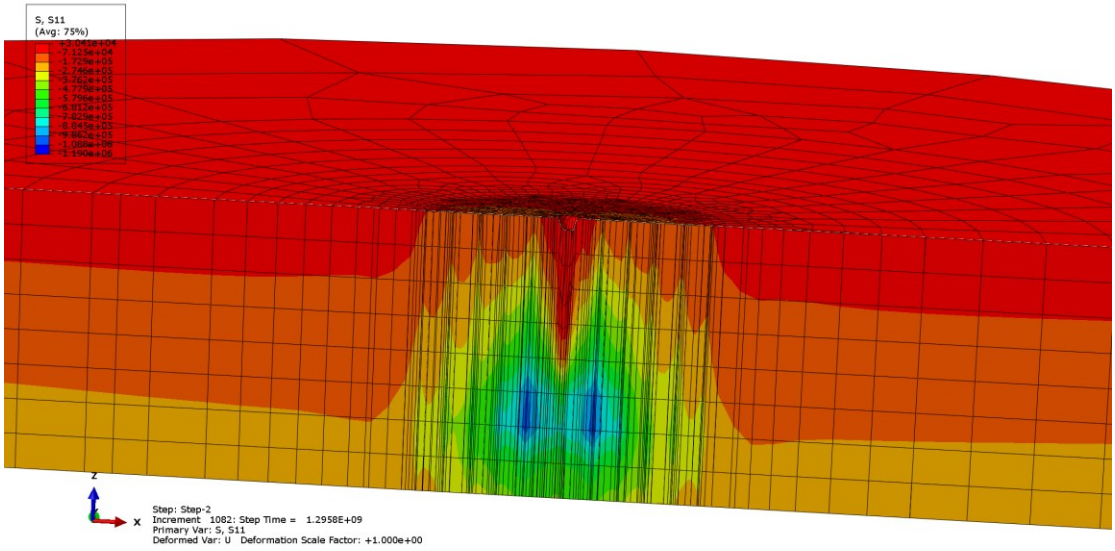

Figure 5.52 Horizontal effective stress contour plot at the end of 41 years for Model 4 (unit = Pa).

Model 5

The influenced zone is a cylinder with a radius of 50 meters. Dramatic pore pressure and effective stress evolution and severe deformation happen in glacial till in the influenced zone. Zone 1, in which 36 boreholes included, is the cuboid with side length of 17.4 meters. Zone 2, where the outer 64 boreholes included, is the rectangular shell surrounding Zone 1. Zone 3 is the rest of the influenced zone.

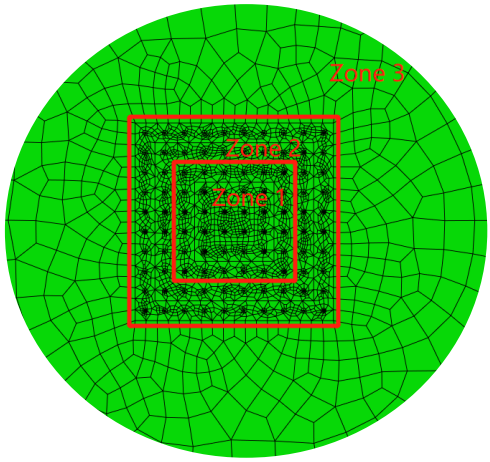

Figure 5.53 The schematic view of five zones for Model 5.

The glacial till in influenced zone expanded vertically in heat injection phase and contracted vertically in heat extraction phase. The maximum vertical expansion is 15 cm, occurred at the end of the 50th heat injection phase. The glacial till in Zone 1 generally heaved behaviour over 50 years. While the glacial till in Zone 2 showed both heave and settlement over 50 years, where ultimate settlement is 4cm.

In the bottom of Zone 1 and the whole Zone 2, effective stresses fluctuated with increasing trend (decreased when heat injection increased when heat extraction). In Zone 3 and upper layer in Zone 1, effective stress fluctuated with decreasing trend. The maximum vertical effective stress,1100 kPa, occurred at the end of 50 years at depth of 25 meters in Zone 2, where initial value is 340 kPa. The maximum horizontal effective stress was 1050 kPa, occurred at the end of 50 years at depth of 30 meters in Zone 2, where the initial value is 180 kPa. The effective stress could increase to near 10 times of initial value.

The deformation and stress path evolution are less significant than Model 3 and 4, although the influenced region is the same and the maximum effective stresses occurred in a similar position.

6 Conclusions and recommendations for further work

6.1 Conclusions

This thesis uses thermal-hydro-mechanical coupled finite element analysis results to demonstrate the effect of geothermal energy storage (GTES) systems of 50-year service life period on thermal consolidation behaviors of surrounding glacial tills formations in northern Quebec. Major conclusions are drawn as the following:

- During the heat injection phase, pore pressure tends to increase, which results in a decrease in the mean effective stress and void ratio. In the heat extraction phase, the pattern of evolution is reversed. The impact of the thermal operation of BTES system on the glacial till formation would aggravate because the difference between increment and reduction in every cycle accumulated over 50 years.

- A BTES system with a larger geometric scale and high operation temperature (60°C in this study) would impose significant influence on the glacial till. The glacial till would sustain effective stresses and pore pressure several times greater than the initial value. As the effective stresses would fluctuate over years as a result of the periodical operation temperature, the stress path moves tortuously. Depending on the location, the glacial till would suffer strain hardening or strain softening behaviour. The glacial till in the upper layer is prone to experience strain softening. While in the lower

layer, where glacial till usually suffers the most severe impact, a strain hardening is expected.

- The deformation usually does not exceed a few tens of centimeters for a single borehole system and a five-borehole system. While it would be over 1 meter in the most severe region for a 100-borehole system. The top layer sustains heave and settlement as the result of thermal expansion and contraction and consolidation. The core area of the whole formation could sustain severe vertical contraction in a 100-borehole system or a five-borehole system with extreme operation temperature. After a 50-year operation, the whole till layer would become uneven as the deformation differs in different zones.

- This study provides a preliminary work to identify the potential geo-risk of BTES systems built in glacial till in northern Quebec region. For the construction of BTES systems, the suggestions include but not limited to 1) ensure the borehole operation temperature within a proper range. 2) a reasonable arrangement of boreholes should be considered to prevent large periodical large deformations within the underground.

6.2 Recommendations for further work

Empirical and simplified data are adopted in this study due to some practical reasons. The author is going to point out the key limitations in this study as the recommendations for further work.

- In-situ measurement on local glacial till. In this study, some of the mechanical properties are referred to tills from other provinces and countries or calculated based on empirical equations. Local data on glacial till would lead to a close result. And other factors including unsaturated soil problem, underground flow, inhomogeneous nature of soil formations should also be considered in a future study.

- Practical borehole temperature evolution rule. Practical temperature evolution could be steeper and more complicated than a sinusoidal rule assumed in this study. The temperature evolution rule directly influences the pore pressure and stresses in the surrounding soil. It is recommended to apply an actual temperature boundary around the BETS boreholes if related data are available.

References

1. Abaqus. (2016). *Applied soil mechanics with Abaqus applications* (Vol. 4, Issue 1).

2. Al-Khazaali, M., Vanapalli, S. K., & Oh, W. T. (2019). Numerical investigation of soil–pipeline system behavior nearby unsupported excavation in saturated and unsaturated glacial till. *Canadian Geotechnical Journal*, *56*(1), 69–88. https://doi.org/10.1139/cgj-2017-0411

3. Atkinson, J. H., & Little, J. A. (1988). Undrained triaxial strength and stress-strain characteristics of a glacial till soil. *Canadian Geotechnical Journal*, *25*(3), 428–439. https://doi.org/10.1139/t88-048

4. Bardet. (1997). *Experimental Soil Mechanics. Prentice Hall*, 1001. http://librosysolucionarios.net/

5. Baser, T., & McCartney, J. S. (2015). Development of a full-scale soil-borehole thermal energy storage system. *Geotechnical Special Publication*, *GSP 256*, 1608–1617. https://doi.org/10.1061/9780784479087.145

6. Bell, F. G. (2002). The geotechnical properties of some till deposits occurring along the coastal areas of Eastern England. *Engineering Geology*, *63*(1–2), 49–68. https://doi.org/10.1016/S0013-7952(01)00068-0

7. Belzile, P., Comeau, F., Raymond, J., & Lamarche, L. (2017). *Arctic Climate Horizontal Ground-Coupled Heat Pump*. *41*.

8. Cao, L., Peaker, S., & Ahmad, S. (2015). Engineering characteristic of glacial tills in GTA. *68e Conférence Canadienne de Géotechnique et 7e Conférence Canadienne Sur Le Pergélisol, 20 Au 23 Septembre 2015, Québec, Québec.*, *1967*.

9. Catolico, Ge, & McCartney. (2016). Numerical Modeling of a Soil-Borehole Thermal Energy Storage System. *Vadose Zone Journal*, *15*(1), vzj2015.05.0078. https://doi.org/10.2136/vzj2015.05.0078

10. Chiasson, A. D., & Yavuzturk, C. (2003). Assessment of the viability of hybrid geothermal heat pump systems with solar thermal collectors. *ASHRAE Transactions*, *109 PART 2*, 487–500.

11. Clarke, B. G. (2018). The engineering properties of glacial tills. *Geotechnical Research*, *5*(4), 262–277. https://doi.org/10.1680/jgere.18.00020

12. Delage, P. (2013). On the thermal impact on the excavation damaged zone around deep radioactive waste disposal. *Journal of Rock Mechanics and Geotechnical Engineering*, *5*(3), 179–190. https://doi.org/10.1016/j.jrmge.2013.04.002

13. Evans, Reay, Riley, Mitchell, & Busby. (2006). *Appraisal of underground energy storage potential in Northern Ireland*.

14. Fortier, Allard, Lemieux, Therrien, Molson, & Fortier. (2011). *Cartographie Des Depots Quateernaires Des Villages Nordiques De Whapmagoostui-Kuujjuarapik, Umijuaq, Salluit, Kuujjuaq*.

15. Fortier, R., LeBlanc, A. M., & Yu, W. (2011). Impacts of permafrost degradation on a road embankment at Umiujaq in Nunavik (Quebec), Canada. *Canadian Geotechnical Journal*, *48*(5), 720–740. https://doi.org/10.1139/t10-101

16. Gabrielsson, Bergdahl, & Moritz. (2000). Thermal energy storage in soils at temperatures reaching 90°c. *Journal of Solar Energy Engineering, Transactions of the ASME*, *122*(1), 3–8. https://doi.org/10.1115/1.556272

17. Gabrielsson, Lehtmets, Moritz, & Bergdahl. (1997). *Heat storage in soft clay*. http://www.swedgeo.se/upload/publikationer/Rapporter/pdf/SGI-R53.pdf

18. Gagnon, & Allard. (2020). *Geomorphological controls over carbon distribution in permafrost soils : the case of*. *528*(July), 509–528.

19. Giordano, Kanzari, Miranda, Dezayes, & Raymond. (2017). Shallow geothermal resource assessments for the northern community of Kuujjuaq, Québec, Canada. *IGCP636 Annual Meeting*, *May 2018*, 1–4.

20. Giordano, & Raymond. (2019). Alternative and sustainable heat production for drinking water needs in a subarctic climate (Nunavik, Canada): Borehole thermal energy storage to reduce fossil fuel dependency in off-grid communities. *Applied Energy*, *252*(June), 113463. https://doi.org/10.1016/j.apenergy.2019.113463

21. Gray, J. T., Pilon, J., & Poitevin, J. (1988). A method to estimate active-layer thickness on the basis of correlations between terrain and climatic parameters as measured in northern Quebec. *Canadian Geotechnical Journal*, *25*(3), 607–616. https://doi.org/10.1139/t88-067

22. Gunawan, Giordano, Jensson, Newson, & Raymond. (2020). Alternative heating systems for northern remote communities: Techno-economic analysis of ground-coupled heat pumps in Kuujjuaq, Nunavik, Canada. *Renewable Energy*, *147*, 1540–1553. https://doi.org/10.1016/j.renene.2019.09.039

23. Han, Z., Vanapalli, S. K., & Kutlu, Z. N. (2016). Modeling Behavior of Friction Pile in Compacted Glacial Till. *International Journal of Geomechanics*, *16*(6), 1–12. https://doi.org/10.1061/(asce)gm.1943-5622.0000659

24. Han, Zheng, Kong, Wang, Li, & Bai. (2008). Numerical simulation of solar assisted ground-source heat pump heating system with latent heat energy storage in severely cold area. *Applied Thermal Engineering*, *28*(11–12), 1427–1436. https://doi.org/10.1016/j.applthermaleng.2007.09.013

25. Hillel, D. (2003). Soil Physics. *Encyclopedia of Physical Science and Technology*, 77–97. https://doi.org/10.1016/B0-12-227410-5/00936-4

26. Huang, B., & Sharma, J. S. (2008). A coupled consolidation shear model for the process of formation of glaciated soils. *Canadian Geotechnical Journal*, *45*(2), 226–237. https://doi.org/10.1139/T07-092

27. Ibrahim, N. M., Rahim, N. L., Amat, R. C., Salehuddin, S., & Ariffin, N. A. (2012). Determination of Plasticity Index and Compression Index of Soil at Perlis. *APCBEE Procedia*, *4*, 94–98. https://doi.org/10.1016/j.apcbee.2012.11.016

28. Işik, N. S. (2009). Estimation of swell index of fine grained soils using regression equations and artificial neural networks. *Scientific Research and Essays*, *4*(10), 1047–1056.

29. Kaliakin, V. N. (2017). Example Problems Related to Compressibility and Settlement of Soils. In *Soil Mechanics*. https://doi.org/10.1016/b978-0-12-804491-9.00008-2

30. Kanzari, I. (2019). *Évaluation Du Potentiel Des Pompes À Chaleur Géothermique Pour La Communauté Nordique De Kuujjuaq*.

31. Klohn, E. J. (1965). The Elastic Properties of a Dense Glacial Till Deposit. *Canadian Geotechnical Journal*, *2*(2), 116–128. https://doi.org/10.1139/t65-014

32. Lajeunesse, P. (2008). *Early Holocene deglaciation of the eastern coast of Hudson Bay*. *99*, 341–352. https://doi.org/10.1016/j.geomorph.2007.11.012

33. Lanini, S., Delaleux, F., Py, X., Olivès, R., & Nguyen, D. (2014). Improvement of borehole thermal energy storage design based on experimental and modelling results. *Energy and Buildings*, *77*, 393–400. https://doi.org/10.1016/j.enbuild.2014.03.056

34. Lehane, B. M., & Simpson, B. (2000). Modelling glacial till under triaxial conditions using a BRICK soil model. *Canadian Geotechnical Journal*, *37*(5), 1078–1088. https://doi.org/10.1139/cgj-37-5-1078

35. Leroueil, S., Bihan, J. Le, Sebaihi, S., & Alicescu, V. (2002). *Hydraulic conductivity of compacted tills from northern Quebec*. *1049*, 1039–1049. https://doi.org/10.1139/T02-062

36. Lewis, R. W., Majorana, C. E., & Schrefler, B. A. (1986). A coupled finite element model for the consolidation of nonisothermal elastoplastic porous media. *Transport in Porous Media*, *1*(2), 155–178.

37. Liang, Y., Cao, L., Liu, J., & Sui, W. (2019). Numerical simulation of mechanical response of glacial tills under biaxial compression with the DEM. *Bulletin of Engineering Geology and the Environment*, *78*(3), 1575–1588. https://doi.org/10.1007/s10064-018-1229-2

38. Long, M., & Menkiti, C. O. (2007). Geotechnical properties of Dublin Boulder Clay. *Geotechnique*, *57*(7), 595–611. https://doi.org/10.1680/geot.2007.57.7.595

39. Mathews, W. H. (1974). Surface profiles of the laurentide ice sheet in its marginal areas. *Journal of Glaciology*, *13*(67), 37–43. https://doi.org/10.3189/s0022143000023352

40. Miranda, Giordano, Kanzari, Raymond, & Dezayes. (2017). *Shallow and deep geothermal resources assessment in northern communities of Québec : preliminary results from Kuujjuaq*. *September*.

41. Miranda, M., Giorfano, N., Kanzari, I., Raymond, J., & Dezayes, C. (2018). *TEMPERATURE-DEPTH PROFILES MEASURED IN THE INUIT COMMUNITY OF KUUJJUAQ , NORTHERN QUÉBEC , CANADA*. *January*.

42. Moradi, A., Smits, K. M., Massey, J., Cihan, A., & McCartney, J. (2015). Impact of coupled heat transfer and water flow on soil borehole thermal energy storage (SBTES) systems: Experimental and modeling investigation. *Geothermics*, *57*, 56–72. https://doi.org/10.1016/j.geothermics.2015.05.007

43. Pahud, D. (2000). Central solar heating plants with seasonal duct storage and short-term water storage: Design guidelines obtained by dynamic system simulations. *Solar Energy*, *69*(6), 495–509. https://doi.org/10.1016/S0038-092X(00)00119-5

44. Pare, Lavallee, & Rosenberg. (1978). Frost Penetration Studies in Glacial Till on the James Bay Hydroelectric Complex. *Canadian Geotechnical Journal*, *15*(4), 473–493. https://doi.org/10.1139/t78-052

45. Paré, Verma, Loiselle, & Pinzariu. (1983). *Seepage through till foundations of dams of the Eastmain - Opinaca - La Grande diversion*.

46. Penrod, E. B., & Prasanna, K. V. (1962). Design of a flat-plate collector for a solar earth heat pump. *Solar Energy*, *6*(1), 9–22. https://doi.org/10.1016/0038-092X(62)90093-2

47. Powrie, W., & Li, E. S. F. (1991). Finite element analyses of an in situ wall propped at formation level. *Geotechnique*, *41*(4), 499–514. https://doi.org/10.1680/geot.1991.41.4.499

48. Rad, F. M., & Fung, A. S. (2016). Solar community heating and cooling system with borehole thermal energy storage - Review of systems. *Renewable and*

Sustainable Energy Reviews, *60*, 1550–1561. https://doi.org/10.1016/j.rser.2016.03.025

49. Rad, F. M., Fung, A. S., & Rosen, M. A. (2017). An integrated model for designing a solar community heating system with borehole thermal storage. *Energy for Sustainable Development*, *36*, 6–15. https://doi.org/10.1016/j.esd.2016.10.003

50. Reuss, M., Beck, M., & Müller, J. P. (1997). Design of a seasonal thermal energy storage in the ground. *Solar Energy*, *59*(4-6–6 pt 4), 247–257. https://doi.org/10.1016/S0038-092X(97)00011-X

51. Roscoe, K. H., & Burland, J. B. (1968). *Roscoe, Burland_1968_On the Generalised Stress-Strain Behaviour of Wet Clay.pdf*.

52. Rosenberg, P., & Journeaux, N. L. (1978). Load bearing slurry trench wall supported by glacial till. *Canadian Geotechnical Journal*, *15*(3), 430–434. https://doi.org/10.1139/t78-040

53. Sauer, E. K., & Christiansen, E. A. (1988). Preconsolidation pressures in intertill glaciolacustrine clay near Blaine Lake, Saskatchewan. *Canadian Geotechnical Journal*, *25*(4), 831–838. https://doi.org/10.1139/t88-091

54. Sauer, E. K., Egeland, A. K., & Christiansen, E. A. (1993a). Compression characteristics and index properties of tills and intertill clays in southern Saskatchewan, Canada. *Canadian Geotechnical Journal*, *30*(2), 257–275. https://doi.org/10.1139/t93-022

55. Sauer, E. K., Egeland, A. K., & Christiansen, E. A. (1993b). Preconsolidation of tills and intertill clays by glacial loading in southern Saskatchewan, Canada. *Canadian Journal of Earth Sciences*, *30*(3), 420–433. https://doi.org/10.1139/e93-031

56. Shah, S. K., Aye, L., & Rismanchi, B. (2018). Seasonal thermal energy storage system for cold climate zones: A review of recent developments. *Renewable and Sustainable Energy Reviews*, *97*(March), 38–49. https://doi.org/10.1016/j.rser.2018.08.025

57. Shaw, R. J., & Hendry, M. J. (1998). *Hydrogeology of a thick clay till and Cretaceous clay sequence , Saskatchewan , Canada*. *1052*, 1041–1052.

58. Sibbitt, B., McClenahan, D., Djebbar, R., Thornton, J., Wong, B., Carriere, J., & Kokko, J. (2012). The performance of a high solar fraction seasonal storage district heating system - Five years of operation. *Energy Procedia*, *30*, 856–865. https://doi.org/10.1016/j.egypro.2012.11.097

59. St-Amour, Clatworthy, & Manzari. (2017). *Jet Grouting within Toronto's Glacial Deposits, a Contractor's Perspective*. 354–364.

60. Sweet, M. L., & McLeskey, J. T. (2012). Numerical simulation of underground Seasonal Solar Thermal Energy Storage (SSTES) for a single family dwelling using TRNSYS. *Solar Energy*, *86*(1), 289–300. https://doi.org/10.1016/j.solener.2011.10.002

61. Thomson, S., Martin, R. L., & Eisenstein, S. (1982). Soft zones in the glacial till in downtown Edmonton. *Canadian Geotechnical Journal*, *19*(2), 175–180. https://doi.org/10.1139/t82-019

62. Trenter, N. . (1999). Engineering in glacial tills. *CIRIA*.

63. Watabe, Y., Leroueil, S., & Le Bihan, J.-P. (2000). Influence of compaction conditions on pore-size distribution and saturated hydraulic conductivity of a glacial till. *Canadian Geotechnical Journal*, *37*(6), 1184–1194. http://www.nrc.ca/cgi-bin/cisti/journals/rp/rp2_abst_e?cgj_t00-053_37_ns_nf_cgj37-00

64. Winterwerp, J. C., & Van Kesteren, W. G. M. (2004). 8 - Mechanical Behaviour. In J. C. Winterwerp & W. G. M. van Kesteren (Eds.), *Introduction to the Physics of Cohesive Sediment in the Marine Environment* (Vol. 56, pp. 253–341). Elsevier. https://doi.org/https://doi.org/10.1016/S0070-4571(04)80009-8

65. Yang, H., Cui, P., & Fang, Z. (2010). Vertical-borehole ground-coupled heat pumps: A review of models and systems. *Applied Energy*, *87*(1), 16–27. https://doi.org/10.1016/j.apenergy.2009.04.038